Aus dem

Helmholtz Zentrum München

Comprehensive Pneumology Center (CPC)


# Mutational processes of thoracic malignancies

Dissertation

zum Erwerb des Doctor of Philosophy (Ph.D.)

an der Medizinischen Fakultät der

Ludwig-Maximilians-Universität München

vorgelegt von
Sabine Behrend

aus
Ebersberg/Deutschland

Jahr
2023

Mit Genehmigung der Medizinischen Fakultät der
Ludwig-Maximilians-Universität München

| | |
|---|---|
| Erstes Gutachten: | Prof. Dr. Jürgen Behr |
| Zweites Gutachten: | Prof. Dr. Georgios Stathopoulos |
| Drittes Gutachten**:** | Priv. Doz. Dr. Gerhard Preissler |
| Viertes Gutachten: | Priv. Doz. Dr. Julian Holch |
| Dekan: | Prof. Dr. med. Thomas Gudermann |
| Tag der mündlichen Prüfung: | 19.10.2023 |

# Affidavit

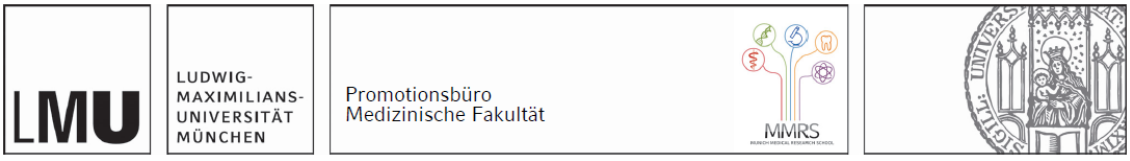


**Affidavit**

Behrend Sabine

Surname, first name

Max-Lebsche-Platz 31

Street

81377 Munich, Germany

Zip code, town, country

I hereby declare that the submitted thesis entitled:

*Mutational processes of thoracic malignancies*

is my own work. I have only used the sources indicated and have not made unauthorized use of services of a third party. Where the work of others has been quoted or reproduced, the source is always given.

I further declare that the submitted thesis or parts thereof have not been presented as part of an examination degree to any other university.

München, den 06.11.2023

Place, date

Sabine Behrend

Signature doctoral candidate

# Confirmation of congruency

LMU LUDWIG-MAXIMILIANS-UNIVERSITÄT MÜNCHEN

Promotionsbüro Medizinische Fakultät

MMRS

**Confirmation of congruency between printed and electronic version of the doctoral thesis**

Behrend Sabine

Surname, first name

Max-Lebsche-Platz 31

Street

81377 Munich, Germany

Zip code, town, country

I hereby declare that the submitted thesis entitled:

*Mutational processes of thoracic malignancies*

is congruent with the printed version both in content and format.

München, den 06.11.2023

Place, date

Sabine Behrend

Signature doctoral candidate

# Table of content

# List of abbreviations

| | |
|---|---|
| **ALK** | Anaplastic lymphoma kinase |
| **ANOVA** | Analysis of variance |
| **AT2 cells** | Alveolar type 2 cells |
| **BAP1** | BRCA1-Assocated Protein 1 |
| **BRAF** | B-Raf proto-oncogene serine/threonine kinase |
| **CCSP** | Clara cell secretory protein, a marker for club cells |
| **CD45** | Cluster of differentiation 45 |
| **CDKN2A** | Cyclin dependent kinase inhibitor 2A |
| **CNA** | Copy number alteration |
| **ddPCR** | Digital droplet polymerase chain reaction |
| **EGFR** | Epidermal growth factor receptor, a proto-oncogene |
| **EML4** | Echinoderm microtubule-associated protein-like |
| **ES-SCLC** | Extensive-stage small-cell lung carcinoma |
| **FFPE** | Formalin-fixed paraffin-embedded |
| **FVIII** | Coagulation factor VIII |
| **KRAS** | KRAS proto-oncogene GTPase |
| **LS-SCLC** | Limited-stage small-cell lung carcinoma |
| **LUAD** | Lung adenocarcinoma |
| **LUSC** | Lung squamous cell carcinoma |
| **LYZ2** | Lysozyme 2, a marker for alveolar type 2 cells and alveolar macrophages |
| **MPE** | Malignant pleural effusion |
| **MPM** | Malignant pleural mesothelioma |
| **mT/mG** | membranous tdTomato/membranous GFP, a CRE reporter mouse line |
| **NF1** | Neurofibromin 1 |
| **NF2** | Moesin-ezrin-radixin like (MERLIN) tumor suppressor |
| **NGS** | Next generation sequencing |
| **NSCLC** | Non-small cell lung carcinoma |
| **PCNA** | Proliferating cell nuclear antigen |
| **PCR** | Polymerase chain reaction |
| **PD-1** | Programmed cell death 1 |
| **PIK3CA** | Phosphatidylinositol-4,5-bisphosphate 3-kinase catalytic subunit alpha |
| **PTEN** | Phosphatase and tensin homolog |

| | |
|---|---|
| **RAF** | Rapidly accelerated fibrosarcoma |
| **RNAseq** | RNA sequencing |
| **SCLC** | Small-cell lung carcinoma |
| **SEM** | Standard error of the mean |
| **SNV** | Single nucleotide variant |
| **STK11** | Serine/threonine kinase 11 |
| **TCGA** | The Cancer Genome Atlas |
| **TP53** | Tumor protein p53, a human tumor suppressor gene |
| **Trp53** | Tumor protein p53, a murine tumor suppressor gene |
| **TUNEL** | Terminal deoxynucleotidyl nick-end labelling |
| **VEGF** | Vascular endothelial growth factor |
| **WT** | Wildtype |

# List of publications

## Publications used for this cumulative dissertation

Marazioti A*, Krontira AC*, **Behrend SJ***, Giotopoulou GA*, Ntaliarda G*, Blanquart C, Bayram H, Iliopoulou M, Vreka M, Trassl L, Pepe MAA, Hackl CM, Klotz LV, Weiss SAI, Koch I, Lindner M, Hatz RA, Behr J, Wagner DE, Papadaki H, Antimisiaris SG, Jean D, Deshayes S, Grégoire M, Kayalar Ö, Mortazavi D, Dilege Ş, Tanju S, Erus S, Yavuz Ö, Bulutay P, Fırat P, Psallidas I, Spella M, Giopanou I, Lilis I, Lamort AS, Stathopoulos GT. KRAS signaling in malignant pleural mesothelioma. EMBO Mol Med. 2022;14(2):e13631. doi: 10.15252/emmm.202013631.

* Equally contributing first authors

Lamort AS, Kaiser JC, Pepe MAA, Lilis I, Ntaliarda G, Somogyi K, Spella M, **Behrend SJ**, Giotopoulou GA, Kujawa W, Lindner M, Koch I, Hatz RA, Behr J, Sotillo R, Schamberger AC, Stathopoulos GT. Prognostic phenotypes of early-stage lung adenocarcinoma. Eur Respir J. 2022;60(1):2101674. doi: 10.1183/13993003.01674-2021.

## Publication additionally appended to this dissertation

**Behrend SJ**, Giotopoulou GA, Spella M, Stathopoulos GT. A role for club cells in smoking-associated lung adenocarcinoma. Eur Respir Rev. 2021;30(162):210122. doi: 10.1183/16000617.0122-2021.

## Further publications of the candidate

Klotz LV, Courty Y, Lindner M, Petit-Courty A, Stowasser A, Koch I, Eichhorn ME, Lilis I, Morresi-Hauf A, Arendt KAM, Pepe M, Giopanou I, Ntaliarda G, **Behrend SJ**, Oplopoiou M, Gissot V, Guyetant S, Marchand-Adam S, Behr J, Kaiser JC, Hatz RA, Lamort AS, Stathopoulos GT. Comprehensive clinical profiling of the Gauting locoregional lung adenocarcinoma donors. Cancer Med. 2019;8(4):1486-1499. doi: 10.1002/cam4.2031.

Abdullahi S, Jäkel M, **Behrend SJ**, Steiger K, Topping G, Krabbe T, Colombo A, Sandig V, Schiergens TS, Thasler WE, Werner J, Lichtenthaler SF, Schmid RM, Ebert O, Altomonte J. A Novel Chimeric Oncolytic Virus Vector for Improved Safety and Efficacy as a Platform for the Treatment of Hepatocellular Carcinoma. J Virol. 2018;92(23):e01386-18. doi: 10.1128/JVI.01386-18.

# Contribution to the publications

## 1 Contribution to paper I

The PhD candidate and co-first author of this publication substantially contributed to the design, experimental work, data analysis and interpretation of this study. Throughout the entire process, she gave valuable intellectual input and wrote portions of the manuscript.

The candidate selected and established the used digital droplet polymerase chain reaction (ddPCR) assays for the precise detection of driver mutations in *KRAS* codons 12, 13, and 61 as well as *TP53* copy number alterations (CNA) in patients suffering pleural effusions from different underlying diseases. Upon DNA extraction she independently designed and performed three different sensitive ddPCR assays on $n$ = 93 samples of 44 patients. She analyzed the data including setting appropriate thresholds and normalization on the programming language R, followed by visualization and statistical calculations of the results and findings derived therof. Additionally, she validated the findings in two further cohorts of malignant pleural mesothelioma (MPM) patients resulting in a total of $n$ = 120 samples of 71 patients. During this process she corresponded with the collaborators from Istanbul, Turkey who provided one of the additional cohorts. With these findings she could significantly help showing the relevance of the specific *KRAS* mutant subset of MPM patients with or without co-occurring *TP53* mutations.

Furthermore, the author participated in the immunostainings of seven MPM and lung adenocarcinoma (LUAD) mouse models with the markers mesothelin, Wilms' tumor 1 and vimentin for a more comprehensive assessment of tumors. Subsequent imaging and scoring were carried out.

In addition, she conducted further analyses which were not used in the final version of the manuscript. Following RNA extraction and coordination for RNA sequencing (RNAseq) submission, she performed mutation detection in a mononucleotide and trinucleotide context, single nucleotide variation (SNV) extraction, gene expression and pathway analysis on $n$ = 6 MPM patients including creating heatmaps and hierarchical clustering of the acquired data. In the publicly available Cancer Genome Atlas (TCGA) PanCancer MPM patient data set ($n$ = 86 patients), she similarly analyzed transcriptomics and pathway activation including their visualization.

The first authorship of this paper was shared among Antonia Marazioti, Anthi C Krontira, Georgia A Giotopoulou, Giannoula Ntaliarda and the candidate due to their equally major contribution to this work. Their common effort in designing the study and conducting experiments was accompanied by discussions throughout the whole progress of the study. All four authors wrote equivalent portions of the manuscript.

## 2 Contribution to paper II

The candidate participated in the tissue processing of the described LUAD cohort with *n* = 366 patients. Biopsies of tumors and adjacent lung tissues were cut in halves, processing one part to formalin-fixed paraffin-embedded (FFPE) blocks and the rest for DNA, RNA, and protein extraction. She furthermore took part in DNA purification which was followed by ddPCR for mutations in the oncogenic driver *KRAS* in codons 12/13 and *EGFR* in exon 19 from *n* = 200 patients representative of the cohort. Additionally, the co-author helped with cutting and immunostaining of the FFPE tissues for the genomic instability marker TP53 and angiogenesis marker FVIII. She provided intellectual input and reviewed the paper draft.

## 3 Contribution to paper III (Appendix)

The author of this PhD thesis helped conceiving the concept, conducted literature research, and analyzed data. She wrote ample parts of the manuscript and helped reviewing the full draft.

# Introductory summary

## 1 Malignant neoplasms of the lower respiratory system

In the chest a variety of distinct types of cancer can arise from different tissues within and surrounding the lung. Besides the genotypic lesions known to crucially drive malignant transformation and progression [1], the cells of origin within one organ also define the tumors [2]. Therefore, within one tissue several subtypes of cancer can be found with again various histologies which determine diagnosis and treatment of the respective malignancies [3]. For the purpose of this thesis, the content will focus on primary cancers of the lungs and pleura.

### 1.1 Malignancies of the lung epithelium

With 1.8 million deaths in 2020, lung cancer is the leading cause of cancer-related mortality worldwide in both men and women [4]. More than 2 million patients were diagnosed with lung cancer, whose clinical signs are characterized by anorexia, weight loss, fatigue, and more specific symptoms such as persisting cough, chest pain, worsening dyspnea, hemoptysis, and reoccurring pneumonia or bronchitis [5]. As these symptoms and thus the diagnosis usually only occur at already advanced stages of this malignancy, the 5-year survival rate amounts to only 10% to 20% [4, 6].

It is scientifically proven that tobacco smoking remains the dominant cause for lung cancer [7, 8]. Tobacco products and its smoke contain over 9,500 chemical compounds of which 83 are provably carcinogens [9]. But there are also other environmental exposures that have been shown to inflict cancer in the respiratory system. These risk factors include secondhand tobacco smoke, radiation, air pollution, radon, and occupational carcinogens such as asbestos [10-18]. Patients with COPD, bronchitis, emphysema, asthma, or another previous history of chronic respiratory diseases are subject to a higher risk of developing neoplasms in the lung [19, 20]. Furthermore, it has been demonstrated that infectious diseases affecting the lung can contribute to carcinogenesis [21-24].

Lung cancer can be divided into two major types, small-cell lung carcinoma (SCLC) and non-small cell lung carcinoma (NSCLC). Globally, SCLC accounts for an incidence of roughly 250,000 and 200,000 deaths every year [25]. Due to its easy relapse, the overall survival rate is with approximately 10 months very low [26]. At a limited stage of this disease (LS-SCLC) the malignant cells are still locally restricted, but 60% of the patients show evidence of extensive-stage SCLC (ES-SCLC). Here, the disease has already progressed and spread beyond the hemithorax [27]. The standard line of treatment is comprised of chemotherapy, radiation therapy, prophylactic cranial radiation, or a combination thereof. Surgery can be an option in LS-SCLC. In the frequent case of recurrence, treatments concentrate on palliative care [28]. Some modest progresses could be achieved in the emerging field of immunotherapeutics targeting molecules such as poly ADP ribose polymerase (PARP), checkpoint kinase 1 (CHK1), programmed cell death 1 (PD-1), programmed death-ligand 1 (PD-L1), fibroblast growth factor receptors (FGFR), and cyclin-dependent kinase 7 (CDK7) in combination with chemotherapy [29]. However, more research needs to be done to develop more effective and comprehensive responses.

NSCLC comprises about 85% of all lung cancer cases and can be further classified into three main categories. 40% of NSCLC patients are diagnosed with lung adenocarcinoma (LUAD) making it the most dominant histopathologic subtype. With 25% lung squamous cell carcinoma (LUSC) ranks second and large cell carcinoma represents 15% of all NSCLC cases. The remaining 20% are composed of other, rare forms such as large cell neuroendocrine, pleomorphic sarcomatoid, and adenosquamous carcinoma, as well as carcinoid tumors [30]. The five-year relative survival rates for NSCLC are generally higher than for SCLC and amount to 23% and 6%, respectively. However, the survival greatly depends on the stage of the disease at diagnosis [30]. When NSCLC patients are diagnosed at an early stage of the disease and the tumor is resectable, surgery together with adjuvant chemotherapy or radiotherapy is the preferred treatment [31, 32]. Nevertheless, as with 70% most patients already have more advanced cancer stages at the time of diagnosis, radiation therapy, combination chemotherapy, laser therapy, and/or targeted therapy are employed [33]. It has been demonstrated that radiation together with chemotherapy improves survival [34, 35]. Generally, the choice of therapeutics is defined by the tumor location, its resectability and the presence of certain mutations. Mutations that can be targeted up to date include epidermal growth factor receptor (*EGFR*), anaplastic lymphoma kinase (*ALK*), proto-oncogene tyrosine-protein kinase (*ROS*), rapidly accelerated fibrosarcoma (*RAF*), tyrosine-protein kinase Met (*MET*), vascular endothelial growth factor (*VEGF*), and others [36]. If there is no actionable mutation present, immunotherapy presents a treatment option. However, acquired resistances are common [36].

## 1.2 Pleural neoplasms

Malignant pleural mesothelioma (MPM) is a rare but devastating malignancy that evolves from the mesothelial cells lining the chest cavity [37, 38]. In 2020, the global incidence reached 31,000 cases and 26,000 deaths could be observed [4]. Since an early detection of MPM is difficult with current diagnostic tools and due to its aggressive nature, the 5-year survival rate is below 5% [37, 39]. Most MPM patients present with chest pain and dyspnea. Other symptoms may include weight loss, fatigue, dry cough, anorexia, sweats, and fever [38, 40]. Progressive breathlessness is usually caused by an elevated accumulation of fluid in the space between the visceral and parietal pleura which contains malignant cells. This phenomenon is called malignant pleural effusion (MPE) and develops in approximately 90% of individuals [41, 42].

The vast majority of MPM (up to 90%) is induced by occupational exposure to the mineral asbestos [43, 44]. It is well established that MPM can bet attributable to other mineral fibers such as erionite or fluoro-edenite, and therapeutic radiation [45-48]. Further risk factors may include chronic pleural inflammation and carbon nanotubes, but the data are sparse [43, 49-51].

MPM can be classified in three histologic subtypes: epithelioid, sarcomatoid, and biphasic. While sarcomatoid histology represents the worst prognosis, epithelioid tumors indicate the longest survival [52]. Patients with biphasic subtype have a more beneficial prognosis the higher the proportion of differentiation towards epithelial cells is [53]. For early stage MPM patients, surgery is debated [40]. Chemotherapy has been proven to prolong the median survival for almost three months and drainage of the MPE fluid can improve dyspnea [54-56]. Despite the toxicity of radiation therapy, it is used palliatively [57, 58]. As lung cancer, MPM can be treated with targeted therapy and immunotherapy including VEGF, EGFR, PDL-1, mesothelin, and cancer vaccines,

dendritic cell-therapy, and chimeric antigen receptor T-cell therapy, respectively [59, 60]. Nevertheless, MPM remains a deadly disease without cure, pointing out the urgent need for further investigations to achieve diagnostic and therapeutic advances.

# 2 Mutational landscapes of thoracic malignancies

Hanahan and Weinberg declared genomic instability and mutations as one of the ten hallmarks of cancer [61]. Genomic changes include base substitutions, so called single nucleotide variants (SNV), insertions and deletions. More extensive damage comprises copy number alterations (CNA), alternative splicing and chromosomal rearrangements such as gene fusions [62]. In addition to these aberrations, epigenetic changes influence tumor progression independent from the DNA. They involve predominantly post-translational histone and DNA methylation pattern modifications leading to abnormal gene expression [63]. Furthermore, gene expression can be modulated by noncoding small RNAs, changes of which are known to act in cancer as well [64].

Organs that build the barrier to the environment such as the skin, but also the respiratory and gastrointestinal system, are directly affected by environmental exposures. Many of these can induce genomic alterations and thus are toxic to the human body. Mutations and other genomic modifications have been proposed to be a hallmark of environmental insults [65]. Hence, tumors in such barrier organs carry a relatively high number of somatic mutations (Figure 1). Studies have already established numerous environmental chemicals as mutagenic. Efforts were made to expose pluripotent stem cells to environmental mutagens inducing alterations in the genome that were comparable to the mutation signatures of human cancers [66]. Similar studies were performed aiming to identify the causative origins of malignancies based on comparing their mutational patterns [67-69].

It is highly valuable to enhance our knowledge about genomic alterations in human tumors. It will not only help to improve the biological understanding of the tumor, its progression and their putative role as driver or passenger mutations of each disease but might also possess prognostic and/or predictive value. New mutations might pose new biomarkers or therapeutic targets influencing clinical decision making, or hint to causative agents.

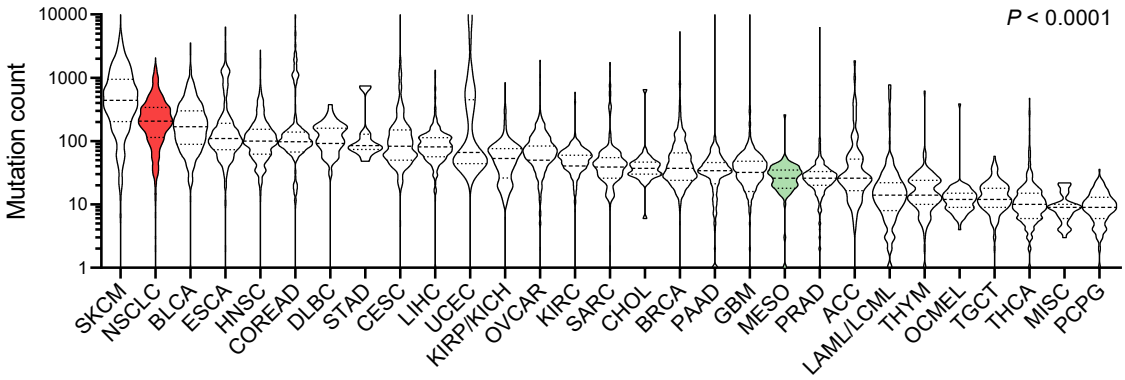


**Figure 1. Mutation numbers of 32 different TCGA cancer studies.** The Cancer Genome Atlas (TCGA) PanCancer Atlas (*n* = 11,133 patients) was queried for mutation numbers for each single cancer study and summarized in this plot. The counts for NSCLC and MPM are highlighted in red and green, respectively. The data are available at https://www.cbioportal.org/. Presented are medians (dashed lines), quartiles (dotted lines), and rotated kernel density plots (violin plots). *P*, probability, ordinary one-way ANOVA. ACC, adrenocortical carcinoma; BLCA, bladder urothelial carcinoma; CESC, cervical squamous cell carcinoma/endocervical adenocarcinoma; CHOL, cholangiocarcinoma; COREAD, colorectal adenocarcinoma; GBM, glioblastoma multiforme; UCEC, uterine corpus endometrial carcinoma; ESCA, esophageal carcinoma; HNSC, head and neck squamous cell carcinoma; LIHC, liver hepatocellular carcinoma; BRCA breast invasive carcinoma; LAML/LCML, acute myeloid leukemia/chronic myelogenous leukemia; DLBC, lymphoid neoplasm diffuse large B-cell lymphoma; SKCM, skin cutaneous melanoma; MISC, miscellaneous; TGCT, testicular germ cell tumors; NSCLC, non-small cell lung carcinoma; OCMEL, ocular melanoma; OVCAR, ovarian serous cystadenocarcinoma; PAAD, pancreatic adenocarcinoma; PCPG, pheochromocytoma/paraganglioma; MESO, mesothelioma; PRAD, prostate adenocarcinoma; KIRC, kidney renal clear cell carcinoma; KIRP/KICH, kidney renal papillary cell carcinoma/kidney chromophobe; SARC, sarcoma; THYM, thymoma; STAD, stomach adenocarcinoma; THCA, thyroid cancer.

But, since cancer is a very heterogenous disease, its characterization and treatment poses a challenge for. Lung cancer and mesothelioma are likewise affected by intra- and inter-tumoral (spatial) but also by clonal (temporal) heterogeneity [70-72]. In lung cancer the most frequent mutations that can be detected in patients differ between the different histologic subtypes, although there are some genes that are common. The most frequent inactivating mutations that can be found in SCLC include tumor protein p53 (*TP53*), RB transcriptional corepressor 1 (*RB1*), lysine methyltransferase 2D (*KMT2D*), phosphatase and tensin homolog (*PTEN*), notch receptor 1 (*NOTCH1*), CREB binding protein (*CREBBP*), FAT atypical cadherin 1 (*FAT1*), neurofibromin 1 (*NF1*), and APC regulator of WNT signaling pathway (*APC*) which are altered at rates of 89, 64, 13, 7, 6, 5, 4, 4, and 4%, respectively [25]. Phosphatidylinositol-4,5-bisphosphate 3-kinase catalytic subunit alpha (*PIK3CA*, 7%), *EGFR* (4%), KRAS proto-oncogene GTPase (*KRAS*, 3%) are prevalently activated oncogenes in this disease [25]. Hence, the most disrupted pathways are PI3K/AKT/mTOR, Ras-Raf-MEK-ERK, cell-cell signaling, transcription regulation, stress response, and chromatin-remodeling.

In NSCLC on the other hand, the genomic alterations can be frequently found in cyclin dependent kinase inhibitor 2A (*CDKN2A*), B-Raf proto-oncogene serine/threonine kinase (*BRAF*), serine/threonine kinase 11 (*STK11*), with *CDKN2A* being more prevalent in LUSC and *BRAF* and *STK11* in LUAD [73]. Similarly to SCLC, high mutational burden can be found in *TP53*, *KRAS*, *EGFR*, *NF1*, *PIK3CA*, and *PTEN*, well known tumor suppressor genes and oncogenes. Especially elevated mutation frequencies can be observed for *TP53* with 46 and 91% in LUAD and LUSC, respectively, and *KRAS* with 33% in LUAD [73]. In addition to these, rearrangements in genes

such as ALK receptor tyrosine kinase, amplification of oncogenes and more extensive deletions e.g., in *CDKN2A* are typical aberrations in lung tumors.

MPM carry an average of only 24 protein-coding alterations which are mainly accumulated in the DNA repair and Hippo pathways [74, 75]. Genetic variation in up to 60% of the tumors can be observed in the tumor suppressor BRCA1-Assocated Protein 1 (*BAP1*) which is involved in DNA repair, cell cycle, and differentiation regulation [76-78]. Furthermore, Bueno et al. and Quetel et al. found that moesin-ezrin-radixin like (MERLIN) tumor suppressor (*NF2*), *CDKN2A*/*B*, *TP53*, and SET domain containing 2 histone lysine methyltransferase (*SETD2*), and large tumor suppressor kinase 2 (*LATS2*) are mutated at high frequency in MPM [74, 77, 79, 80]. Mutations in oncogenes such as *EGFR*, *KRAS*, and *PIK3CA* upregulating the Ras/Raf/MEK/ERK and PI3K/AKT/mTOR pathways and thus driving cellular survival and proliferation are rather rare in MPM, although recent data suggest an underestimated role for *KRAS* mutations in this malignancy [39, 81]. Table 1 summarizes the most abundant mutations which can be found in both diseases, lung cancer and MPM.

**Table1.** Most abundant somatic mutations common among lung cancer and MPM and their frequencies.

| Gene | Mutation frequency [%] | | | | Main function |
|---|---|---|---|---|---|
| | SCLC | LUAD | LUSC | MPM | |
| *TP53* | 90 | 46 | 91 | 8 | Tumor suppressor; cell cycle control, DNA repair, apoptosis |
| *CDKN2A* | | 4 | 17 | | Tumor suppressor; cell cycle control, TP53 pathway |
| *NF1* | 4 | 11 | | | Tumor suppressor; PI3K/AKT/mTOR signaling, Ras/Raf/MEK/ERK signaling |
| *PTEN* | 6 | | 8 | | Tumor suppressor; PI3K/AKT/mTOR signaling |
| *KRAS* | 3 | 33 | | rare | Oncogene; PI3K/AKT/mTOR signaling, Ras/Raf/MEK/ERK signaling |
| *EGFR* | 4 | 14 | | rare | Oncogene; PI3K/AKT/mTOR signaling, Ras/Raf/MEK/ERK signaling |
| *PIK3CA* | | 7 | 16 | rare | Oncogene; PI3K/AKT/mTOR signaling |

Data collected from [25, 73, 74]

# 3 Digital droplet PCR

Digital droplet polymerase chain reaction (ddPCR) is a molecular method that allows direct quantification of nucleic acid molecules with a very high level of precision and sensitivity [82]. It can be used in various applications including mutation and genome edit detection, copy number examination, absolute quantification of nucleic acids, gene expression, and identification of microorganisms [83]. This method can be a powerful tool for molecular diagnostics, especially for detecting rare mutations.

By creating a water-in-oil emulsion of the sample, it is partitioned into up to 20,000 nanoliter droplets which ideally contain only one copy of the target molecule and all PCR reagents. Then, PCR amplification runs in every single droplet providing high accuracy. The readout is performed by

detecting two-color fluorescent Taqman probes. In the subsequent analysis thresholds are set in order to discriminate positive and negative signals as e.g., wildtype from mutant droplets of a certain target gene (Figure 2).

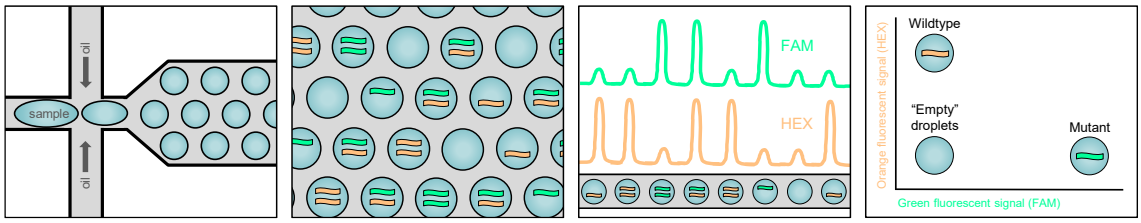


**Figure 2. Schematic workflow of ddPCR.** The single steps including droplet generation, PCR amplification, droplet reading, and analysis are visualized. Exemplary, wildtype copies of a target molecule are labelled with the fluorescent marker FAM (turquoise) and mutant copies with HEX (orange).

As the detection of the PCR products happens at the end of the reaction, the outcome is much less influenced by its amplification efficiency and no standards or calibration is required, making ddPCR superior to conventional PCR and qPCR [84, 85]. This method allows the user absolute quantification of the target nucleic acid without bias and detection at a very low frequency of 1:10,000 [82, 85]. The necessity of only low sample and reagent quantity poses another benefit reducing costs and saving precious samples. Thus, ddPCR is among other applications a suitable tool for molecular diagnostics.

Next generation sequencing (NGS) or massively parallel sequencing represents another rising highly effective tool to analyze exomes, transcriptomes, and genomes in a comprehensive and high-throughput fashion [86]. With NGS, one can evaluate somatic mutations not only in known disease-related genes, but also previously uncharted genetic or epigenetic alterations. In comparison with ddPCR, it is not necessary to know the target sequence, but NGS will take more time and be more costly [87]. Additionally, NGS requires extensive computer capacity, storage space and bioinformatic expertise for analysis, which is not the case with ddPCR. Signatures extracted from NGS data pose approximations dependent on the mathematical approach and thresholds used [68]. Regarding the detection limit, both methods show high sensitivity levels with 0.001% and 0.001-1% for ddPCR and NGS, respectively, making ddPCR more sensitive in most cases [82, 87-89]. Despite its advantages, the target sequence needs to be known to develop specific assays for each single base alteration when applying ddPCR [88].

We and others have observed that compared to NGS, ddPCR is faster and more sensitive for detecting specific mutations or pathogens in human specimen [89-91]. Taken together, ddPCR represents a very well-suited technique for the detection of especially rare mutations in known target sequences.

# 4 Spatiotemporal evolution of *Kras* mutations in murine lung adenocarcinoma

**Behrend SJ**, Giotopoulou GA, Spella M, Stathopoulos GT. A role for club cells in smoking-associated lung adenocarcinoma. Eur Respir Rev. 2021;30(162):210122. doi: 10.1183/16000617.0122-2021

and unpublished data (manuscript in preparation).

With lung cancer being the number one cancer killer worldwide, we decided to investigate the mutation pattern and cell of origin of LUAD, the most abundant type of lung cancer, in a spatiotemporal manner. Generally, the tumor initiating cells and their genetic alterations determine cancer formation and progression [92]. Thus, and due to their potential role as therapeutic targets, defining and studying the cell of origin is of high relevance. Together with cancer stem cells and mature cancer cells they share upregulation of self-renewal pathways [93]. Based on this fact, all pulmonary cell lineages that possess stem cell characteristics such as basal, club, alveolar type 2 (AT2), and bronchioalveolar stem cells are potential cells of origin in LUAD [94-101]. It is plausible that the enormous diversity of causes of this dreadful disease results in different tumor initiating cells ultimately leading to the existing heterogeneity of patient subgroups [102]. This is a fact which should be covered in research addressing the cell of origin.

Next to genetic mouse models which artificially introduce driver mutations found in patients, murine LUAD models which are inflicted by environmental carcinogens such as the tobacco chemicals urethane (ethyl carbamate), N-nitrosodiethylamine, N-methyl-N-nitrosourea, 4-(methylnitrosamino)-1-(3-pyridyl)-1-butanone, or N'-nitrosonornicotine better recapitulate complex carcinogenic processes, mutation accumulation signatures and pathophysiology [102-104]. These chemicals do not necessarily cause the exact mutation found in humans, but the relevant mutation range [104, 105]. The tobacco carcinogen urethane is able to reliably induce LUAD in susceptible FVB mice by a single injection of the chemical [106]. This mouse model displays the complex mutation patterns which can be found in human LUAD, and which reproducibly include *Kras*$^{Q61R}$ mutations [104, 105, 107]. In patients *KRAS* mutations are predominantly found in codon 12, and some in codons 13 and 61 [108].

*KRAS* is a key driver oncogene which is mutated in about one third of all LUAD patients and is associated with tobacco smoking [73, 109, 110]. Patients carrying a *KRAS* activation display a poorer prognosis and targeted therapies have been demonstrated to be challenging due to the biological heterogeneity of *KRAS* mutant lung cancer. Numerous clinical trials for new therapeutics haven't shown promising results so far [111]. The *KRAS* gene encodes a cell membrane bound GTPase which when carrying an activating mutation, enables various signal pathways such as enhanced proliferation, apoptosis repression, upregulated cell metabolism, angiogenesis, suppressed antitumor immunity, and metastasis [112].

A valuable approach to investigate the spatial LUAD development is lineage marking. Since the time axis of *Kras*$^{Q61R}$ mutation acquisition and the afflicted cell lineages are still obscure, we combined this strategy with the urethane mouse model of environmentally induced LUAD to scrutinize when and which pulmonary cell types gain *Kras*$^{Q61R}$ mutations and ultimately conclude on the question whether urethane inflicted LUAD develops from the alveoli or airways. Clara cell secretory protein (*CCSP*) and lysozyme 2 (*LYZ2*) are well established markers that are specifically

expressed in club cells of the bronchi and in AT2 cells and alveolar macrophages, respectively [98, 100]. Hence, different CRE-driver strains expressing the Cre recombinase under the promoters of these two genes were intercrossed with a double fluorescent CRE-reporter strain (mT/mG) that switches from expression of membranous tdTomato (*mT*) to membranous GFP (*mG*) upon CRE recombination [113]. The heterozygous offspring CCSP.CRE;mT/mG and LYZ2.CRE;mT/mG with permanently labelled club cells, and AT2 cells and alveolar macrophages, respectively, received a single dose of urethane. Lungs were taken 0, 1, 2, 4, and 8 weeks post-urethane and tumors were resected at 16, 24, and 32 weeks following the treatment (Figure 3A-B).

We developed a duplexed ddPCR assay for the parallel detection of two targets. With this specialized method we checked for CRE recombination by probes against *mT* and the presence of *Kras*$^{Q61R}$ mutations by probes spanning the codons 57-64 of wildtype *Kras*. In both, lung samples at early phases following urethane administration and tumors at advanced stages of LUAD, we found an increasing proportion of lineage marked mG+ and *Kras*$^{Q61R}$ mutant droplets in CCSP.CRE;mT/mG mice and thus *Kras*$^{Q61R}$ mutant club cells. In AT2 cells the opposite effect could be observed for both sample types, indicating that club cells in the airways maintain driver *Kras* mutations while these tend to get lost in alveolar cells (Figure 3C-D). These findings suggest that club cells are cells of origin of LUAD induced by smoking as opposed to most of the current literature which shows AT2 cells as major progenitors in genetic mouse models of *Kras*$^{G12D}$ driven LUAD [114-116]. However, there has also been proof that tobacco specifically sensitizes epithelial cells of the bronchi and, similar to our results, the tobacco carcinogen urethane causes early *Kras* mutations in club cells which can lead to murine LUAD in sensitive mice [98, 117, 118].

As the data about the cell of origin of LUAD are contradictory, there is a high need for further investigation which takes into account the great heterogeneity of the underlying disease and its causes. Human studies scrutinizing the tumor initiating cells are challenging and sparse, since the disease usually is already progressed, and reconstruction of the clonal evolution can be solely done by correlation [119]. LUAD of smokers and never-smokers may arise from distinct cells acquiring different molecular characteristics [102, 120]. Thus, application of mouse models, lineage tracing studies, single cell RNAseq, and verification in human relevant pre-clinical models might deliver valuable insights in the future.

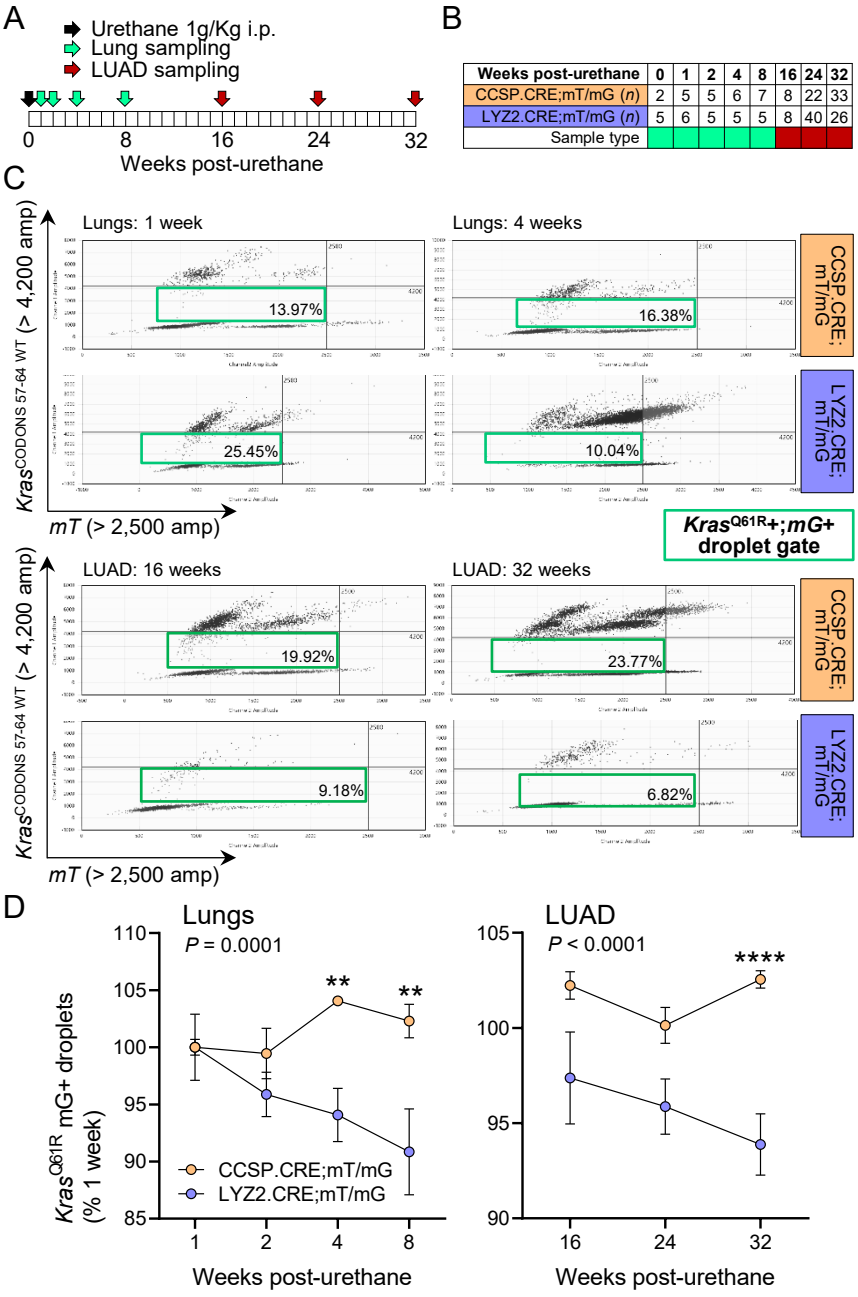


**Figure 3. Airway cells sustain *Kras*$^{Q61R}$ mutations during LUAD development.** (A, B) The timeline shows the design of this study (A). A single dose of 1 g/Kg urethane was administered to CCSP.CRE;mT/mG and LYZ2.CRE;mT/mG mice (FVB strain). Whole lungs were harvested at 1, 2, 4, and 8 weeks and lung tumors were taken at 16, 24, and 32 weeks post-urethane. DNA was extracted from lungs (*n* = 36-45 samples/strain) and tumors (*n* = 63-74 samples/strain) at different time points (B). Duplexed ddPCR with specific primers and probes against Tomato (*mT*) and wildtype for *Kras* codon 61 (*Kras*$^{Q61WT}$) alleles was performed and *mG*+ (lineage marked) and *Kras*$^{Q61R}$ (mutant) droplets were calculated by exclusion. (C) Representative amplitude graphs demonstrating the gating strategy for quantification of Kras$^{Q61R}$ mutant and mG+ droplets (green boxes). (D, E) Percentage of *Kras*$^{Q61R}$ mutant and mG+ droplets normalized to time-point 1 week post-urethane in whole lungs (D; *n* = 5-7/data point) and LUAD (E; *n* = 8-40/data-point) over time. Shown are mean (circles) ± standard error of the mean (SEM) (bars). *P*, probability, two-way ANOVA. ** and ****, $P < 0.01$ and $P < 0.0001$, respectively, for comparison between strains, Sidak's test.

# 5 Immunopathologic features reveal new human lung adenocarcinoma patient phenotypes independent of oncogenic driver mutation status

Lamort AS, Kaiser JC, Pepe MAA, Lilis I, Ntaliarda G, Somogyi K, Spella M, **Behrend SJ**, Giotopoulou GA, Kujawa W, Lindner M, Koch I, Hatz RA, Behr J, Sotillo R, Schamberger AC, Stathopoulos GT. Prognostic phenotypes of early-stage lung adenocarcinoma. Eur Respir J. 2022;60(1):2101674. doi: 10.1183/13993003.01674-2021.

Moving on to the human malady, we were able to obtain a cohort of 366 LUAD patients with resected tumor and adjacent tissue samples [121]. In order to characterize a large set of patients, we performed ddPCR for driver mutation detection and histologic stainings for examination of seven cancer hallmarks in 200 patients representative of the cohort [61, 122].

We screened the specimen for alterations in the two most frequently mutated oncogenes in LUAD, *KRAS* and *EGFR* [73]. EGFR is a transmembrane receptor with tyrosine kinase function. It triggers a signaling cascade inducing maintenance and growth of epithelial cells and preventing apoptosis [123]. Most mutations in *EGFR* comprise smaller deletions in exon 19 or the point mutation L858R in exon 21, while *KRAS* mutations predominantly can be found in codons 12, 13 and occasionally 61 [108, 124, 125]. Thus, we were scrutinizing alterations in *KRAS* codons 12/13 and in *EGFR* exon 19 by sensitive ddPCR. In addition, the samples were checked for a common fusion with oncogenic action. An inversion in chromosome 2 leads to the fusion of the N-terminal half of echinoderm microtubule-associated protein-like 4 (*EML4*) with the kinase domain of *ALK* [124]. The resulting fusion *EML4-ALK* was detected in our human LUAD samples by reverse transcription.

The cancer hallmarks that were stained and scored using immunohistochemistry include proliferating cell nuclear antigen (PCNA), TP53, NF1, terminal deoxynucleotidyl nick-end labelling (TUNEL), cluster of differentiation 45 (CD45), PD-1, and Coagulation factor VIII (FVIII) indicative of proliferation, genomic instability, KRAS pathway activation, apoptosis, inflammation, immune checkpoint activity, and angiogenesis, respectively [61].

Since survival varies among LUAD patients, prognostic biomarkers are imperative. Immunohistochemistry poses a well-established method in pathology to provide a platform for biomarker detection. By scoring the expression of these seven cancer hallmarks, we were able to identify two patient clusters with either high TUNEL (apoptotic cluster) or high expression of the markers PCNA, TP53, NF1, CD45, PD-1, and FVIII (proliferative cluster) [122]. No or only slight correlation could be determined with clinical parameters, but with 70% the 5-year survival was elevated in patients within the apoptotic cluster as compared to 50% in the proliferative group. No connection could be observed with the presence of the tested driver mutations in *KRAS*, *EGFR* or *EML4-ALK*. Hence, we were able to make out two different LUAD phenotypes in our cohort by solely immunostaining which could be verified in the TCGA PanCancer cohort [122].

Examination of the single markers and their correlation to overall survival revealed that specifically enhanced TP53 and PCNA expression can predict worse survival. All markers were included in an immunophenotypic LUAD death score to prognosticate overall survival and were validated in

the cohort and using the KMplot lung cancer module. Comparison revealed that TNM7 classification is superior to our score which in turn outperforms WHO histology. As there is only marginal correlation with the TNM classification, this death score can be used alone or in combination with established clinical scores to predict patients' survival [122]. Furthermore, we developed a formula with 96% accuracy to predict the LUAD phenotype using the expression scores of PCNA, TP53, NF1, TUNEL, CD45, and FVIII which is easily applicable in the clinic.

Taken together, these data highlight the role of immunohistochemistry as a valuable tool to predict overall survival in patients with resected LUAD as it is already applied in breast cancer [126]. We provide formulas which are ready to use in the clinic and it would be worthwhile to explore these patient clusters for potential prediction in response to therapies. Existence of different clusters also supports our hypothesis that there are multiple subtypes and several molecular ways to LUAD. The clusters identified in this study are not grouped by driver mutation or clinicopathologic parameters and may thus be explained by the cell of origin or environmental causes [122].

# 6 Underestimated role of *KRAS* mutations in human malignant mesothelioma

Marazioti A*, Krontira AC*, **Behrend SJ***, Giotopoulou GA*, Ntaliarda G*, Blanquart C, Bayram H, Iliopoulou M, Vreka M, Trassl L, Pepe MAA, Hackl CM, Klotz LV, Weiss SAI, Koch I, Lind-ner M, Hatz RA, Behr J, Wagner DE, Papadaki H, Antimisiaris SG, Jean D, Deshayes S, Gré-goire M, Kayalar Ö, Mortazavi D, Dilege Ş, Tanju S, Erus S, Yavuz Ö, Bulutay P, Fırat P, Psallidas I, Spella M, Giopanou I, Lilis I, Lamort AS, Stathopoulos GT. KRAS signaling in ma-lignant pleural mesothelioma. EMBO Mol Med. 2022;14(2):e13631. doi: 10.15252/emmm.202013631.

Mutations found in MPM affect patient survival as it had been shown for deactivating alterations in *TP53* and *CDKN2A* to predict poor survival [76, 127]. Although *KRAS* mutations are scarcely detected in MPM, it has been found that RAS signaling is commonly upregulated in this disease [128]. Furthermore, Matallanas et al. could demonstrate a functional link between mutated *KRAS* and the activation of TP53 [129]. Along this line, we decided to scrutinize *KRAS* alterations and their putative interplay with *TP53* loss-of-function during MPM evolution.

Analysis of ten MPM studies revealed that *KRAS* and *TP53* mutations made up 2 and 18% of all mutated genes [74, 76, 80, 130-136]. However, detailed exploration of the TCGA PanCancer MPM dataset unveiled a higher number of patients carrying mutations in *KRAS* and *TP53*, considering mutations, CNA, mRNA and protein expression [80]. In total, 20% of the patients carried a *KRAS* alteration, while 12% displayed a mutation in *KRAS* alone and 8% in both, *KRAS* and *TP53* [90]. The MPM patients suffering *KRAS* mutations in general presented a tendency towards biphasic histology and thus worse survival. By unsupervised hierarchical clustering of gene expression data, the double mutant specimen formed an own cluster and showed higher aneuploidy and genome alteration indices. These findings indicate a molecular subclass of MPM in the TCGA dataset displaying alterations in *KRAS* alone or together with *TP53* [90].

To verify this subset of patients, we screened our cohort for mutations in *KRAS* codons 12, 13, and 61 as well as *TP53* CNA using ddPCR. Cell pellets and pleural effusions of 45 patients caused by benign medical conditions, LUAD, MPM, or other metastatic tumors were scrutinized [121, 137]. Out of 12 MPM samples we found 3 to be *KRAS* mutant and another 2 to be *KRAS*/*TP53* altered. To expand these data, we additionally tested two more cohorts of MPM inflicted MPE samples including 6 from Nantes, France and 17 from Istanbul, Turkey for alteration in these two genes [138, 139]. Here, we discovered 9 *KRAS* mutant and 3 *KRAS*/*TP53* double altered patients. Sensitive ddPCR revealed that the obtained KRAS mutations had a copy number of below 10% in most cases, which would be likely missed by other molecular tools due to their lower sensitivity, low read depth and/or too stringent detection thresholds. In summary, we detected standalone *KRAS* mutations in 33% and co-occurring *KRAS*/*TP53* alterations in 17% of all patients out of three different MPM cohorts [90]. These results suggest the existence of a molecular subgroup of MPM with *KRAS* and *TP53* alterations or mutated *KRAS* alone.

To this day suitable MPM models for functional studies such as cell lines and mouse models are limited and hard to obtain [140-143]. Surprisingly, single mutations in the most frequently altered genes in MPM such as *BAP1*, *NF2*, *CDKN2A*, *TP53*, or *TSC1* alone are not sufficient to induce MPM [144-147]. Thus, there has been no mouse model displaying the complex mutational landscape together with clinicopathologic signs of MPM, enabling functional validation of driver mutations.

For validation of mutated *KRAS* as a driver in MPM, wildtype (WT) and conditional *KRAS*$^{G12D}$ and/or *Trp*$^{f/f}$ mice received intrapleural injection of Adenovirus expressing CRE recombinase. Consequently, upon CRE recombination the mice carried the respective alterations in the pleural mesothelium, but not in the surrounding tissues [143, 148-150]. While WT, *Trp*$^{f/WT}$, and *Trp*$^{f/f}$ didn't show any disease, cachexia, pleural lesions, and reduced survival could be observed in *KRAS*$^{G12D}$ mice. Epithelioid MPM was diagnosed, and inflammatory cells were infiltrating the pleura, similar to the inflammation upon pleural asbestos exposure [151]. However, in *KRAS*$^{G12D}$;*Trp*$^{f/f}$ mice we found MPE, pleural tumors invading the adjacent tissues, distress, and shortened lifespan. The tumors could be identified as biphasic MPM and the MPE displayed numerous typical features of patients with advanced MPM [152, 153]. *KRAS*$^{G12D}$;*Trp*$^{f/WT}$ mice revealed an intermediate disease with biphasic MPM [90].

To ascertain that in these mice indeed suffered MPM and not LUAD, we performed immunostaining with widely used MPM and LUAD markers. Our mice showed high Wilms' tumor 1, calretinin, osteopontin, podoplanin, and mesothelin as well as moderate vimentin, and cytokeratin 5/6, but no surfactant protein C expression. Hence, *KRAS*$^{G12D}$ expressed in the mesothelium can cause biphasic MPM, and in co-occurrence with *Trp53* deletion, inflicts more aggressive biphasic MPM with MPE in mice. Trp53 loss alone was not sufficient to induce MPM.

Out of the *KRAS*$^{G12D}$;*Trp*$^{f/f}$ mice, we isolated 3 MPM cell lines, which displayed quick growth, elevated expression of Cdkn2a and Bap1, caused tumors bearing the initial alterations when injected in the flanks of mice, and generated the same disease upon pleural instillation [154]. Administration of the KRAS inhibitor deltarasin in a mouse model with intrapleurally injected MPM cell lines resulted in decreased cellularity and fewer and smaller effusions as compared to the untreated control [155]. RNAseq of these MPM cell lines identified several mutations in *Bap1*, which is the most commonly mutated gene in human MPM. In comparison with normal mesothelial cells from the pleura, the MPM cells showed transcriptomic upregulation of well-known MPM

markers and novel potential mesothelioma markers. Furthermore, a publicly available MPM signature of 113 patients was enriched in our isolated MPM cell lines [90, 156]. In summary, the proposed mice and tumor cell lines derived thereof present a valid *KRAS*/*TP53*-driven MPM model with high similarity to the human disease and potential use in transplantation and drug screening of MPM.

Taken together, these findings corroborate the presence of a subset in MPM patients which is driven by oncogenic KRAS, which has been underestimated so far. Due to its heterozygous nature and thus low allelic frequency, mutations in *KRAS* may get lost during sampling and/or sequencing similar to other subclonal alterations in LUAD [118, 119, 157]. Additionally, most sequencing techniques show lower sensitivity and stringent detection thresholds resulting in the omission of many alterations. Therefore, very sensitive detection methods such as ddPCR or maximal depth sequencing should be utilized to identify this specific subgroup of MPM patients.

*Trp53* mutations alone could not induce mesothelioma but contributed to *KRAS* driven MPM carcinogenesis and a biphasic histologic subtype. Likewise, *Trp53* promoted MPM evolution of *Nf2* or *Tsc1* driven MPM in other studies [144, 145]. Hence, *Trp53* loss-of-function mutations seem to cooperate with oncogenes driving MPM progression, metastasis, and poor survival. Further investigations of drugs targeting TP53 may advance personalized therapy for a large group of MPM patients.

# Paper I

Reproduced with permission of the EMBO Press: EMBO Molecular Medicine 14 (2) e13631; doi: 10.15252/emmm.202013631 Published 13 December 2021

*Article*

SOURCE DATA | TRANSPARENT PROCESS | OPEN ACCESS

EMBO Molecular Medicine

# KRAS signaling in malignant pleural mesothelioma

Antonia Marazioti[1,2,†], Anthi C Krontira[2,†], Sabine J Behrend[1,3,†], Georgia A Giotopoulou[1,2,3,†], Giannoula Ntaliarda[2,†], Christophe Blanquart[4], Hasan Bayram[5,6], Marianthi Iliopoulou[2], Malamati Vreka[1,2,3], Lilith Trassl[1,3], Mario A A Pepe[1,3], Caroline M Hackl[1,3], Laura V Klotz[1,3], Stefanie A I Weiss[1,3], Ina Koch[3,7], Michael Lindner[3,7], Rudolph A Hatz[3,7], Juergen Behr[3,8], Darcy E Wagner[1,3,9], Helen Papadaki[10], Sophia G Antimisiaris[11,12], Didier Jean[13], Sophie Deshayes[4], Marc Grégoire[4], Özgecan Kayalar[6], Deniz Mortazavi[6], Şükrü Dilege[14], Serhan Tanju[14], Suat Erus[14], Ömer Yavuz[14], Pınar Bulutay[15], Pınar Fırat[15], Ioannis Psallidas[2], Magda Spella[2], Ioanna Giopanou[2], Ioannis Lilis[2], Anne-Sophie Lamort[1,3,‡] & Georgios T Stathopoulos[1,2,3,*,‡]

## Abstract

**Malignant pleural mesothelioma (MPM) arises from mesothelial cells lining the pleural cavity of asbestos-exposed individuals and rapidly leads to death. MPM harbors loss-of-function mutations in *BAP1*, *NF2*, *CDKN2A*, and *TP53*, but isolated deletion of these genes alone in mice does not cause MPM and mouse models of the disease are sparse. Here, we show that a proportion of human MPM harbor point mutations, copy number alterations, and over-expression of *KRAS* with or without *TP53* changes. These are likely pathogenic, since ectopic expression of mutant *KRAS*$^{G12D}$ in the pleural mesothelium of conditional mice causes epithelioid MPM and cooperates with *TP53* deletion to drive a more aggressive disease form with biphasic features and pleural effusions. Murine MPM cell lines derived from these tumors carry the initiating *KRAS*$^{G12D}$ lesions, secondary *Bap1* alterations, and human MPM-like gene expression profiles. Moreover, they are transplantable and actionable by KRAS inhibition. Our results indicate that *KRAS* alterations alone or in accomplice with *TP53* alterations likely play an important and underestimated role in a proportion of patients with MPM, which warrants further exploration.**

**Keywords** asbestos; BAP1; KRAS; NF2; TP53
**Subject Categories** Cancer; Respiratory System
**DOI** 10.15252/emmm.202013631 | Received 22 October 2020 | Revised 28 October 2021 | Accepted 15 November 2021
**EMBO Mol Med (2021) e13631**

## Introduction

Malignant mesothelioma annually kills up to forty persons per million population worldwide (Liu *et al*, 2017; Carbone *et al*, 2019). It most commonly arises from the mesothelium of the pleural cavities that line the lungs (visceral pleura) and the interior chest wall (parietal pleura) and only occasionally from the peritoneal mesothelium (Bibby *et al*, 2016; Mutti *et al*, 2018). Human malignant pleural mesothelioma (MPM) is mainly caused by inhaled asbestos, which caused 145,235 deaths in 1990 increasing by 51% to 218,827 deaths in 2016, most of them in high-income countries (GBD 2016 Occupational Carcinogens Collaborators, 2020). However, other bioactive materials such as nanofibers can also cause mesothelioma in rodents and possibly in humans (Ryman-Rasmussen *et al*, 2009;

1 Comprehensive Pneumology Center (CPC) and Institute for Lung Biology and Disease (iLBD), Helmholtz Center Munich-German Research Center for Environmental Health (HMGU) and Ludwig-Maximilian-University (LMU) Munich, Munich, Germany
2 Laboratory for Molecular Respiratory Carcinogenesis, Department of Physiology, Faculty of Medicine, University of Patras, Rio, Greece
3 German Center for Lung Research (DZL), Gießen, Germany
4 Université de Nantes, CNRS, INSERM, CRCINA, Nantes, France
5 Department of Pulmonary Medicine, Koc University School of Medicine, Istanbul, Turkey
6 Koc University Research Center for Translational Medicine (KUTTAM), Koc University School of Medicine, Istanbul, Turkey
7 Center for Thoracic Surgery Munich, Ludwig-Maximilian-University (LMU) Munich and Asklepios Medical Center, Gauting, Germany
8 Department of Medicine V, University Hospital, Ludwig-Maximilian-University (LMU) Munich, Munich, Germany
9 Lung Bioengineering and Regeneration, Department of Experimental Medical Sciences, Lund Stem Cell Center, Wallenberg Molecular Medicine Center, Faculty of Medicine, Lund University, Lund, Sweden
10 Department of Anatomy, Faculty of Medicine, University of Patras, Rio, Greece
11 Laboratory for Pharmaceutical Technology, Department of Pharmacy, School of Health Sciences, University of Patras, Rio, Greece
12 Foundation for Research and Technology Hellas, Institute of Chemical Engineering, FORTH/ICE-HT, Rio, Greece
13 Centre de Recherche des Cordeliers, INSERM, Sorbonne Université, Université de Paris, Functional Genomics of Solid Tumors, Paris, France
14 Department of Thoracic Surgery, Koc University School of Medicine, Istanbul, Turkey
15 Department of Pathology, Koc University School of Medicine, Istanbul, Turkey
*Corresponding author. Tel: +49 (89) 3187 1194; Fax: +49 (89) 3187 4661; E-mail: stathopoulos@helmholtz-muenchen.de
†These authors contributed equally to this work as first authors
‡These authors contributed equally to this work as senior authors

Nagai *et al*, 2011). MPM manifests with or without a malignant pleural effusion (MPE), that is, exudative fluid accumulation that causes chest pain and dyspnea, and is histologically classified into epithelioid, sarcomatoid, or biphasic subtypes (Scherpereel *et al*, 2010; Galateau-Salle *et al*, 2016; Thomas *et al*, 2017; Paajanen *et al*, 2018). The disease progresses relentlessly despite contemporary combination therapies, with a median survival of mere 9–18 months (Zalcman *et al*, 2016; Yap *et al*, 2017; Scherpereel *et al*, 2018; Courtiol *et al*, 2019). The clinicopathologic manifestation of MPM at diagnosis impacts patient survival, with advanced stage, sarcomatoid histologic subtype, poor physical performance status, elevated numbers of peripheral blood leucocytes, male sex, uncontrolled pleural effusion, and other factors portending dismal prognosis (Fennell *et al*, 2005; Tsao *et al*, 2009; Pass *et al*, 2016; Rusch *et al*,

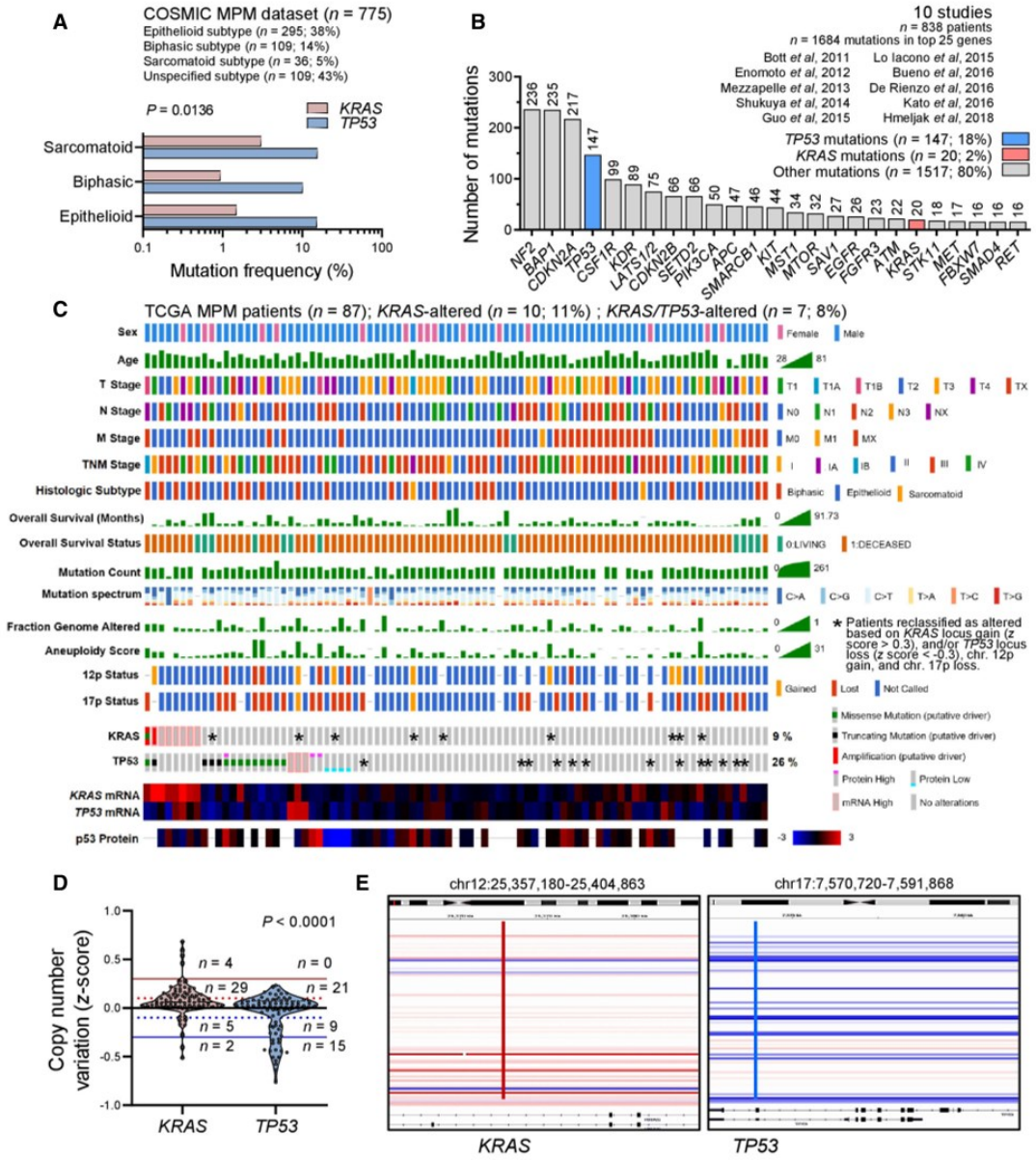


**Figure 1.**

**Figure 1. *KRAS* alterations in human MPM from published datasets and the cancer genome atlas (TCGA) pan-cancer MPM cohort.**

A *KRAS* and *TP53* mutation frequencies in MPM from the catalogue of somatic mutations in cancer (COSMIC) stratified by histologic subtype ($n$ = 775 patients).

B Top 25 mutated genes from 10 molecular studies of human MPM ($n$ = 838 patients).

C–E *KRAS* and *TP53* alterations in the cancer genome atlas (TCGA) pan-cancer MPM dataset ($n$ = 86 patients). Shown are clinical and molecular data plot with alteration frequencies (C) and patients reclassified as *KRAS*- or *TP53*-altered (asterisks), copy number variation data summary (D), and segments of the *KRAS* and *TP53* loci (E).

Data information: In (A), data are presented as cumulative percentages of patients tested mutant respective to patients tested for every gene. *P*, overall probability, two-way ANOVA. In (B), data are presented as cumulative numbers ($n$; numbers above bars) and percentages (%) of patients with *KRAS* (red bar), *TP53* (blue bar), and other (gray bars) mutations. In (C), each column represents one patient and each row one clinical or molecular feature. Asterisks indicate *KRAS* and *TP53* alterations not identified by the TCGA, but reclassified as altered in this study due to 12p gain, 17p loss, *KRAS* locus gain ($z > 0.3$), and/or *TP53* locus loss ($z < -0.3$). In (D), data are presented as raw data points (circles), rotated kernel density distributions (violins), and patient numbers ($n$) between thresholds of normal (solid black line at $z = 0$), low amplification (dotted red line at $z = 0.1$), low loss (dotted blue line at $z = -0.1$), high amplification (solid red line at $z = 0.3$), and deep loss (solid blue line at $z = -0.3$). *P*, probability, paired Wilcoxon rank sum test. In (E), *KRAS* (red line) and *TP53* (blue line) loci segments of all 87 patients are shown. Each horizontal segment represents one patient. White and shades of red and blue indicate no change and magnitude of gain and loss, respectively.
Source data are available online for this figure.

2016; Cheah *et al*, 2017; Thomas *et al*, 2017; Kindler *et al*, 2018; Hassan *et al*, 2019).

Multiple comprehensive analyses of MPM genomes identified a mosaic mutational landscape characterized by widespread loss-of-function of tumor suppressor genes (*BAP1*, *NF2*, *CDKN2A*, *TP53*, *TSC1*, etc), sporadic gain-of-function of proto-oncogenes (*PIK3CA*, *EGFR*, *KRAS*, *NRAS*, *HRAS*, *BRAF*, etc), and inconclusive addiction/exclusion patterns thereof (Bott *et al*, 2011; Enomoto *et al*, 2012; Mezzapelle *et al*, 2013; Shukuya *et al*; 2014; Guo *et al*, 2015; Lo Iacono *et al*, 2015; Bueno *et al*, 2016; De Rienzo *et al*, 2016; Kato *et al*, 2016; Hmeljak *et al*, 2018). Interestingly, KRAS proto-oncogene GTPase (*KRAS*) alterations were detected more frequently using targeted compared with massive parallel sequencing approaches by the studies above. In addition, *NF2* mutations that cause persistent KRAS signaling (Tikoo *et al*, 1994), as well as *BAP1* and *CDKN2A* mutations that are functionally related with *TP53* loss-of-function (Stott *et al*, 1998; Arizti *et al*, 2000; Bi *et al*, 2016), are very common in MPM. *KRAS* mutations have also been shown to activate the *TP53* cell cycle checkpoint (Matallanas *et al*, 2011). In addition to clinicopathologic presentation, MPM mutations also impact prognosis, with *TP53* and *CDKN2A* loss-of-function occurring more frequently in non-epithelioid MPM and portending poor survival (Bott *et al*, 2011; Yap *et al*, 2017).

There is an unmet clinical need for mouse models that recapitulate the mutation spectrum and clinicopathologic manifestations of human MPM. In this regard, MPM cell lines for transplantable models, asbestos-induced mouse models, and genetic models of the disease are characterized by scarcity, limited availability, and significant difficulty of implementation (Ikediobi *et al*, 2006; Fridlender *et al*, 2009; Forbes *et al*, 2015; Agalioti *et al*, 2017). Interestingly, standalone mesothelial loss-of-function of *BAP1*, *NF2*, *CDKN2A*, *TP53*, and *TSC1* is not sufficient to cause MPM in mice, rendering the drivers of the disease resistant to functional validation (Jongsma *et al*, 2008; Guo *et al*, 2014; Menges *et al*, 2014; Xu *et al*, 2014; Kukuyan *et al*, 2019). Moreover, faithful models of MPM are urgently needed, as most existing studies have focused on the rare

**Figure 2. KRAS pathway activation in MPM from the cancer genome atlas (TCGA) pan-cancer MPM dataset.**

A–F Molecular and clinical features of the cancer genome atlas (TCGA) pan-cancer MPM patients ($n$ = 87) stratified by the presence of *KRAS* standalone ($n$ = 10) and combined *KRAS*/*TP53* ($n$ = 7) alterations. Shown are unsupervised hierarchical clustering of $n$ = 86 patients (gene expression data were not available for one patient) by 40 genes significantly overexpressed in *KRAS*/*TP53*-altered over *KRAS*-altered over *KRAS*/*TP53*-normal patients (A) and data summaries of mononucleotide change signatures (B), of indices of genomic instability and mutation burden (C), of clinical features and *KRAS*/*TP53*/*NF2* co-mutation frequency (D, E), and of overall survival (F).

G KRAS/TP53 pathway adapted from Matallanas *et al* (2011) and Tikoo *et al* (1994). Color-coded genes were identified by TCGA and PANTHER pathway analyses.

H, I PANTHER and Reactome KRAS and TP53 pathways significantly altered in the cancer genome atlas (TCGA) pan-cancer MPM patients. Shown are volcano plot of fold-enrichment versus $-\log_{10}$(probability) (H), and data summary of fold-enrichment of KRAS and TP53 versus all other pathways with fold-enrichment > 0.5 (I).

Data information: In (A), data are presented as heatmap of 40 differentially expressed genes (rows) in 86 individual patients (columns), color code of unsupervised hierarchical clusters, *KRAS*/*TP53* status, and heatmap (legend), and probabilities (*P*) for enrichment of *KRAS*- and *KRAS*/*TP53*-altered patients in cluster 1. The scale bar represents the color-coded $z$-scores. In (B), data are presented as heatmap of six different possible mononucleotide changes (rows) in patients grouped by *KRAS*/*TP53* status (columns) and color code of mean mutation number (legend). ****, FDR $q < 2 \times 10^{-7}$ compared with all other mononucleotide changes, 2-way ANOVA with Benjamini, Krieger, and Yekutieli two-stage linear step-up procedure. In (C) and (I), data are presented as raw data points (circles), rotated kernel density distributions (violins), medians (solid lines), and quartiles (dotted lines). *P*, overall probability, Kruskal–Wallis test. (C): * and **: $P < 0.05$ and $P < 0.01$, respectively, compared with *KRAS*/*TP53*-normal patients, Dunn's post-tests. (I): ** and ****: $P < 0.01$ and $P < 0.0001$, respectively, compared with other pathways, Dunn's post-tests. In (D) and (E), data are presented as patient numbers ($n$) and overall probability (*P*) by $\chi^2$ or Kruskal–Wallis tests (D) or hypergeometric test for enrichment of *KRAS* mutations in *TP53*-altered or biphasic MPM (E). In (F), data are presented as sample size ($n$), Kaplan–Meier survival estimates (lines), censored observations (line marks), log-rank *P* value, and hazard ratio (HR) with 95% confidence interval (95% CI). In (H), data are presented as color-coded individual pathways (circles), threshold of significance (horizontal dotted line), no enrichment baseline reference (vertical dotted line), and selected pathway names and codes. P and R initials in pathway codes denote PANTHER and Reactome pathways, respectively. $n$, sample size; FDR $q$, probability, false discovery rate; ΔGE, differential gene expression.
Source data are available online for this figure.

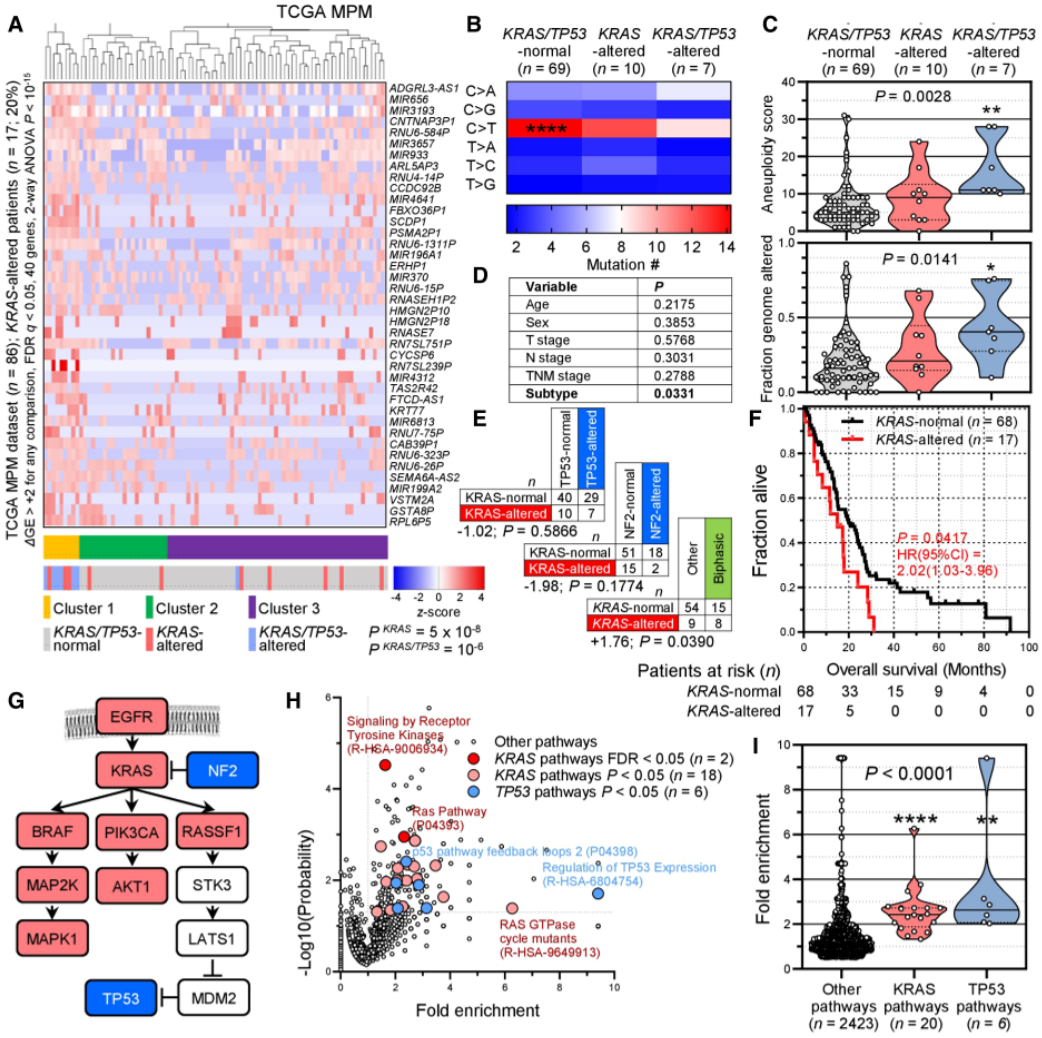


**Figure 2.**

peritoneal disease and only one elegant study targeted *NF2/CDKN2A/TP53* deletions to the pleural mesothelium (Jongsma *et al*, 2008). Such mouse models would represent different molecular subtypes of MPM, would have high penetrance, and would also be specific for MPM with or without MPE development.

Based on our previous observation of a $Kras^{G12C}$ mutation (*Kras*, *Mus musculus* Kirsten rat sarcoma viral oncogene homolog) in an asbestos-induced murine MPM cell line (Agalioti *et al*, 2017; Marazioti *et al*, 2018), on published work that showed RAS pathway activation in MPM (Patel *et al*, 2007), and on the functional interconnection between mutant *KRAS* and *TP53* signaling (Matallanas *et al*, 2011), we hypothesized that *KRAS* alterations are involved in MPM development, alone or in accomplice with *TP53* alterations. Indeed, here we query the TCGA MPM dataset and employ sensitive methods in our own clinical cohorts to discover *KRAS* and *TP53* alterations in a subset of patients with MPM. We further show that targeting oncogenic $KRAS^{G12D}$ alone to the murine pleural mesothelium causes MPM and, when combined with *Trp53* deletion, triggers aggressive MPM with MPE. Murine MPM is shown to carry the initiating $KRAS^{G12D}$ mutations, to harbor *Bap1* inactivating mutations, to be transmissible to naïve mice, and to resemble the molecular signatures of human MPM. Hence, *KRAS* mutations are implicated in MPM pathobiology, the contributions of *TP53* in shaping the disease's manifestations are described, and new mouse models are provided for the study of the biology and therapy of a molecular subclass of MPM that is driven by *KRAS* signaling.

## Results

### *KRAS* and *TP53* alterations in human MPM

In MPM from the catalogue of somatic mutations in cancer (COSMIC; Forbes *et al*, 2015), *KRAS* and *TP53* mutation frequencies of 1–3% and 10–20%, respectively, were evident (Fig 1A; dataset available at https://cancer.sanger.ac.uk/cosmic/browse/tissue?wgs=off&sn=pleura&ss=all&hn=mesothelioma&sh=&in=t&src=tissue&all_data=n). *KRAS* and *TP53* mutations comprised, respectively, 2 and 18% of all mutated genes in a dataset composed of 10 large MPM studies (Bott *et al*, 2011; Enomoto *et al*, 2012; Mezzapelle *et al*, 2013; Shukuya *et al*, 2014; Guo *et al*, 2015; Lo Iacono *et al*, 2015; Bueno *et al*, 2016; De Rienzo *et al*, 2016; Kato *et al*, 2016; Hmeljak *et al*, 2018) (Fig 1B). The aforementioned analysis consisted of manual curation of the main and supplementary data, while the latter study, the cancer genome atlas (TCGA) pan-cancer MPM dataset ($n$ = 86 patients; Hmeljak *et al*, 2018) available at https://www.cbioportal.org/study/summary?id=meso_tcga_pan_can_atlas_2018 (Cerami *et al*, 2012), was analyzed in detail, via a systematic query of mutations, copy number alterations, and mRNA and protein expression of *KRAS* and *TP53*. According to TCGA criteria, eight patients showed alterations in *KRAS* two of which had dual *KRAS*/*TP53* changes. However, when copy number alterations (CNA) at the *KRAS*12p12.1 (position chr12:25,357,180–25,404,863) and *TP53* 17p13.1 (position chr17:7,570,720–7,591,868) loci were scrutinized using integrative genomics viewer (Robinson *et al*, 2011), additional high *KRAS* gains were discovered in nine and deep *TP53* losses in 13 patients, with five patients harboring changes in both genes (Fig 1C–E). For this, *KRAS* locus gain ($z > 0.3$) and/or *TP53* locus loss ($z < -0.3$), as well as chromosome 12p gains and 17p losses, were taken into account (Smith & Sheltzer, 2018). Hence, a *KRAS* alteration alone was determined in $n$ = 10 patients (12%) and a combined *KRAS*/*TP53* alteration in $n$ = 7 (8%), for a total *KRAS* alteration rate of 20%.

We subsequently examined the transcriptomes of TCGA MPMs (available at https://xenabrowser.net/datapages/?dataset=TCGA-MESO.htseq_fpkm-uq.tsv&host=https%3A%2F%2Fgdc.xenahubs.net&removeHub=https%3A%2F%2Fxena.treehouse.gi.ucsc.edu%3A443) stratified by the presence of a *KRAS* alteration alone ($n$ = 10), a combined *KRAS*/*TP53* alteration ($n$ = 7), or none of the above ($n$ = 69). Forty genes were biologically and statistically significantly overrepresented in *KRAS*/*TP53*-altered over *KRAS*-altered over normal patients, which were able to cluster patients by genetic alteration in an unsupervised hierarchical fashion (Fig 2A). *KRAS*/*TP53*-altered patients showed loss of a C>T mononucleotide signature that preponderated in *KRAS*/*TP53*-normal patients and displayed higher aneuploidy and genome alteration indices (Figs 2B and C). *KRAS* and *TP53* alterations were co-occurring at a rate expected by chance, while *KRAS*-altered patients displayed a non-significant repulsion of *NF2* mutations, a statistically significant preponderance of biphasic histology, and significantly worse prognosis (Figs 2D–F). Interestingly, when all mutated genes from this cohort were entered into the Protein Analysis Through Evolutionary Relationships System (PANTHER; http://www.pantherdb.org/), multiple KRAS and TP53 signaling pathways were biologically and statistically significantly enriched in MPM, which, together with the *KRAS-NF2* repulsion described above, aligned along a biological KRAS-TP53 pathway proposed elsewhere (Tikoo *et al*, 1994; Matallanas *et al*, 2011) (Fig 2G–I). Our results were concordant with the TCGA pan-cancer pathway analysis that reported 9 and 21% alteration frequencies of the RTK/RAS and p53 pathways in MPM (Sanchez-Vega *et al*, 2018). Hence, we describe a molecular subclass of MPM patients in the TCGA dataset that involves ~ 20% of patients, which harbor *KRAS* gain-of-function with or without *TP53* loss-of-function. This molecular MPM subset features KRAS pathway activation, different mutation spectra, gene expression profiles, histology, and survival compared to other MPMs.

To further test this, we interrogated *KRAS* and *TP53* in our MPM patients, whose clinical characteristics are given in Appendix Table S1. We employed digital droplet polymerase chain reaction (ddPCR) in order to detect *KRAS* codon 12/13 and 61 mutations, as well as *TP53* CNA in pleural fluid and cell pellets of 45 patients with pleural effusions from our cohorts in Munich, Germany (Klotz *et al*, 2019a, 2019b). The effusions were caused

**Figure 3. *KRAS* and *TP53* alterations in human MPM from Germany and human MPM cell lines from France.**

A–D Pleural fluid cell pellets and supernatants from 45 patients (called ASK #) with pleural effusion from Munich, Germany (Klotz *et al*, 2019a, 2019b), were subjected to digital droplet polymerase chain reaction (ddPCR) for the detection of mutant ($^{MUT}$) copies of *KRAS* codon 12/13 ($KRAS^{G12/13}$) and *KRAS* codon 61 ($KRAS^{Q61}$), as well as copies of *TP53* and *TERT*. Diagnoses were benign pleural effusion ($n$ = 5), lung adenocarcinoma (LUAD; $n$ = 16), MPM ($n$ = 12), and other extrathoracic cancers ($n$ = 12). The assays were designed for detection of down to 1:20,000 copies using EKVX ($KRAS^{WT}TP53^{G610T}$), A549 ($KRAS^{G12S}TP53^{WT}$), NCI-H460 ($KRAS^{Q61H}TP53^{WT}$), NCI-H3122 ($KRAS^{WT}TP53^{E285V}$), and NCI-H3255 ($KRAS^{WT}TP53^{G560-1A}$) human LUAD cells as controls. Shown are individual patient (*KRAS* plot) and individual sample (*TP53* plot) allelic frequencies with color code and limits of normal *TP53* allelic frequency as vertical dashed lines in the *TP53* plot (A), representative gated dotplots of codon 12/13 *KRAS* ddPCR (B) and *TP53*/*TERT* (C), and results summary table (D). Any number of *KRAS*-mutant droplets detected in any sample (*KRAS* plot in A) and any patient that failed to achieve normal *TP53* ploidy by any sample (*TP53* plot in A) was deemed altered.

E–G Results summary (E), representative *KRAS* CNA segments (F), and data summary of individual cell line CNA $z$-score (G) from Affymetrix CytoScanHD Arrays of 33 primary MPM cell lines (called MESO #) from Nantes, France (GEO dataset GSE134349). Red lines denote the KRAS locus on chromosome 12p12.1.

H Data summary of mutant allelic frequency of *KRAS* compared with *NF2* and *BAP1* in all mutated samples from (A–G).

Data information: In (A), data are presented as data summary of the highest mutant copy percentage detected per individual sample (*KRAS* plot) or of all individual samples assessed (*TP53* plot). In (D), data are presented as number of patients ($n$). $P$, probability, hypergeometric test for enrichment of *KRAS* mutations in MPM versus other tumors. In (E), data are presented as individual cell lines (columns), genes (rows), legend, and number of patients ($n$ in table). $P$, probability, hypergeometric test for enrichment of *KRAS* mutations in *TP53*-mutant MPM. In (G), data are presented as raw data points (circles), rotated kernel density distribution (violins), and cell line numbers ($n$) outside thresholds of amplification (dotted red line at 2.3) and loss (solid blue line at 1.7). $P$, probability, paired Wilcoxon rank sum test. In (H), data are presented as raw data points (circles), rotated kernel density distributions (violins), and medians (lines). $P$, overall probability, one-way ANOVA. * and **: $P < 0.05$ and $P < 0.01$, respectively, compared with *KRAS*, Tukey's post-test.
Source data are available online for this figure.

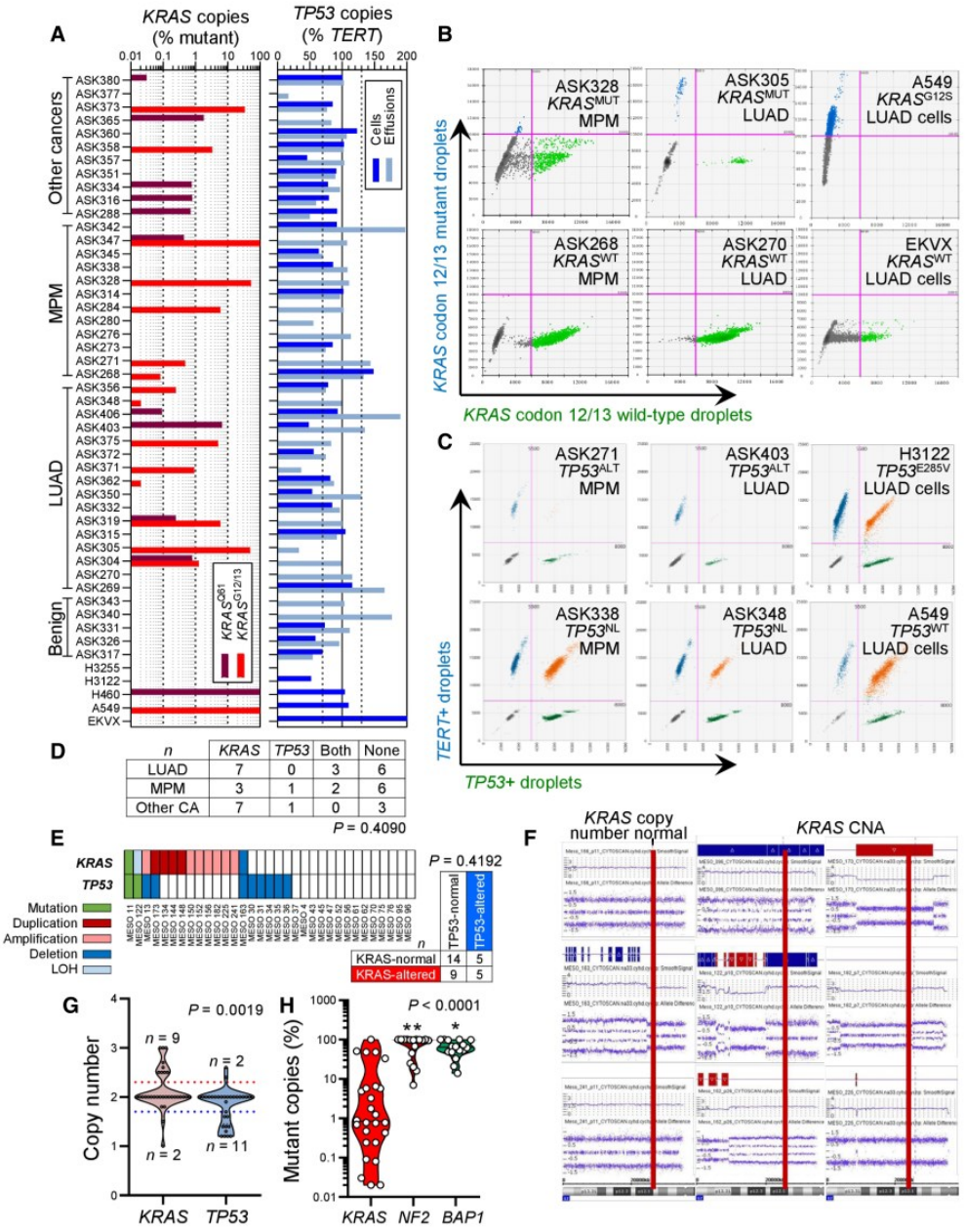


**Figure 3.**

from benign etiologies ($n$ = 5), MPM ($n$ = 12), metastatic lung adenocarcinoma (LUAD; $n$ = 16), or metastatic other bodily tumors ($n$ = 12). The assays were designed for the detection of down to 1:20,000 mutant ($^{MUT}$) or wild-type ($^{WT}$) copies. We detected standalone *KRAS* mutations and combined *KRAS*/*TP53* alterations in three and two of our 12 patients with MPM, respectively (Fig 3A–C). *KRAS* and *TP53* alterations co-occurred at a rate expected by chance (Fig 3D). We next used sensitive Affymetrix CytoScanHD

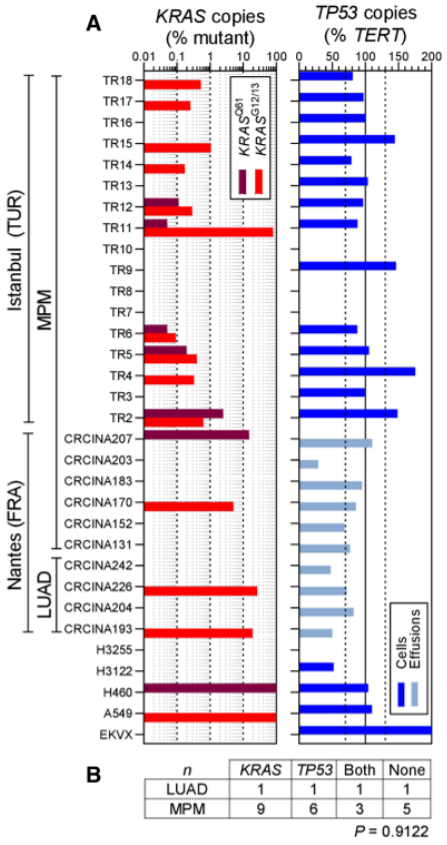


**Figure 4. *KRAS* and *TP53* alterations in MPM patients from France and Turkey.**

A, B Pleural fluid cell pellets and supernatants from 10 patients (called CRCINA #) with pleural effusion from Nantes, France (Gueugnon *et al*, 2011; Smeele *et al*, 2018), and pleural tumor samples from 17 patients (called TR#) with MPM from Istanbul, Turkey, were subjected to digital droplet polymerase chain reaction (ddPCR) for the detection of mutant ($^{MUT}$) copies of *KRAS* codon 12/13 ($KRAS^{G12/13}$) and *KRAS* codon 61 ($KRAS^{Q61}$), as well as copies of *TP53* and *TERT*. Diagnoses were lung adenocarcinoma (LUAD; $n$ = 4) and MPM ($n$ = 23). The assays were designed for detection of down to 1:20,000 copies using EKVX ($KRAS^{WT}TP53^{G610T}$), A549 ($KRAS^{G12S}TP53^{WT}$), NCI-H460 ($KRAS^{Q61H}TP53^{WT}$), NCI-H3122 ($KRAS^{WT}TP53^{E285V}$), and NCI-H3255 ($KRAS^{WT}TP53^{G560-1A}$) human LUAD cells as controls. Shown are individual patient (*KRAS* plot) and individual sample (*TP53* plot) allelic frequencies with color code and limits of normal *TP53* allelic frequency as vertical dashed lines in the *TP53* plot (A) and results summary table (B). Any number of *KRAS*-mutant droplets detected in any sample (*KRAS* plot in A) and any patient that failed to achieve normal *TP53* ploidy by any sample (*TP53* plot in A) was deemed altered.

Data information: In (A), data are presented as data summary of the highest mutant copy percentage detected per individual sample (*KRAS* plot) or of all individual samples assessed (*TP53* plot). In (B), data are presented as number of patients ($n$). $P$, probability, $\chi^2$ test.
Source data are available online for this figure.

Arrays utilizing 2.67 million markers and targeted next-generation sequencing to identify *KRAS* and *TP53* alterations in a cohort of 33 primary MPM cell lines from Nantes, France (GEO dataset GSE134349; Gueugnon *et al*, 2011; Data ref: Blanquart *et al*, 2019; Delaunay *et al*, 2020; Quetel *et al*, 2020) The clinical characteristics of the cell line donors are given in Appendix Table S2. We detected standalone *KRAS* and combined *KRAS*/*TP53* alterations in nine and five cell lines, respectively, and *KRAS* and *TP53* alterations again co-occurred at a rate expected by chance (Fig 3E). In addition, the *KRAS* and *TP53* loci were statistically significantly amplified and deleted, respectively, across all cell lines irrespective of genotype (Fig 3F and G). Interestingly, 80% of the samples with $KRAS^{MUT}$ copies from both studies displayed low mutant copy numbers (< 10%) that would be likely missed by other techniques with lower read depths or stringent detection thresholds (Fig 3H). We also tested a patient with MPM from the Malignancy of Pleural Effusions in the Emergency Department (MAPED; ClinicalTrials.gov # NCT03319472) Study (preprint: Marazioti *et al*, 2021) for *KRAS* and *TP53* status by Sanger sequencing, RT–PCR, and qPCR. We found four different KRAS point mutations in this patient, as well as discrepant *TP53* expression levels by RT–PCR and qPCR, strongly indicative of a *TP53* mutation (Fig EV1). To obtain definitive validation, we finally examined by ddPCR for *KRAS* codon 12/13 and 61 mutations, as well as *TP53* CNA, additional six MPM-associated MPE samples from Nantes (Gueugnon *et al*, 2011; Smeele *et al*, 2018) and 17 MPM tumor samples from Istanbul, Turkey (patients' clinical characteristics are given in Appendix Table S3). Indeed, we found that nine patients had standalone KRAS mutations, whereas another three had combined *KRAS*/*TP53* alterations (Fig 4A and B). Taken together, we examined 36 human tumor/effusion samples from four countries to find standalone *KRAS* alterations in 12 (33%) and combined *KRAS*/*TP53* alterations in 6 (17%) patients. These results indicate that a molecular subset of MPM that is driven by *KRAS* with/without *TP53* alterations indeed exists outside the TCGA cohort.

### MPM in mice expressing mesothelial-targeted $KRAS^{G12D}$

To functionally validate *KRAS* mutations in MPM, we targeted transgenes to mesothelial surfaces using type 5 adenoviral vectors (Ad). For this, *mT*/*mG* CRE-reporter mice that switch from somatic cell membranous tomato (mT) to green fluorescent protein (mG) expression upon *Cre*-mediated recombination (Muzumdar *et al*, 2007) received $5 \times 10^8$ plaque-forming units (PFU) intrapleural Ad encoding *Melanotus* luciferase (Ad-*Luc*) or *Cre* recombinase (Ad-*Cre*) followed by serial bioluminescence imaging. Ad-*Luc*-treated mice developed intense bilateral chest light emission (mice lack mediastinal separations; Stathopoulos *et al*, 2006) that peaked at 4–7 and subsided by 14 days post-injection (Fig EV2A). At this time point, when transient Ad-*Luc* expression ceased and therefore maximal Ad-*Cre*-mediated recombination was achieved, Ad-*Cre*-treated mice displayed widespread recombination of the pleural mesothelium even in contralateral pleural fissures, but not of the lungs, chest wall, or pleural immune cells (Fig EV2B–E). Similar results were obtained from intraperitoneal $5 \times 10^8$ PFU Ad-*Cre*-treated *mT*/*mG* mice after 2 weeks (Fig EV2F). Importantly, Ad-*Cre* did not cause inflammation in wild-type (*Wt*) mice, as evident by imaging and cellular analyses of luminescent bone marrow chimeras used as real-time myeloid tracers

(Cao *et al*, 2004; Giannou *et al*, 2015; Agalioti *et al*, 2017; Fig EV3). These results show that intraserosal Ad-*Cre* treatment efficiently and specifically recombines mesothelial surfaces *in vivo*.

To test whether oncogenic *KRAS* can cause MPM, *Wt* mice and mice carrying conditional $KRAS^{G12D}$ and/or *Trp53f/f* alleles expressed or deleted, respectively, upon *Cre*-mediated recombination (Marino *et al*, 2000; Jackson *et al*, 2001; Meylan *et al*, 2009) received $5 \times 10^8$ PFU intrapleural Ad-*Cre* and were longitudinally followed and sampled (Fig 5A–F). *Wt*, *Trp53f/Wt*, and *Trp53f/f* mice survived up to 16 months post-Ad without clinical or pathologic disease manifestations (median survival undefined). In contrast, $KRAS^{G12D}$ mice developed cachexia and succumbed by 6–12 months post-injection (median [95% CI] survival = 339 [285–379] days; $P = 0.005$ compared with controls, log-rank test). At necropsy, no pleural fluid or inflammatory cell accumulation was evident, but diffuse visceral and parietal pleural nodular and peel-like lesions were found in all mice. These lesions expressed proliferating cell nuclear antigen (PCNA) unlike the normal pleura and were diagnosed by a board-certified pathologist as epithelioid MPM (Fig 5G). In addition, chimeric $KRAS^{G12D}$ recipients adoptively transplanted with luminescent bone marrow revealed an early pleural inflammatory infiltrate composed of $CD11b^+Gr1^+$ myeloid cells at

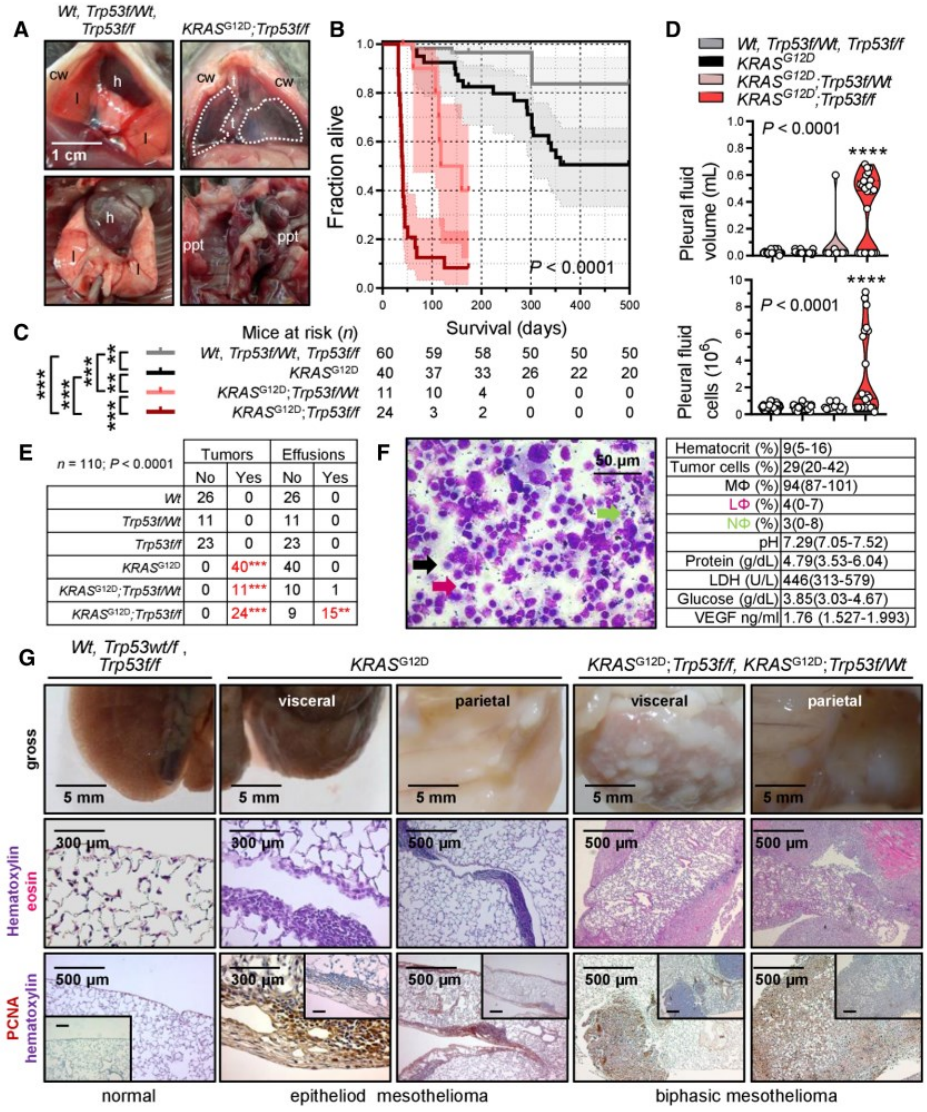


**Figure 5.**

**Figure 5. Human-like malignant pleural mesotheliomas and effusions of mice with pleural mesothelial-targeted oncogenic *KRAS*$^{G12D}$ and/or *Trp53* deletion.**

Wild-type (*Wt*), *KRAS*$^{G12D}$, and *Trp53f/f* mice (all *C57BL/6*) were intercrossed and all possible offspring genotypes received 5 × 10$^8$ PFU intrapleural Ad-*Cre* (*n* is given in survival table in [C]).

A Representative photographs of the thorax before (top) and after (bottom) chest opening (t, tumors; l, lungs; cw, chest wall; h, heart; dashed lines, effusion; ppt, parietal pleural tumors).
B Kaplan–Meier survival plot.
C Survival table.
D Data summary of pleural effusion volume and nucleated cells (*n* is given in table in [C]).
E Incidence of pleural tumors and effusions.
F Representative May–Gruenwald–Giemsa-stained pleural fluid cytocentrifugal specimen from a *KRAS*$^{G12D}$;*Trp53f/f* mouse showing macrophages (MΦ, black arrow), lymphocytes (LΦ, purple arrow), and neutrophils (NΦ, green arrow) and summary of cellular and biochemical features of effusions of *KRAS*$^{G12D}$;*Trp53f/f* mice (*n* = 10).
G Gross macroscopic and microscopic images of visceral and parietal tumors stained with hematoxylin and eosin or PCNA (*n* is given in table in [E]).

Data information: In (B) and (C), data are presented as Kaplan–Meier survival estimates (lines), censored observations (line marks) 95% confidence interval (shaded areas) and number of mice at risk. *P*, overall probability, log-rank test. ** and ***: $P < 0.01$ and $P < 0.001$, respectively, for the comparisons indicated, log-rank test. In (D), data are presented as raw data points (circles), rotated kernel density distribution (violins), and medians (lines). *P*, overall probability, one-way ANOVA. ****: $P < 0.0001$, for comparison with all other groups, Bonferroni post-tests. In (E), data are presented as number of mice (*n*). *P*, probability for comparison with the top-three groups, Fischer's exact test. In (F), data are presented as mean ± 95% confidence interval. *Wt*, wild-type; *KRAS*$^{G12D}$, Lox-STOP-Lox.*KRAS*$^{G12D}$; *Trp53f/f*, conditional *Trp53*-deleted; Ad, adenovirus type 5; PFU, plaque-forming units; *Cre*, CRE recombinase gene; PCNA, proliferating cell nuclear antigen; LDH, lactate dehydrogenase; ANOVA, analysis of variance; VEGF, vascular endothelial growth factor.
Source data are available online for this figure.

7–14 days post-Ad-*Cre* (Fig EV3), emulating the inflammatory response observed after pleural asbestos instillation (Nagai *et al*, 2011) that is thought to drive MPM development (Fridlender *et al*, 2009; Patil *et al*, 2018; Courtiol *et al*, 2019).

The phenotype of intrapleural Ad-*Cre*-injected *KRAS*$^{G12D}$;*Trp53f/f* mice was fulminant, with respiratory and locomotor distress and retracted body posture culminating in death by 3–6 weeks post-Ad-*Cre* (median [95% CI] survival = 41 [38–73] days; $P < 0.001$ compared with any other genotype, log-rank test). Examination of the thorax revealed massive MPE in most and visceral/parietal pleural tumors in all mice, which invaded the lungs, chest wall, and mediastinum and uniformly presented as PCNA$^+$ biphasic MPM with mixed sarcomatoid/epithelioid features. Effusions were bloody but non-coagulating, contained abundant cancer and inflammatory cells, and had low pH and glucose and high protein, VEGF, and lactate dehydrogenase levels, resembling effusions of human advanced MPM (Robinson *et al*, 2005; Patil *et al*, 2018) and of *C57BL/6* mice injected with *KRAS*$^{G12C}$-mutant AE17 mesothelioma cells (Agalioti *et al*, 2017). *KRAS*$^{G12D}$;*Trp53f/Wt* mice displayed an intermediate phenotype (median [95% CI] survival = 118 [97–160] days; $P < 0.003$ compared with any other genotype, log-rank test), biphasic histology, and a single MPE occurrence. *Wt*, *Trp53f/f*, and *KRAS*$^{G12D}$;*Trp53f/f* mice also received 5 × 10$^8$ PFU intraperitoneal Ad-*Cre* (Fig EV4). Again, *Wt* and *Trp53f/f* mice displayed unlimited survival without signs of disease (median survival undefined), but K*RAS*$^{G12D}$;*Trp53f/f* mice developed abdominal swelling and succumbed by 2–5 months post-Ad-*Cre* (median [95% CI] survival = 95 [60–123] days; $P < 0.001$ compared with controls, log-rank test). At necropsy, nodular and diffuse tumors throughout the abdominal cavity and loculated ascites with features similar to MPM with MPE were detected.

To corroborate that our mice had mesothelioma and not pleural spread of LUAD (Jackson *et al*, 2001), immunostaining for specific markers of both tumor types was performed based on expert guidelines for distinguishing human MPM from LUAD (Scherpereel *et al*, 2010; Galateau-Salle *et al*, 2016; Courtiol *et al*, 2019) and on previous published experience from mouse models (Jongsma *et al*, 2008). In parallel, LUAD of intratracheal Ad-*Cre*-treated (5 × 10$^8$ PFU) *KRAS*$^{G12D}$ and of urethane-treated mice were examined (Mason *et al*, 2000; Spella *et al*, 2019). Our murine MPM displayed ubiquitous strong Wilms' tumor 1, patchy moderate vimentin, ubiquitous moderate mesothelin, ubiquitous strong calretinin/podoplanin/osteopontin, and patchy moderate cytokeratin 5/6 expression, but no evidence of surfactant protein C expression, in contrast with LUAD that expressed some of these markers and SFTPC (Fig 6), supporting that our tumors are indeed MPM of the biphasic subtype. These results show that pleural mesothelial-targeted *KRAS*$^{G12D}$ causes epithelioid MPM in mice. Furthermore, that standalone *TP53* loss does not trigger MPM, but cooperates with mutant *KRAS* to accelerate MPM development, to promote biphasic histology, and to precipitate effusion formation.

**Figure 6. Molecular phenotyping of murine mesothelioma.**

Wild-type (*Wt*), *KRAS*$^{G12D}$, and *Trp53f/f* mice were intercrossed, and all possible offspring genotypes received 5 × 10$^8$ PFU intrapleural or intratracheal Ad-*Cre* and were sacrificed when moribund. In parallel, *C57BL/6* mice received 10 consecutive weekly intraperitoneal injections of 1 g/kg urethane and were sacrificed after 6 months. Data summary (heatmap) and representative images of immunoreactivity of tissue sections of pleural and pulmonary tissues and tumors from these mice for different markers of human malignant pleural mesothelioma (MPM) and lung adenocarcinoma (LUAD). *n* = 10 mice/group were analyzed for each marker. Brown color indicates immunoreactivity and blue color nuclear hematoxylin counterstaining. Note the ubiquitous strong expression of Wilms' tumor 1 (WT1), patchy moderate expression of vimentin (VIM), ubiquitous moderate expression of mesothelin (MSLN), ubiquitous strong expression of calretinin (CALB2), podoplanin (PDPN), and osteopontin (SPP1), patchy moderate expression of cytokeratin 5/6 (CK5/6), and the absence of expression of surfactant protein C (SFTPC) in murine *KRAS*-driven mesotheliomas. Note also the ubiquitous strong expression of WT1, the patchy moderate expression of VIM, the ubiquitous low-level expression of MSLN, the ubiquitous strong expression of CALB2 and SPP1, the ubiquitous low-level expression of PDPN, the variable moderate expression of CK5/6, and the ubiquitous moderate expression of SFTPC in murine *KRAS*$^{G12D}$-driven and urethane-induced LUAD.

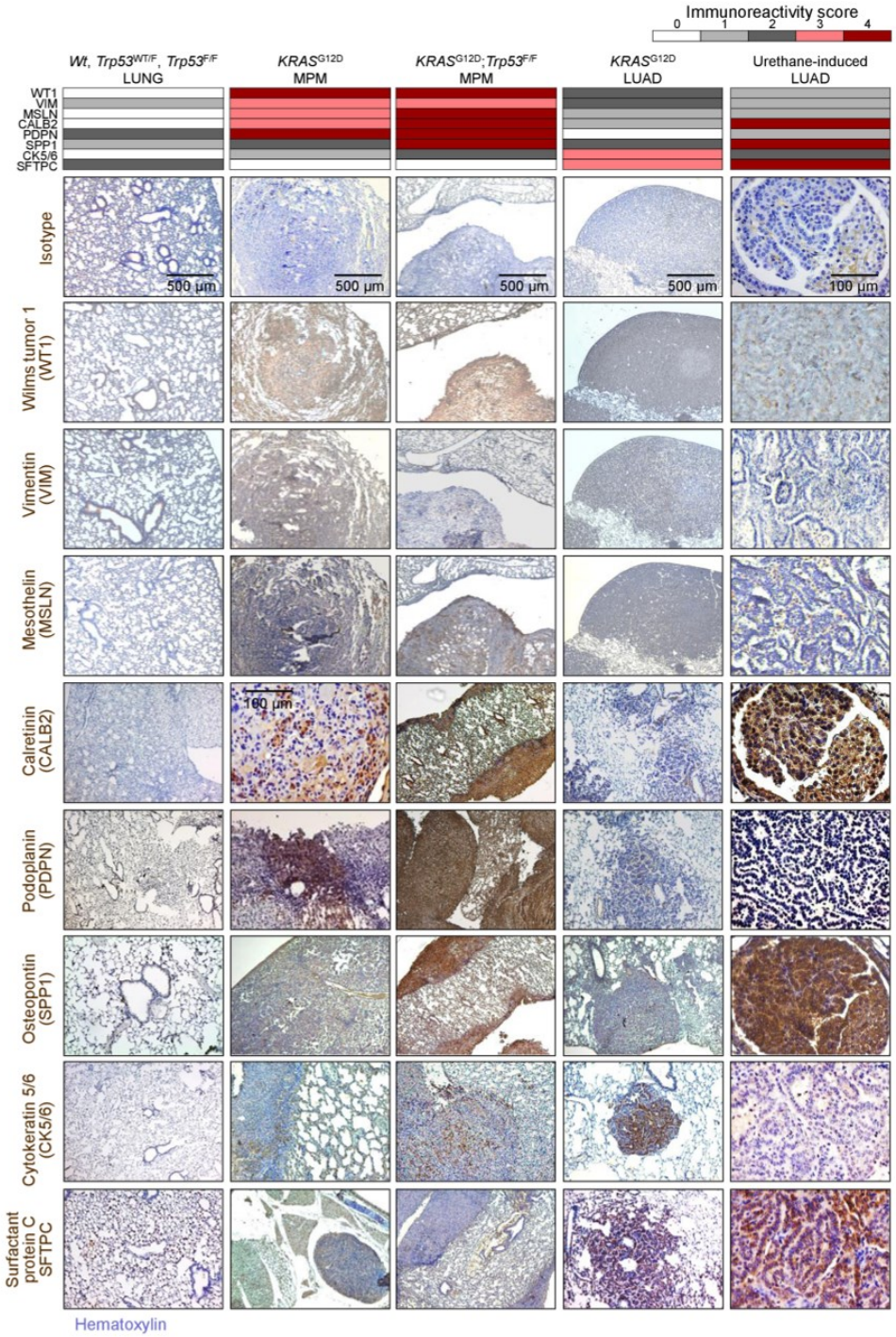


**Figure 6.**

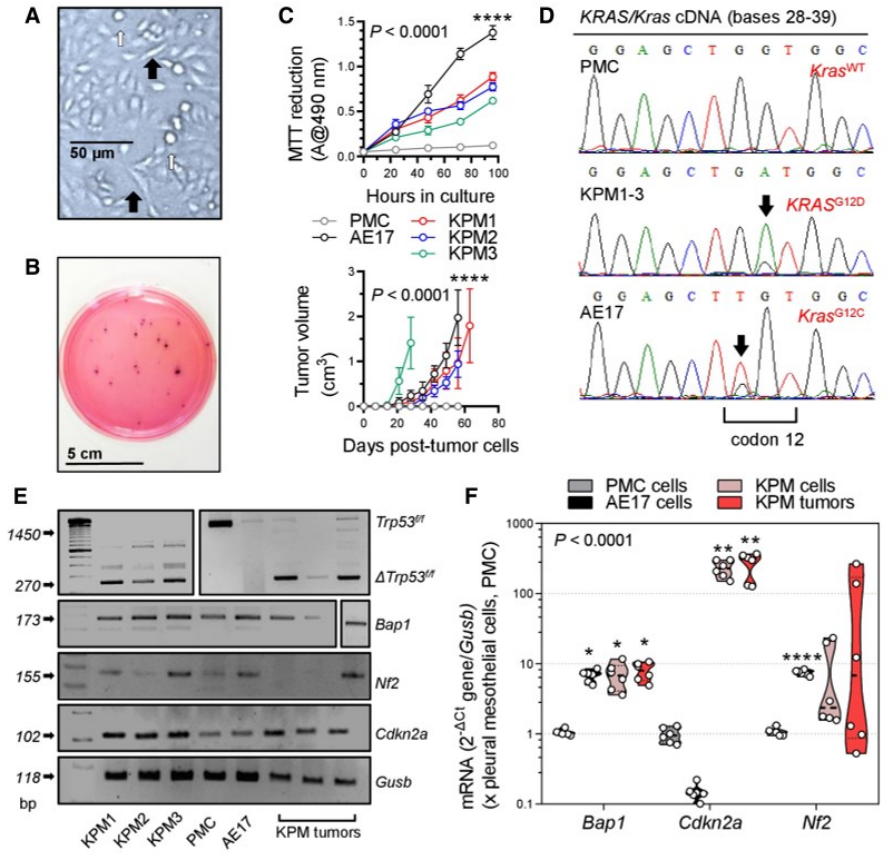


**Figure 7. Transplantable *KRAS/TP53*-mutant murine mesothelioma (KPM) cell lines.**

*KRAS*$^{G12D}$;*Trp53f/f* pleural mesothelioma (KPM), pleural mesothelial (PMC), and asbestos-induced AE17 mesothelioma cells (all from *C57BL/6* mice) were analyzed.

A KPM cell culture showing anoikis (white arrows) and spindle-shaped morphology (black arrows).

B Representative colonies of KPM1 cells ($7.5 \times 10^3$ cells/vessel) seeded on a soft agar-containing 60-mm petri dish and stained with crystal violet after a month ($n$ = 3/group).

C Data summaries from *in vitro* MTT reduction (top; $2 \times 10^4$ cells/well; $n$ = 6 independent experiments) and *in vivo* subcutaneous tumor growth after injection of $10^6$ cells per *C57BL/6* mouse (bottom; $n$ = 5/group).

D *KRAS/Kras* mRNA Sanger sequencing shows wild-type *Kras* (*Kras*$^{WT}$) of PMC and mutant murine *Kras*/human *KRAS* alleles (*KRAS*$^{G12D}$ and *Kras*$^{G12C}$) of KPM and AE17 cells (arrows).

E, F RT–PCR (E) and qPCR (F) of KPM cells and parental tumors show *Trp53f/f* allele deletion (*Δ*) and *Bap1* and *Cdkn2a* overexpression compared with PMC.

Data information: In (C), data are presented as mean (circles) and 95% confidence interval (bars). *P*, overall probability, two-way ANOVA. ****: $P < 0.0001$ for AE17 cells (top) or for KPM cells (bottom) compared with all other groups, Bonferroni post-tests. In (F), data are presented as raw data points (circles), rotated kernel density distribution (violins), and medians (lines). *P*, overall probability, two-way ANOVA. *, **, and ****: $P < 0.05$, $P < 0.01$, and $P < 0.0001$, respectively, for comparison with PMC, Bonferroni post-tests.

Source data are available online for this figure.

### Transplantable and actionable murine MPM cell lines with *KRAS*$^{G12D}$, *Trp53*, and *Bap1* mutations, and a human-like transcriptome

We subsequently isolated three different MPM cell lines from Ad-*Cre*-treated *KRAS*$^{G12D}$;*Trp53f/f* mice (called KPM1–3) using long-term tumor culture (Pauli *et al*, 2017; Kanellakis *et al*, 2019, 2020). KPM cells displayed anchorage-independent growth (anoikis), spindle-shaped morphology, and rapid growth in minimal-supplemented media and in soft agar. In addition, KPM cells were tumorigenic when injected subcutaneously into the flank of *C57BL/6* mice and carried the original *KRAS*$^{G12D}$/*Trp53* lesions (Fig 7A–E, and Appendix Fig S1). KPM cells and their parental tumors featured enhanced *Bap1* and *Cdkn2a*, but not *Nf2* expression (Fig 7E and F, and Appendix Fig S1), consistent with previous work that identified *TP53*-mediated repression of *BRCA1* and *CDKN2A* expression (Stott

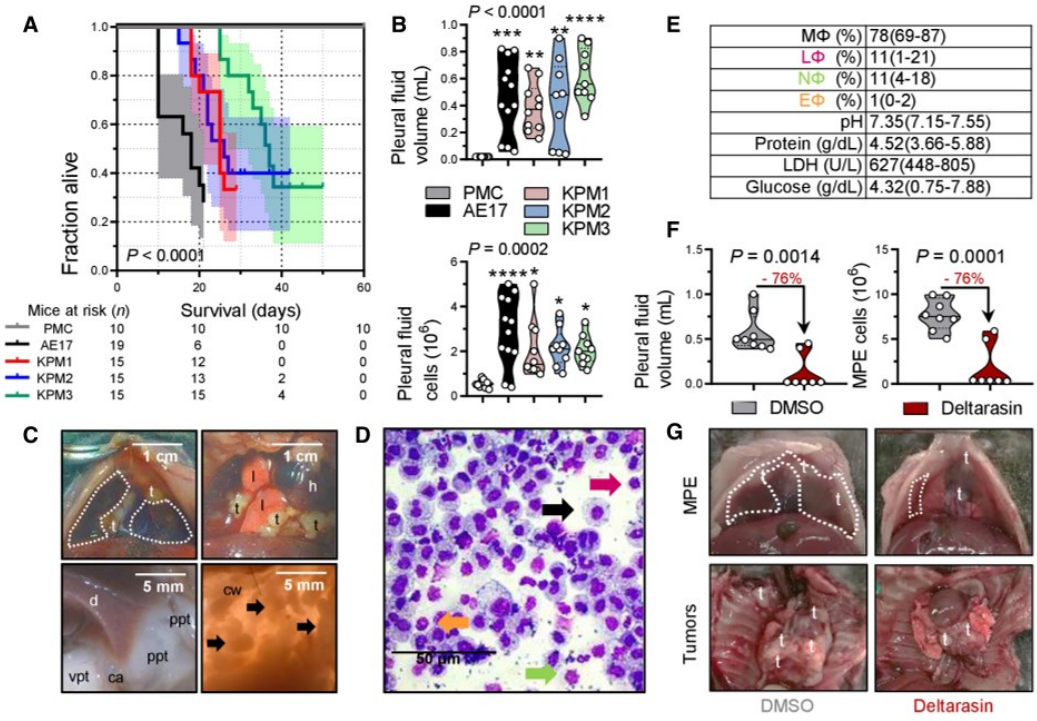


**Figure 8. Transplantable and actionable murine mesothelioma models using KPM cells.**

*C57BL/6* mice received $2 \times 10^5$ intrapleural *KRAS*$^{G12D}$;*Trp53f/f* pleural mesothelioma cells (KPM), pleural mesothelial cells (PMC), or asbestos-induced AE17 MPM cells.

A Kaplan–Meier survival plot with survival table.

B Data summary of pleural effusion volume and total cells ($n$ = 10, 12, 10, 9, and 9 mice/group, respectively, from left to right).

C Images of the chest before and after opening, showing effusion (dashed lines), visceral (vpt), and parietal (ppt) pleural tumors on the costophrenic angle (ca), the diaphragm (d), and the chest wall (cw, arrows). t, tumors; l, lungs; h, heart.

D May–Gruenwald–Giemsa-stained pleural cells (macrophages, MΦ: black arrow; lymphocytes, LΦ: purple arrow; neutrophils, NΦ: green arrow; eosinophils, EΦ: orange arrow).

E Effusion cytology and biochemistry data summary (total $n$ = 10 mice; $n$ = 4, 3, and 3 effusions from mice injected with KPM1, KPM2, and KPM3 cells, respectively, were analyzed and shown are pooled data).

F, G *C57BL/6* mice received pleural KPM1 cells followed by a single intrapleural injection of liposomes containing 1% DMSO or 15 mg/kg deltarasin in 1% DMSO at day 9 post-tumor cells. Shown are data summaries of MPE volume ($n$ = 8 and 7 DMSO and deltarasin-treated mice/group, respectively) and pleural fluid nucleated cells at day 19 post-KPM1 cells (F), as well as representative images of pleural effusions (dashed lines) and tumors (t in [G]).

Data information: In (A), data are presented as Kaplan–Meier survival estimates (lines), 95% confidence interval (shaded areas), and number of mice at risk ($n$). $P$, probability of overall comparison and of any comparison to PMC, log-rank test. In (B) and (F), data are presented as raw data points (circles), rotated kernel density distribution (violins), and medians (lines). Numbers in red font and arrows in (F) indicate end-point reduction by deltarasin effect. $P$, probability, one-way ANOVA (B) or Student's $t$-test (F). *, **, ***, and ****: $P < 0.05$, $P < 0.01$, $P < 0.001$, and $P < 0.0001$, respectively, for comparison with PMC, Bonferroni post-tests. In (E), data are presented as mean ± 95% confidence interval. LDH, lactate dehydrogenase.
Source data are available online for this figure.

*et al*, 1998; Arizti *et al*, 2000). RNA sequencing of KPM cells (GEO dataset GSE94415; Data ref: Stathopoulos *et al*, 2017) revealed that they carry the pathogenic *KRAS*$^{G12D}$/*Trp53* lesions, but also multiple stochastic single nucleotide variants in exon 6 and insertions in exon 11 of *Bap1*, all validated by Sanger sequencing, although immunohistochemistry revealed persistent nuclear BAP1 expression rendering these Bap1 mutations of uncertain functional significance (Nasu *et al*, 2015) (Fig EV5). Finally, $2 \times 10^5$ pleural-delivered KPM cells could inflict to naïve *C57BL/6* mice secondary disease identical to primary MPM of *KRAS*$^{G12D}$;*Trp53f/f* mice in terms of manifestation, pathology, cytology, and biochemistry (Fig 8A–E), fulfilling modified Koch's postulates (Byrd & Segre, 2016).

To determine the potential efficacy of KRAS inhibition against murine KRAS/TP53-driven MPM, *C57BL/6* mice received pleural KPM1 cells, followed by a single intrapleural injection of liposomal-encapsulated KRAS inhibitor deltarasin (15 mg/kg; Zimmermann *et al*, 2013) or empty liposomes on day nine post-tumor cells, in order to allow initial tumor implantation in the pleural space (Agalioti *et al*, 2017). At day 19 after pleural injection of KPM1 cells, deltarasin-treated *C57BL/6* mice developed fewer and smaller MPE

with decreased cellularity compared with controls (Fig 8F and G). These results collectively show that our murine MPM is indeed malignant, originate from recombined mesothelial cells, and cause transplantable disease that can be used for hypothesis and drug testing.

Finally, RNA sequencing of KPM cells comparative to normal pleural mesothelial cells revealed a distinctive transcriptomic signature that included classic mesothelioma markers (*Msln, Spp1, Efemp1, Pdpn, Wt1*) as well as new candidate mesothelioma genes (Fig 9A–C and Appendix Table S4). A human 150–gene mesothelioma signature derived from a cohort of 113 patients via comparison of MPM against multiple other malignancies (GSE42977; De Rienzo *et al*, 2013; Data ref: De Rienzo *et al*, 2012) was highly enriched in our KPM cell line signature (Fig 9D). These data indicate that murine *KRAS*/*TP53*-driven MPM present *Bap1* mutations, a gene expression profile that is highly similar to human MPM, and can be used for transplantable and druggable MPM models in syngeneic mice. Collectively, the murine and human findings support the existence of a *KRAS*-driven subset of MPM patients or clones that are likely missed during sequencing and/or sampling (Comertpay *et al*, 2014; Li *et al*, 2020).

## Discussion

Our results demonstrate that, alone or in combination with *TP53*, *KRAS* is perturbed in a proportion of human MPM and can potentially drive the murine mesothelium toward MPM development. *KRAS* mutations, amplifications, and overexpression, as well as chromosome 12p gains, are shown to exist in 20% of patients from the TCGA MPM dataset and low allelic frequency *KRAS* mutations are discovered in 50% of MPM samples from our own human cohorts using sensitive techniques. Furthermore, *KRAS* mutations are shown to occasionally co-exist with *TP53* mutations, to repulse *NF2* mutations, and to be associated with biphasic MPM histology. Targeting of oncogenic $KRAS^{G12D}$ alone to the pleural mesothelium caused epithelioid MPM in mice and together with *Trp53* deletion resulted in biphasic MPM with MPE. We further show that murine MPM carry the initiating $KRAS^{G12D}$/*Trp53* mutations and multiple secondary *Bap1* mutations, are transplantable and druggable, and highly similar to human MPM in terms of molecular markers and gene expression. Collectively, the data support a pathogenic role for *KRAS* mutations in a fraction of MPMs and provide new models to study this patient group.

Our striking findings can be reconciled with the sporadic nature of *KRAS* mutations in human MPM sequencing studies (Bott *et al*, 2011; Guo *et al*, 2015; Bueno *et al*, 2016; Hmeljak *et al*, 2018) and the incomplete penetrance of standalone *Bap1*, *Cdkn2a*, *Nf2*, or *Trp53* deletions in causing MPM in mice (Jongsma *et al*, 2008; Guo *et al*, 2014; Menges *et al*, 2014; Xu *et al*, 2014; Kukuyan *et al*, 2019). To this end, mesothelial *KRAS* mutations may initiate MPM in some patients, but may be lost during sampling and sequencing, as has been shown for other mutations in LUAD that persist at a subclonal level (Abbosh *et al*, 2017; Jamal-Hanjani *et al*, 2017). The low allelic frequency of *KRAS* mutations is explicable by their heterozygous nature and the robust inflammatory responses *KRAS*-mutant tumors generate (Agalioti *et al*, 2017; Marazioti *et al*, 2018) and is not limiting their driver capabilities in other tumor types (Abbosh *et al*, 2017; Jamal-Hanjani *et al*, 2017; Li *et al*, 2020). The fact that these mutations were not detected by most next-generation sequencing studies of MPM can be explained by the relative low sensitivity of these methods compared with ddPCR, as well as the low allelic frequency of KRAS mutations. To this end, typical read depths of 50–100 are employed in most next-generation sequencing studies yielding a sensitivity of 1–2%, compared with the theoretical 0.005% or actual 0.1% of ddPCR (Demuth *et al*, 2018). In addition, most next-generation sequencing studies set discovery cutoffs of 25% allelic frequency, likely rendering many *KRAS* mutations undiscovered. Our findings are plausible, since MPM is likely polyclonal (Comertpay *et al*, 2014), cell lines display *KRAS* activation and mutations (Patel *et al*, 2007; Agalioti *et al*, 2017), *NF2* is a *KRAS* suppressor (Tikoo *et al*, 1994), and *KRAS* signaling is interconnected with the *TP53* cell cycle checkpoint (Matallanas *et al*, 2011). The postulation that KRAS mutations in MPM might be early events can be tested in the future by genome doubling analyses. Taken together, our data and the literature support that, in a subset of patients, low allelic frequency *KRAS* alterations conditionally accomplice with *TP53* to drive mesothelial cells toward MPM. These tumors may be selectively responsive to *KRAS* blockade and detectable by sensitive methods like ddPCR or maximal depth sequencing (Li *et al*, 2020).

We also corroborate the critical role of *TP53* in MPM progression, since *TP53* mutations are frequent in MPM. Although standalone T*rp53* deletion did not induce MPM in mice, it promoted $KRAS^{G12D}$-driven MPM progression and biphasic histology, as was also observed in combination with *Nf2* and *Tsc1* deletion (Jongsma *et al*, 2008; Guo *et al*, 2014), suggesting that *Trp53* loss may conditionally cooperate with other oncogenes in MPM. In addition, *Trp53*-deleted $KRAS^{G12D}$ MPM was accompanied by effusions, a human MPM phenotype that likely affects survival (Ryu *et al*, 2014) and that was previously not reproducible in mice. Again, *Trp53* loss was not causative, but likely potentiated the effusion-promoting effects of *KRAS*, which we recently identified in metastatic effusions (Agalioti *et al*, 2017). Taken together with published work, our findings functionally validate the role of *TP53* mutations in human MPM in driving biphasic histology, tumor progression and metastasis, and poor survival (Bueno *et al*, 2016; Yap *et al*, 2017). Hence, TP53-targeted therapies may be prioritized for biphasic MPM when available (Brown *et al*, 2009).

Another surprising finding was the multiple and different *Bap1* mutations of our MPM cell lines, since they originated from tumors inflicted by $KRAS^{G12D}$ and *Trp53* loss. Frequent copy number loss and recurrent somatic mutations in *BAP1* have been identified in MPM (Bott *et al*, 2011; Guo *et al*, 2015; Nasu *et al*, 2015). Based on the multiplicity and variety of the *Bap1* mutations we observed, we postulate that they were secondarily triggered by the genomic instability caused from combined *KRAS* mutation and *TP53* loss. Whatever their cause may be, their presence strengthens our findings of an involvement of KRAS signaling in MPM pathobiology, as well as the relevance of the novel mouse models we developed, since *Bap1* is the single most commonly mutated gene in human MPM.

Research on MPM is hampered by the paucity of mouse models (Blanquart *et al*, 2020). We provide multiple new mouse models with defined phenotype, histology, and latency: (i) a genetic mouse model of pleural epithelioid MPM; (ii) genetic and transplantable models of pleural and peritoneal biphasic MPM with accompanying effusion; and (iii) three new MPM cell lines of defined genotype, transcriptome, and phenotype that are syngeneic to *C57BL/6* mice.

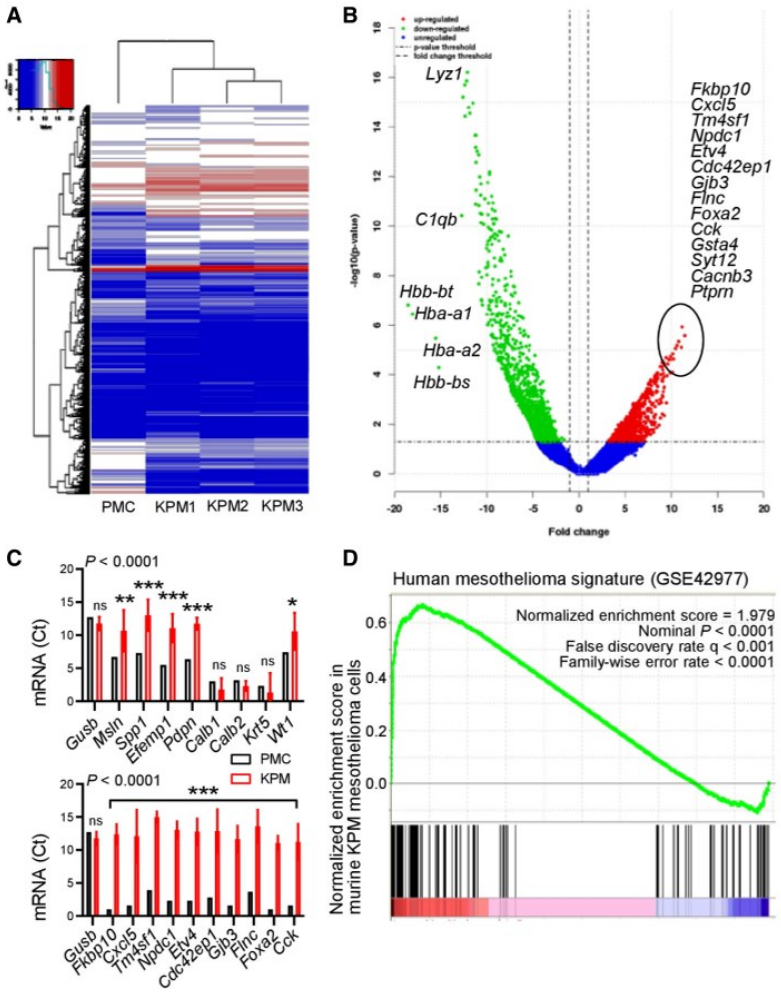


**Figure 9. The molecular signature of KPM cells is enriched in human mesothelioma.**

RNA sequencing results (GEO dataset GSE94415) of *KRAS*$^{G12D}$;*Trp53f/f* mesothelioma (KPM) cells ($n$ = 3) compared with pleural mesothelial cells (PMC; $n$ = 1 pooled triplicate). $n$ denotes biological replicates, since pooled triplicate technical replicates from each cell line were sequenced.

A Unsupervised hierarchical clustering shows distinctive gene expression of KPM versus PMC.

B Volcano plot showing some top KPM versus PMC differentially expressed genes.

C KPM and PMC expression of classic mesothelioma markers (top) and top KPM versus PMC overexpressed genes (bottom).

D Gene set enrichment analysis, including enrichment score and nominal probability value of the 150 gene-signature specifically over-represented in human mesothelioma compared with other thoracic malignancies derived from 113 patients (GSE42977) within the transcriptome of KPM cells versus PMC shows significant enrichment of the human mesothelioma signature in KPM cells.

Data information: In (C), data are presented as mean (columns) and 95% confidence interval (bars). *P*: probability, two-way ANOVA. ns, *, **, and ***: $P > 0.05$, $P < 0.05$, $P < 0.01$, and $P < 0.001$, respectively, compared with PMC, Bonferroni post-tests.
Source data are available online for this figure.

These are positioned to enhance MPM research by overcoming the need for immune compromise providing intact immune responses critical for MPM pathogenesis (Burt *et al*, 2012; Westbom *et al*, 2014; Kadariya *et al*, 2016; Patil *et al*, 2018), by widening the repertoire of existing cell lines, by recapitulating MPM with effusion, and by addressing pleural MPM.

In conclusion, our findings support that oncogenic *KRAS* signaling causes MPM in a proportion of humans and in mice. As some

 

mutations along this signaling pathway are currently druggable or are likely to become such in the near future (Herbst *et al*, 2002; Brown *et al*, 2009; Flaherty *et al*, 2010; Stephen *et al*, 2014), our findings may facilitate therapeutic innovation. Pending validation of our human findings in larger cohorts, we provide novel tools for the study of a molecular subclass of MPM that will hopefully aid in drug discovery and personalized treatment of patients with MPM driven by KRAS signaling.

## Materials and Methods

### Computational biologic analyses

The dataset for Fig 1A was generated by manual curation of COSMIC data (https://cancer.sanger.ac.uk/cosmic/browse/tissue?wgs=off&sn=pleura&ss=all&hn=mesothelioma&sh=&in=t&src=tissue&all_data=n). The dataset for Fig 1B was generated by manual curation of the main text and supplementary data of publications (Bott *et al*, 2011; Enomoto *et al*, 2012; Mezzapelle *et al*, 2013; Shukuya *et al*; 2014; Guo *et al*, 2015; Lo Iacono *et al*, 2015; Bueno *et al*, 2016; De Rienzo *et al*, 2016; Kato *et al*, 2016; Hmeljak *et al*, 2018). Raw data from 86 human TCGA MPM patients were retrieved from the cBioPortal for Cancer Genomics (www.cbioportal.org/) using inputs "mesothelioma", "Mesothelioma (TCGA, PanCancer Atlas)", "Query by Gene *KRAS* and *TP53*", "Mutations", "Putative copy-number alterations from GISTIC", "mRNA expression *z*-scores", and "Protein expression *z*-scores" were downloaded and analyzed. Gene expression data from these patients, normalized with the $\log_2$(fpkm-uq + 1) method, were downloaded (https://xenabrowser.net/datapages/?dataset=TCGA-MESO.htseq_fpkm-uq.tsv&host=https%3A%2F%2Fgdc.xenahubs.net&removeHub=https%3A%2F%2Fxena.treehouse.gi.ucsc.edu%3A443), ENSEMBL gene IDs were converted to gene symbols using https://www.biotools.fr/mouse/ensembl_symbol_converter, the data were filtered, differential gene expression (ΔGE) was analyzed, and heatmap visualization was performed using R* and packages limma R version 3.42.2 (https://bioconductor.org/packages/release/bioc/html/limma.html) and edgeR (https://bioconductor.org/packages/release/bioc/html/edgeR.html). Both rows and columns were clustered using Pearson correlation and complete linkage. All mutations ($n$ = 2,150) of all patients ($n$ = 86) with MPM from the TCGA pan-cancer dataset were retrieved from www.cbioportal.org/ and were fed into the protein analysis through evolutionary relationships (PANTHER) Classification System (www.pantherdb.org/) using parameters: organism, *Homo Sapiens*; analysis, statistical overrepresentation test > PANTHER pathways or reactome pathways (both analyses were done); whole-genome reference list: *Homo Sapiens*; test type: binomial; and correction: false discovery rate. All raw data from the two independent PANTHER and reactome pathway analyses were retrieved, merged, and analyzed. Gene set enrichment analysis (GSEA) was performed with the Broad Institute pre-ranked GSEA module software (http://software.broadinstitute.org/gsea/index.jsp;Subramanian *et al*, 2005). All aforementioned raw data were downloaded from the sources referenced above in *.csv format, are provided as source data files with this publication, and were reanalyzed using R*, Prism v8.0 (GraphPad, La Jolla, CA), and Excel (Microsoft, Redmont, WA).

### Reagents

Adenoviruses type 5 (Ad) encoding *Melanotus* luciferase (*Luc*) or CRE-recombinase (*Cre*) were from the Vector Development Laboratory, Baylor College of Medicine (Houston, TX); 3-(4,5-dimethylthiazol-2-yl)-2,5-diphenyltetrazolium bromide (MTT) assay from Sigma-Aldrich (St. Louis, MO), and D-luciferin from Gold Biotechnology (St. Louis, MO). Primers and antibodies are listed in Appendix Tables S5 and S6. All cell culture reagents were from Thermo Fisher Scientific.

### Human studies

All human experiments conformed to the principles set out in the WMA Declaration of Helsinki and the Department of Health and Human Services Belmont Report. The Munich clinical study was prospectively approved by the Ludwig-Maximilians-University Munich Ethics Committee (approvals #623–15 and #711–16). All patients gave written informed consent *a priori*. Diagnoses were made according to current standards by a board-certified pathologist at the Asklepios Fachkliniken Gauting, Munich, Germany. Pleural fluid was centrifuged at 300 *g* for 10 min at 4°C, genomic DNA was extracted from cell pellets, supernatants, and pleural tumor tissues using TRIzol (Thermo Fisher) and purified using GenElute Mammalian Genomic DNA Miniprep (Sigma Aldrich), and 200 ng DNA were used to analyze *KRAS* codons 12/13 and 61, and *TP53* copies with ddPCR *KRAS* G12/G13, *KRAS* G61, *TP53* CNV, and TERT CNV Kits and QuantaSoft Analysis Pro software (BioRad, Hercules, CA) as described elsewhere (Poole *et al*, 2019). Thresholds for $KRAS^{WT}$, $KRAS^{MUT}$, *TP53*, and *TERT* droplet amplitude gates were, respectively, 6,000, 10,000, 5,500, and 7,000. Data were normalized by accepted droplet numbers to yield absolute mutant ($^{MUT}$) and wild-type ($^{WT}$) droplet percentages, which were determined using thresholds derived from cell line controls and from LUAD patient samples clinically confirmed to have *KRAS* mutations and *TP53* copy number changes, according to the formula:

$$KRAS\,\text{mutant copies}\,\% = \frac{n_{\text{positive mutant droplets}}}{\left(n_{\text{positive mutant droplets}} + n_{\text{positive wild type droplets}}\right)} * 100$$

$$TP53\ \text{copies}\ \% = \frac{n_{\text{TP53 positive droplets}}}{n_{\text{TERT positive droplets}}} * 100.$$

In the Nantes Study, MPM cell lines, as well as pleural fluid cells and supernatants, were derived from pleural fluid aspirates obtained for diagnostic and therapeutic purposes. The study was approved by the French Ministry of Research (DC-2011-1399), and all patients gave written informed consent *a priori* for their excess pleural fluid to be used for the establishment of cell lines. MPE samples from over 120 patients with MPM were used to generate the 33 cell lines, since the success rate is < 30%, as described elsewhere (Gueugnon *et al*, 2011; Delaunay *et al*, 2020). Diagnoses were established by both fluid cytology and immunohistochemical staining of pleural biopsies performed by the pathology department at Laënnec Hospital (St-Herblain, France) and then externally confirmed by MESOPATH, the French panel of pathology experts for the diagnosis of mesothelioma. All recruited patients had received no prior

anticancer therapy. All cell lines were maintained in RPMI-1640 medium supplemented with 2 mM L-glutamine, 100 IU/ml penicillin, 0.1 mg/ml streptomycin, and 10% heat-inactivated fetal calf serum and cultured at 37°C in 5% $CO_2$-95% air. Genomic DNA from 33 MPM cell lines was extracted with Nucleospin Blood kit (Macherey-Nagel, Düren, Germany) and 500 ng were hybridized to Affymetrix CytoScanHD Arrays (Thermo Fisher). Detection, quantification, and visualization of single nucleotide variations (SNV) and copy number alterations (CNA) were performed using Affymetrix Chromosome Analysis Suite v3.1.1.27 (Thermo Fisher) and data are available at GEO datasets (GSE134349; Data ref: Blanquart *et al*, 2019). The cell lines were also sequenced in a targeted fashion focusing on 21 genes and the TERT promoter on a MiSeq system (Illumina, San Diego, CA) (Quetel *et al*, 2020). The MAPED (Clinical identification of malignant pleural effusions in the emergency department) study entailed a few samples from patients enrolled in a prospective clinical trial (preprint: Marazioti *et al*, 2021). MAPED was registered with ClinicalTrials.gov (#NCT03319472), and written informed consent was obtained from all patients *a priori*. MAPED was approved by the University of Patras Ethics Committee (approval #22699/21.11.2013). Pleural fluid was centrifuged at 300 *g* for 10 min at 4°C, RNA and DNA were extracted from cell pellets using TRIzol (Thermo Fisher) and purified using GenElute Mammalian Genomic DNA Miniprep (Sigma-Aldrich), and 200 ng RNA/DNA were used for RT–PCR, qPCR, and Sanger sequencing. The Istanbul study was approved by the Koç University Ethics Committee on Human Research (approval #2021.223.IRB2.042/06.05.2021). Both Nantes pleural fluid and Istanbul pleural tumor specimens were processed and analyzed identical to the Munich study.

#### Mice

*C57BL/6* (#000664), *B6.129(Cg)-Gt(ROSA)26Sor*$^{tm4(ACTB-tdTomato,-EGFP)Luo}$*/J* (*mT/mG*; #007676; Muzumdar *et al*, 2007), *FVB-Tg(CAG-luc,-GFP) L2G85Chco/J* (*CAG.Luc.eGFP*; #008450; Cao *et al*, 2004)[64], B6.129S4-*Kras*$^{tm4Tyj}$*/J* (*KRAS*$^{G12D}$; #008179; Jackson *et al*, 2001), and B6.129P2-*Trp53*$^{tm1Brn}$*/J* (*Trp53f/f*; #008462; Meylan *et al*, 2009) mice were obtained from Jackson Laboratories (Bar Harbor, ME) and bred on the *C57BL/6* background at the University of Patras Center for Animal Models of Disease. Experiments were approved by the Prefecture of Western Greece's Veterinary Administration (approval 118018/578-30.04.2014) and were conducted according to Directive 2010/63/EU (http://eur-lex.europa.eu/legal-content/EN/TXT/?uri=CELEX%3A32010L0063). Sex-, weight (20–25 g)-, and age (6–12 week)-matched experimental mice were used, and their numbers (total $n = 432$) are detailed in Appendix Table S7.

#### Mesothelial transgene delivery

Isoflurane-anesthetized *C57BL/6* and *mT/mG* mice received $5 \times 10^8$ PFU intrapleural or intraperitoneal Ad-*Cre* or Ad-*Luc* in 100 μl PBS and were serially imaged for bioluminescence on a Xenogen Lumina II (Perkin-Elmer, Waltham, MA) after receiving 1 mg retro-orbital D-luciferin under isoflurane anesthesia, and data were analyzed using Living Image v.4.2 (Perkin-Elmer; Stathopoulos *et al*, 2006; Spella *et al*, 2019), or were euthanized and pleural lavage was performed, lungs were explanted, and parietal pleura was stripped. For pleural lavage, 1 ml PBS was injected, was withdrawn after 30 s, and was cytocentrifuged onto glass slides ($5 \times 10^4$ cells, 300 *g*, 10 min) using CellSpin (Tharmac, Marburg, Germany). Lungs were embedded in optimal cutting temperature (OCT; Sakura, Tokyo, Japan) and sectioned into 10-μm cryosections. The parietal pleura was placed apical side up onto glass slides. Samples were stained with Hoechst 55238 and were examined on AxioObserver D1 (Zeiss, Jena, Germany) or TCS SP5 (Leica, Heidelberg, Germany) microscopes.

#### Primary MPM models

Wild-type (*Wt*), *KRAS*$^{G12D}$, and *Trp53f/f* mice were intercrossed and all possible offspring genotypes received isoflurane anesthesia and $5 \times 10^8$ PFU intrapleural or intraperitoneal Ad-*Cre*. Mice were monitored daily and sacrificed when moribund or prematurely for pathology. Mice with pleural fluid volume ≥ 100 μl were judged to have effusions that were aspirated. Animals with pleural fluid volume < 100 μl were judged not to have effusions and underwent pleural lavage. For isolation of primary murine pleural mesothelial cells (PMC), pleural myeloid and lymphoid cells were removed by pleural lavage followed by pleural instillation of 1 ml DMEM, 2% trypsin EDTA, aspiration after 1 min, and culture.

#### Bone marrow transfer

For adoptive BMT, *C57BL/6* mice received $10^7$ bone marrow cells obtained from *CAG.Luc.eGFP* donors i.v. 12 h after total-body irradiation (1,100 Rad). Full bone marrow reconstitution was completed after one month, as described elsewhere (Agalioti *et al*, 2017).

#### Transplantable mesothelioma cell lines

Murine *KRAS*$^{G12D}$*;Trp53f/f* pleural mesotheliomas were minced and cultured in DMEM 10% FBS for > 30 passages, yielding three *KRAS*$^{G12D}$*;Trp53f/f* mesothelioma (KPM1–3) cell lines, which were compared to AE17 cells (*Kras*$^{G12C}$-mutant asbestos-induced murine mesothelioma) and PMC (Agalioti *et al*, 2017). PMC were generated in our laboratory as primary cultures of murine pleural lavage with DMEM 2% trypsin, whereas AE17 cells were donated by Dr. YC Gary Lee (University of Western Australia, Perth, Australia) and have been both extensively described elsewhere (Giannou *et al*, 2015, 2017; Agalioti *et al*, 2017; Marazioti *et al*, 2018). For this, $2 \times 10^5$ cells in 100 μl PBS were delivered intrapleurally to isoflurane-anesthetized *C57BL/6* mice that were followed as above. For solid tumor formation, *C57BL/6* mice received $10^6$ subcutaneous PMC, KPM, or AE17 cells in the rear flank, three vertical tumor dimensions ($\delta^1$, $\delta^2$, $\delta^3$) were monitored serially, and the formula $\pi\delta^1\delta^2\delta^3/6$ was used to calculate tumor volume. RNA sequencing was done on an IonTorrent sequencer (Thermo Fisher); data were deposited at GEO datasets (GSE94415) and were analyzed using Bioconductor (Data ref: Stathopoulos *et al*, 2017). Gene set enrichment was done with the Broad Institute pre-ranked GSEA module (Subramanian *et al*, 2005).

#### PCR and Sanger sequencing

Cellular RNA was isolated using TRIzol (Thermo Fisher Scientific, Waltham, MA) followed by RNAeasy purification and genomic DNA removal (Qiagen, Hilden, Germany). For tumor RNA, tissues were

 

passed through 70-μm strainers (BD Biosciences, San Jose, CA) and $10^7$ cells were subjected to RNA extraction. One μg RNA was reverse-transcribed using Oligo$(dT)_{18}$ and Superscript III (Thermo Fisher). cDNAs were amplified using specific primers (Appendix Table S5) and Phusion Hot Start Flex polymerase (New England Biolabs, Ipswich, MA). DNA fragments were run on 2% agarose gels or were purified with NucleoSpin gel and PCR clean-up columns (Macherey-Nagel, Düren, Germany) and were sequenced using their primers by VBC Biotech (Vienna, Austria). qPCR was performed using specific primers (Appendix Table S5) and SYBR FAST qPCR Kit (Kapa Biosystems, Wilmington, MA) in a StepOne cycler (Applied Biosystems, Carlsbad, CA). Ct values from triplicate reactions were analyzed with the $2^{-\Delta CT}$ method (Pfaffl, 2001). mRNA abundance was determined relative to glycuronidase beta (*Gusb*) and is given as $2^{-\Delta CT} = 2^{-(\text{Ct of transcript})-(\text{Ct of Gusb})}$. The Sanger sequencing trace files were further analyzed for double peak parser using Bioconductor (https://www.bioconductor.org/) with a threshold of 25 Phred quality core (Ewing *et al*, 1998). The mismatch basecalls in respect to the wild-type samples were grouped by sample and used as template to generate the lollipop plot per each KPM cell line for a visual representation of all the mutations detected (Jay & Brouwer, 2016). Lollipop plots were generated using MutationMapper (https://www.cbioportal.org/mutation_mapper; Cerami *et al*, 2012).

#### RNA sequencing

RNA sequencing was done on an IonTorrent sequencer (Thermo Fisher), and data were analyzed using Bioconductor (https://www.bioconductor.org/). File alignments were performed with Tmap (https://github.com/iontorrent/TMAP). Coverage and alignments plot from sequencing were generated using Integrative genome viewer (Robinson *et al*, 2011). Alignments are represented as gray polygons with reads mismatching the reference indicated by color. Loci with a large percentage of mismatches relative to the reference are flagged in the coverage plot as color-coded bars. Alignments with inferred small insertion or small deletion are represented with vertical or horizontal bars, respectively. Gene set enrichment analysis (GSEA) was performed with the Broad Institute pre-ranked GSEA module software (http://software.broadinstitute.org/gsea/index.jsp; Subramanian *et al*, 2005). The raw *.bam files, one for each RNA-Seq sample, were summarized to a gene read counts table, using the Bioconductor package GenomicRanges. In the final read counts table, each row represented one gene, each column one RNAseq sample, and each cell the corresponding read counts associated with each row and column. The gene counts table was normalized for inherent systematic or experimental biases (e.g., sequencing depth, gene length, and GC content bias) using the Bioconductor package DESeq after removing genes that had zero counts over all RNASeq samples (20,007 genes). The output of the normalization algorithm was a table with normalized counts, which can be used for differential expression analysis with statistical algorithms developed specifically for count data. Prior to the statistical testing procedure, the gene read counts were filtered for possible artifacts that could affect the subsequent statistical testing procedures. Genes presenting any of the following were excluded from further analysis: (i) genes with length less than 500 bp (2,051 genes), (ii) genes whose average reads per 100 bp was less than the $25^{th}$ percentile of the total normalized distribution of average reads per 100 bp (0 genes with cutoff value 0.02248 average reads per 100 bp), (iii) genes with read counts below the median read counts of the total normalized count distribution (11,358 genes with cutoff value 16 normalized read counts). The total number of genes excluded due to the application of gene filters was 5,298. The total (unified) number of genes excluded due to the application of all filters was 32,595. The resulting gene counts table was subjected to differential expression analysis for the contrast KPM versus PMC using the Bioconductor package DESeq. The final numbers of statistically significant differentially expressed genes were 2,344 genes and of these, 650 were up-regulated and 1,694 were down-regulated according to an absolute fold-change cutoff value of 2.

#### Cell culture

All KPM cell lines are available upon request. Cells were cultured at 37°C in 5% $CO_2$-95% air using DMEM 10% FBS, 2 mM L-glutamine, 1 mM pyruvate, 100 U/ml penicillin, and 100 mg/ml streptomycin and were tested biannually for identity (by short tandem repeats) and *Mycoplasma Spp*. (by PCR). *In vitro* cell proliferation was determined using 3-(4,5-dimethylthiazol-2-yl)-2,5-diphenyltetrazolium bromide (MTT) assay. For *in vivo* injections, cells were harvested with trypsin, incubated with Trypan blue, counted on a hemocytometer, and > 95% viable cells were injected into the pleural space ($2 \times 10^5$) or into the skin ($10^6$) as described elsewhere (Agalioti *et al*, 2017). Mouse numbers used are detailed in Appendix Table S7.

#### Cell and tissue analyses

MPE fluid was diluted in 10-fold excess red blood cells lysis buffer (155 mM $NH_4Cl$, 12 mM $NaHCO_3$, 0.1 mM EDTA). Total pleural cell counts were determined microscopically in a hemocytometer and cytocentrifugal specimens ($5 \times 10^4$ cells each) of pleural fluid cells were fixed with methanol for 2 min. Cells were stained with May–Grünwald stain in 1 mM $Na_2HPO_4$, 2.5 mM $KH_2PO_4$, pH = 6.4 for 6 min and Giemsa stain in 2 mM $Na_2HPO_4$, 5 mM $KH_2PO_4$, pH = 6.4 for 40 min, washed with $H_2O$, and dried. Slides were mounted with Entellan (Merck Millipore, Darmstadt, Germany), coverslipped, and analyzed. For flow cytometry, $10^6$ nucleated pleural fluid cells suspended in 50 μl PBS supplemented with 2% FBS and 0.1% $NaN_3$ were stained with the indicated antibodies according to manufacturer's instructions (Appendix Table S6) for 20 min in the dark, washed, and resuspended in buffer for further analysis. Lungs, visceral pleural tumors, parietal pleural tumors, and chest walls were fixed in 4% paraformaldehyde overnight, embedded in paraffin or optimal cutting temperature (OCT) and were stored at room temperature or −80°C, respectively. Five-μm paraffin or 10-μm cryosections were mounted on glass slides. Sections were labeled using the indicated antibodies (Appendix Table S6), counterstained with Envision (Dako, Carpinteria, CA) or Hoechst 33258 (Sigma-Aldrich, St. Louis, MO), and mounted with Entellan new (Merck Millipore) or Mowiol 4-88 (Calbiochem, Gibbstown, NJ). For isotype control, primary antibody was omitted. Bright-field and fluorescent microscopy were done on AxioLab.A1 (Zeiss), AxioObserver.D1 (Zeiss), or TCS SP5 (Leica) microscopes and digital images were processed with Fiji (Schindelin *et al*, 2012).

**The paper explained**

**Problem**
In a proportion of patients with human malignant pleural mesothelioma (MPM), a dreadful disease most commonly inflicted by occupational asbestos inhalation but also possibly by smoking, sporadic mutations of KRAS is observed. However, their functional impact and significance have not been addressed and experimental model systems suitable for the study of this molecular subclass of MPM are not available.

**Results**
We systematically interrogate *KRAS* alterations in the TCGA pan-cancer dataset of human MPM and in MPM patients from our centers employing sensitive techniques. 20% of TCGA and 50% of our patients show activating mutations or amplification of *KRAS*, in 30% of the cases accompanied by *TP53* mutations or loss. These changes are associated with enhanced signaling downstream of *KRAS*. *KRAS* and *TP53* are shown to cooperate for MPM development in conditional mouse models. Three new MPM cell lines are developed that are highly similar to the human disease, and these experimental MPM models are shown to be actionable by a novel KRAS inhibitor.

**Impact**
Multiple new tools for investigations on MPM biology are provided together with proof-of-concept data that support involvement of *KRAS* signaling in MPM pathogenesis. The findings can be rapidly translated to clinical trials of KRAS pathway inhibition in a molecular subset of MPM patients.

#### Liposomal deltarasin preparation and treatment

Deltarasin-encapsulating liposomes were prepared as described elsewhere (Markoutsa *et al*, 2014; Marazioti *et al*, 2019), by freeze-drying 30 mg of empty DSPC/PG/Chol (9:1:5 mol/mol/mol) unilamelar sonicated vesicles with 1 ml of deltarasin solution (5 mg/ml) in PBS, or plain PBS (for empty liposomes), followed by controlled rehydration. Liposome size was decreased by extrusion though Lipo-so-fast extruder polycarbonate membranes (Avestin Europe, Mannheim, Germany) with 400-nm pore diameter. Liposome lipid concentration, size distribution, surface charge (zeta-sizer, Malvern Panalytical Ltd, Malvern, United Kingdom), and drug encapsulation efficiency were estimated by measuring non-liposomal drug absorption at 284 nm as reported elsewhere (Markoutsa *et al*, 2014; Marazioti *et al*, 2019). Deltarasin-encapsulating liposomes were delivered intrapleurally into *C57BL/6* mice 9 days post-intrapleural KPM1 cells, when the first pleural tumors were already established (Agalioti *et al*, 2017).

#### Statistics

Sample size was estimated using G*power (Faul *et al*, 2007) assuming $\alpha = 0.05$, $\beta = 0.05$, and effect size $d$ or $\varphi = 1.5$. Animals were allocated to treatments by alternation and transgenic animals case-control-wise. Data acquisition was blinded and no data were excluded from analyses. Data were tested for normality of distribution by Kolmogorov–Smirnov test and are given as mean $\pm$ 95% confidence interval (CI). Sample size ($n$) refers to biological replicates. Differences in means or medians were examined by $t$-test, Mann–Whitney test, Wilcoxon matched-pairs signed rank test, one-way analysis of variance (ANOVA) with Tukey's or Bonferroni's post-tests, or Kruskal–Wallis test with Dunn's post-tests, as indicated and appropriate. Differences in frequencies were tested by Fischer's exact or $\chi^2$ tests. Molecular and longitudinal (bioluminescence, MTT, tumor growth) data were analyzed by two-way ANOVA with Bonferroni's, Sidak's, Dunnett's, or Tukey's post-tests, or with two-stage linear step-up procedure of Benjamini, Krieger, and Yekutieli. Survival was analyzed using Kaplan–Meier estimates, log-rank (Mantel–Cox) test for probability, and Mantel–Haenszel estimates of hazard ratio. Probability ($P$) values are two-tailed and $P < 0.05$ was considered significant. Analyses and plots were done on Prism v8.0 (GraphPad, La Jolla, CA) and Excel (Microsoft, Redmont, WA).

## Data availability

Affymetrix CytoScanHD Microarray data: GEO dataset GSE134349 (https://www.ncbi.nlm.nih.gov/geo/query/acc.cgi?acc=GSE134349).
IonTorrent RNA sequencing data: GEO dataset GSE94415 (https://www.ncbi.nlm.nih.gov/geo/query/acc.cgi?&acc=GSE94415).

**Expanded View** for this article is available online.

### Acknowledgements
The authors thank Dr. YC Gary Lee (University of Western Australia, Perth, Australia) for donating AE17 cells and the cluster LUNG innovation (LUNG O2) for logistic support. This work was supported by European Research Council 2010 Starting Independent Investigator (#260524) and 2015 Proof of Concept (#679345) grants, the Graduate College (Graduiertenkolleg, GRK) #2338 of the German Research Society (Deutsche Forschungsgemeinschaft, DFG), the target validation project for pharmaceutical development ALTERNATIVE of the German Ministry for Education and Research (Bundesministerium für Bildung und Forschung, BMBF), and a Translational Research Grant by the German Center for Lung Research (Deutsches Zentrum für Lungenforschung, DZL) (all to GTS); the Greek State Scholarship Foundation Program "Reinforcement of Postdoctoral Researchers-1st and 2nd cycles" co-financed by the European Union Social Fund and Greek national funds (NSRF 2014–2020 and MIS-5033021) (to IG, MS, and IL); General Secretariat for Research and Innovation and Hellenic Foundation for Research and Innovation grant #1853a (to MS); REPSIRE European Respiratory Society Fellowship (LTRF 2015-1824) (to IP); INSERM, CNRS, the "Institut de Recherche en Santé Respiratoire des Pays de la Loire", ARSMESO44, the National Research Agency under the Programme d' Investissements d' Avenir (ANR-16-IDEX-0007), and the Pays de la Loire Region research program (all to CB, MG, and SD); as well as INSERM, the Ligue Contre le Cancer (Ile de France committee), and the Chancellerie des Universités de Paris (Legs POIX) (all to DJ). Open Access funding enabled and organized by Projekt DEAL.

### Author contributions
AM, ACK, GAG, SJB, and GN designed and carried out experiments, analyzed data, provided critical intellectual input, and generated portions of the paper draft; CB, DJ, SD, and MG designed and carried out microarray analyses, provided the French MPM cell line cohort, and provided and characterized the Nantes patient cohort; HB, ÖK, DM, ŞD, ST, SE, ÖY, PB, and PF provided and characterized the Istanbul patient cohort; SAIW, LT, MAAP, and CMH designed and carried out sequencing experiments and analysis, immunohistochemistry,

RNA sequencing analysis, and digital droplet PCR; LVK, IK, ML, RAH, and JB provided the German MPM and LUAD tumor cohort; MI and MV performed *in vivo* CRE reporter assays and experiments using *KRAS*$^{G12D}$ mice; ACK and IL performed molecular phenotyping of murine tumors; DEW performed GSEA; HP evaluated and diagnosed mouse pathology; SGA prepared liposomes; IP, MS, and IG designed and performed experiments and provided critical intellectual input and partial funding; A-SL carried out and analyzed immunohistochemistry and digital droplet PCR, and organized the experiments for the revision of the manuscript; and GTS conceived the idea, obtained funding, supervised the study, designed experiments, analyzed the data, performed statistics, analyzed public datasets, generated graphs and figures, wrote the original paper and its revised form, and is the guarantor of the study's integrity. All authors reviewed and concur with the submitted manuscript.

### Conflict of interest

IP works as a Senior Director in AstraZeneca Pharmaceutical in a non-related field with the publication. The remaining authors declare no competing financial interests.

### For more information

Institute of Lung Biology and Disease (ILBD) & Comprehensive Pneumology Center (CPC): https://www.helmholtz-muenchen.de/ilbd/index.html
Helmholtz Center Munich-German Research Center for Environmental Health (HMGU): https://www.helmholtz-muenchen.de/en/helmholtz-zentrum-muenchen/index.html
Ludwig-Maximilian-University (LMU) Munich: https://www.en.uni-muenchen.de/index.html
The Regional Center for Research in Cancerology and Immunology Nantes / Angers: https://www.crcina.org/?lang=en
The Koc University School of Medicine: https://medicine.ku.edu.tr/en/
The cancer genome atlas (TCGA) pan-cancer human malignant pleural mesothelioma (MPM) dataset available at cBioportal: https://www.cbioportal.org/study/summary?id=meso_tcga_pan_can_atlas_2018
The cancer genome atlas (TCGA) pan-cancer human malignant pleural mesothelioma (MPM) gene expression dataset available at: https://xenabrowser.net/datapages/?dataset=TCGA-MESO.htseq_fpkm-uq.tsv&host=https%3A%2F%2Fgdc.xenahubs.net&removeHub=https%3A%2F%2Fxena.treehouse.gi.ucsc.edu%3A443
The catalogue of somatic mutations in cancer (COSMIC) human MPM dataset: https://cancer.sanger.ac.uk/cosmic/browse/tissue?wgs=off&sn=pleura&ss=all&hn=mesothelioma&sh=&in=t&src=tissue&all_data=n
Human MPM datasets at Gene Expression Omnibus: https://www.ncbi.nlm.nih.gov/geo/query/acc.cgi?acc=GSE51024, https://www.ncbi.nlm.nih.gov/geo/query/acc.cgi?acc=GSE134349, https://www.ncbi.nlm.nih.gov/geo/query/acc.cgi?acc=GSE42977
Novel mouse MPM cell line and normal mesothelial cell RNA sequencing dataset at Gene Expression Omnibus: https://www.ncbi.nlm.nih.gov/geo/query/acc.cgi?&acc=GSE94415
Using Pleural Effusions to Diagnose Cancer (MAPED) study page at ClinicalTrials.gov: https://www.clinicaltrials.gov/ct2/show/NCT03319472?term=maped&draw=2&rank=1
Links to patient support, advocate, and charity organizations: https://www.mesotheliomagroup.com/, https://www.mesothelioma.com/, https://www.mesotheliomahelp.org/, https://www.asbestos.com/support/, https://mesothelioma.net/mesothelioma-support/, https://www.curemeso.org/, https://www.mesotheliomahope.com/resources/cancer-foundations/, https://www.mesothelioma.uk.com/.

## References

Abbosh C, Birkbak NJ, Wilson GA, Jamal-Hanjani M, Constantin T, Salari R, Le Quesne J, Moore DA, Veeriah S, Rosenthal R *et al* (2017) Phylogenetic ctDNA analysis depicts early-stage lung cancer evolution. *Nature* 545: 446 – 451

Agalioti T, Giannou AD, Krontira AC, Kanellakis NI, Kati D, Vreka M, Pepe M, Spella M, Lilis I, Zazara DE *et al* (2017) Mutant KRAS mediates malignant pleural effusion formation. *Nat Commun* 8: 15205

Arizti P, Fang L, Park I, Yin Y, Solomon E, Ouchi T, Aaronson SA, Lee SW (2000) Tumor suppressor p53 is required to modulate BRCA1 expression. *Mol Cell Biol* 20: 7450 – 7459

Bi M, Zhao S, Said JW, Merino MJ, Adeniran AJ, Xie Z, Nawaf CB, Choi J, Belldegrun AS, Pantuck AJ *et al* (2016) Genomic characterization of sarcomatoid transformation in clear cell renal cell carcinoma. *Proc Natl Acad Sci USA* 113: 2170 – 2175

Bibby AC, Tsim S, Kanellakis N, Ball H, Talbot DC, Blyth KG, Maskell NA, Psallidas I (2016) Malignant pleural mesothelioma: an update on investigation, diagnosis and treatment. *Eur Respir Rev* 25: 472 – 486

Blanquart C, Fonteneau J, Minvielle S (2019) Gene Expression Omnibus GSE134349 (https://www.ncbi.nlm.nih.gov/geo/query/acc.cgi?acc=GSE134349). [DATASET]

Blanquart C, Jaurand MC, Jean D (2020) The biology of malignant mesothelioma and the relevance of preclinical models. *Front Oncol* 10: 388

Bott M, Brevet M, Taylor BS, Shimizu S, Ito T, Wang LU, Creaney J, Lake RA, Zakowski MF, Reva B *et al* (2011) The nuclear deubiquitinase BAP1 is commonly inactivated by somatic mutations and 3p21.1 losses in malignant pleural mesothelioma. *Nat Genet* 43: 668 – 672

Brown CJ, Lain S, Verma CS, Fersht AR, Lane DP (2009) Awakening guardian angels: drugging the p53 pathway. *Nat Rev Cancer* 9: 862 – 873

Bueno R, Stawiski EW, Goldstein LD, Durinck S, De Rienzo A, Modrusan Z, Gnad F, Nguyen TT, Jaiswal BS, Chirieac LR *et al* (2016) Comprehensive genomic analysis of malignant pleural mesothelioma identifies recurrent mutations, gene fusions and splicing alterations. *Nat Genet* 48: 407 – 416

Burt BM, Bader A, Winter D, Rodig SJ, Bueno R, Sugarbaker DJ (2012) Expression of interleukin-4 receptor alpha in human pleural mesothelioma is associated with poor survival and promotion of tumor inflammation. *Clin Cancer Res* 18: 1568 – 1577

Byrd AL, Segre JA (2016) Infectious disease. Adapting Koch's postulates. *Science* 351: 224 – 226

Cao YA, Wagers AJ, Beilhack A, Dusich J, Bachmann MH, Negrin RS, Weissman IL, Contag CH (2004) Shifting foci of hematopoiesis during reconstitution from single stem cells. *Proc Natl Acad Sci USA* 101: 221 – 226

Carbone M, Adusumilli PS, Alexander HR, Baas P, Bardelli F, Bononi A, Bueno R, Felley-Bosco E, Galateau-Salle F, Jablons D *et al* (2019) Mesothelioma: scientific clues for prevention, diagnosis, and therapy. *CA Cancer J Clin* 69: 402 – 429

Cerami E, Gao J, Dogrusoz U, Gross BE, Sumer SO, Aksoy BA, Jacobsen A, Byrne CJ, Heuer ML, Larsson E *et al* (2012) The cBio cancer genomics portal: an open platform for exploring multidimensional cancer genomics data. *Cancer Discov* 2: 401 – 404

Cheah HM, Lansley SM, Varano Della Vergiliana JF, Tan AL, Thomas R, Leong SL, Creaney J, Lee YC (2017) Malignant pleural fluid from mesothelioma has potent biological activities. *Respirology* 22: 192 – 199

Comertpay S, Pastorino S, Tanji M, Mezzapelle R, Strianese O, Napolitano A, Baumann F, Weigel T, Friedberg J, Sugarbaker P *et al* (2014) Evaluation of clonal origin of malignant mesothelioma. *J Transl Med* 12: 301

Courtiol P, Maussion C, Moarii M, Pronier E, Pilcer S, Sefta M, Manceron P, Toldo S, Zaslavskiy M, Le Stang N *et al* (2019) Deep learning-based

classification of mesothelioma improves prediction of patient outcome. *Nat Med* 25: 1519–1525

De Rienzo A, Richards WG, Yeap BY, Coleman MH, Sugarbaker PE, Chirieac LR, Wang YE, Quackenbush J, Jensen RV, Bueno R (2012) Gene Expression Omnibus GSE42977 (https://www.ncbi.nlm.nih.gov/geo/query/acc.cgi?acc=GSE42977). [DATASET]

De Rienzo A, Richards WG, Yeap BY, Coleman MH, Sugarbaker PE, Chirieac LR, Wang YE, Quackenbush J, Jensen RV, Bueno R (2013) Sequential binary gene ratio tests define a novel molecular diagnostic strategy for malignant pleural mesothelioma. *Clin Cancer Res* 19: 2493–2502

De Rienzo A, Archer MA, Yeap BY, Dao N, Sciaranghella D, Sideris AC, Zheng Y, Holman AG, Wang YE, Dal Cin PS *et al* (2016) Gender-specific molecular and clinical features underlie malignant pleural mesothelioma. *Cancer Res* 76: 319–328

Delaunay T, Achard C, Boisgerault N, Grard M, Petithomme T, Chatelain C, Dutoit S, Blanquart C, Royer P-J, Minvielle S *et al* (2020) Frequent homozygous deletions of type I interferon genes in pleural mesothelioma confer sensitivity to oncolytic measles virus. *J Thorac Oncol* 15: 827–842

Demuth C, Spindler KG, Johansen JS, Pallisgaard N, Nielsen D, Hogdall E, Vittrup B, Sorensen BS (2018) Measuring KRAS mutations in circulating tumor DNA by droplet digital PCR and next-generation sequencing. *Transl Oncol* 11: 1220–1224

Enomoto Y, Kasai T, Takeda M, Takano M, Morita K, Kadota E, Iizuka N, Maruyama H, Haratake J, Kojima YU *et al* (2012) Epidermal growth factor receptor mutations in malignant pleural and peritoneal mesothelioma. *J Clin Pathol* 65: 522–527

Ewing B, Hillier L, Wendl MC, Green P (1998) Base-calling of automated sequencer traces using phred I accuracy assessment. *Genome Res* 8: 175–185

Faul F, Erdfelder E, Lang AG, Buchner A (2007) G*Power 3: a flexible statistical power analysis program for the social, behavioral, and biomedical sciences. *Behav Res Methods* 39: 175–191

Fennell DA, Parmar A, Shamash J, Evans MT, Sheaff MT, Sylvester R, Dhaliwal K, Gower N, Steele J, Rudd R (2005) Statistical validation of the EORTC prognostic model for malignant pleural mesothelioma based on three consecutive phase II trials. *J Clin Oncol* 23: 184–189

Flaherty KT, Puzanov I, Kim KB, Ribas A, McArthur GA, Sosman JA, O'Dwyer PJ, Lee RJ, Grippo JF, Nolop K *et al* (2010) Inhibition of mutated, activated BRAF in metastatic melanoma. *N Engl J Med* 363: 809–819

Forbes SA, Beare D, Gunasekaran P, Leung K, Bindal N, Boutselakis H, Ding M, Bamford S, Cole C, Ward S *et al* (2015) COSMIC: exploring the world's knowledge of somatic mutations in human cancer. *Nucleic Acids Res* 43: D805–D811

Fridlender ZG, Sun J, Kim S, Kapoor V, Cheng G, Ling L, Worthen GS, Albelda SM (2009) Polarization of tumor-associated neutrophil phenotype by TGF-beta: "N1" versus "N2" TAN. *Cancer Cell* 16: 183–194

Galateau-Salle F, Churg A, Roggli V, Travis WD; World Health Organization Committee for Tumors of the Pleura (2016) The 2015 World Health Organization classification of tumors of the pleura: advances since the 2004 classification. *J Thorac Oncol* 11: 142–154

Giannou AD, Marazioti A, Kanellakis NI, Giopanou I, Lilis I, Zazara DE, Ntaliarda G, Kati D, Armenis V, Giotopoulou GA *et al* (2017) *NRAS* destines tumor cells to the lungs. *EMBO Mol Med* 9: 672–686

Giannou AD, Marazioti A, Spella M, Kanellakis NI, Apostolopoulou H, Psallidas I, Prijovich ZM, Vreka M, Zazara DE, Lilis I *et al* (2015) Mast cells mediate malignant pleural effusion formation. *J Clin Invest* 125: 2317–2334

Global Burden of Disease (GBD) 2016 Occupational Carcinogens Collaborators (2020) Global and regional burden of cancer in 2016 arising from occupational exposure to selected carcinogens: a systematic analysis for the Global Burden of Disease Study 2016. *Occup Environ Med* 77: 151–159

Gueugnon F, Leclercq S, Blanquart C, Sagan C, Cellerin L, Padieu M, Perigaud C, Scherpereel A, Gregoire M (2011) Identification of novel markers for the diagnosis of malignant pleural mesothelioma. *Am J Pathol* 178: 1033–1042

Guo Y, Chirieac LR, Bueno R, Pass H, Wu W, Malinowska IA, Kwiatkowski DJ (2014) Tsc1-Tp53 loss induces mesothelioma in mice, and evidence for this mechanism in human mesothelioma. *Oncogene* 33: 3151–3160

Guo G, Chmielecki J, Goparaju C, Heguy A, Dolgalev I, Carbone M, Seepo S, Meyerson M, Pass HI (2015) Whole-exome sequencing reveals frequent genetic alterations in BAP1, NF2, CDKN2A, and CUL1 in malignant pleural mesothelioma. *Cancer Res* 75: 264–269

Hassan M, Mercer RM, Maskell NA, Asciak R, McCracken DJ, Bedawi EO, Shaarawy H, El-Ganady A, Psallidas I, Miller RF *et al* (2019) Survival in patients with malignant pleural effusion undergoing talc pleurodesis. *Lung Cancer* 137: 14–18

Herbst RS, Maddox A-M, Rothenberg ML, Small EJ, Rubin EH, Baselga J, Rojo F, Hong WK, Swaisland H, Averbuch SD *et al* (2002) Selective oral epidermal growth factor receptor tyrosine kinase inhibitor ZD1839 is generally well-tolerated and has activity in non-small-cell lung cancer and other solid tumors: results of a phase I trial. *J Clin Oncol* 20: 3815–3825

Hmeljak J, Sanchez-Vega F, Hoadley KA, Shih J, Stewart C, Heiman D, Tarpey P, Danilova L, Drill E, Gibb EA *et al* (2018) Integrative molecular characterization of malignant pleural mesothelioma. *Cancer Discov* 8: 1548–1565

Ikediobi ON, Davies H, Bignell G, Edkins S, Stevens C, O'Meara S, Santarius T, Avis T, Barthorpe S, Brackenbury L *et al* (2006) Mutation analysis of 24 known cancer genes in the NCI-60 cell line set. *Mol Cancer Ther* 5: 2606–2612

Jackson EL, Willis N, Mercer K, Bronson RT, Crowley D, Montoya R, Jacks T, Tuveson DA (2001) Analysis of lung tumor initiation and progression using conditional expression of oncogenic K-ras. *Genes Dev* 15: 3243–3248

Jamal-Hanjani M, Wilson GA, McGranahan N, Birkbak NJ, Watkins TBK, Veeriah S, Shafi S, Johnson DH, Mitter R, Rosenthal R *et al* (2017) Tracking the evolution of non-small-cell lung cancer. *N Engl J Med* 376: 2109–2121

Jay JJ, Brouwer C (2016) Lollipops in the clinic: information dense mutation plots for precision medicine. *PLoS One* 11: e0160519

Jongsma J, van Montfort E, Vooijs M, Zevenhoven J, Krimpenfort P, van der Valk M, van de Vijver M, Berns A (2008) A conditional mouse model for malignant mesothelioma. *Cancer Cell* 13: 261–271

Kadariya Y, Menges CW, Talarchek J, Cai KQ, Klein-Szanto AJ, Pietrofesa RA, Christofidou-Solomidou M, Cheung M, Mossman BT, Shukla A *et al* (2016) Inflammation-related IL1β/IL1R signaling promotes the development of asbestos-induced malignant mesothelioma. *Cancer Prev Res (Phila)* 9: 406–414

Kanellakis NI, Giannou AD, Pepe MAA, Agalioti T, Zazara DE, Giopanou I, Psallidas I, Spella M, Marazioti A, Arendt KAM *et al* (2019) Tobacco chemical-induced mouse lung adenocarcinoma cell lines pin the prolactin orthologue proliferin as a lung tumour promoter. *Carcinogenesis* 40: 1352–1362

Kanellakis NI, Asciak R, Hamid MA, Yao X, McCole M, McGowan S, Seraia E, Hatch S, Hallifax RJ, Mercer RM *et al* (2020) Patient-derived malignant pleural mesothelioma cell cultures: a tool to advance biomarker-driven treatments. *Thorax* 75: 1004–1008

Kato S, Tomson BN, Buys TP, Elkin SK, Carter JL, Kurzrock R (2016) Genomic landscape of malignant mesotheliomas. *Mol Cancer Ther* 15: 2498–2507

 

Kindler HL, Ismaila N, Armato SG, Bueno R, Hesdorffer M, Jahan T, Jones CM, Miettinen M, Pass H, Rimner A *et al* (2018) Treatment of malignant pleural mesothelioma: American Society of Clinical Oncology Clinical Practice Guideline. *J Clin Oncol* 36: 1343 – 1373

Klotz LV, Courty Y, Lindner M, Petit-Courty A, Stowasser A, Koch I, Eichhorn ME, Lilis I, Morresi-Hauf A, Arendt KAM *et al* (2019) Comprehensive clinical profiling of the Gauting locoregional lung adenocarcinoma donors. *Cancer Med* 8: 1486 – 1499

Klotz LV, Lindner M, Eichhorn ME, Grützner U, Koch I, Winter H, Kauke T, Duell T, Hatz RA (2019) Pleurectomy/decortication and hyperthermic intrathoracic chemoperfusion using cisplatin and doxorubicin for malignant pleural mesothelioma. *J Thorac Dis* 11: 1963 – 1972

Kukuyan AM, Sementino E, Kadariya Y, Menges CW, Cheung M, Tan Y, Cai KQ, Slifker MJ, Peri S, Klein-Szanto AJ *et al* (2019) Inactivation of Bap1 cooperates with losses of Nf2 and Cdkn2a to drive the development of pleural malignant mesothelioma in conditional mouse models. *Cancer Res* 79: 4113 – 4123

Liu B, van Gerwen M, Bonassi S, Taioli E; International Association for the Study of Lung Cancer Mesothelioma Task Force (2017) Epidemiology of Environmental Exposure and Malignant Mesothelioma. *J Thorac Oncol* 12: 1031 – 1045

Li S, MacAlpine DM, Counter CM (2020) Capturing the primordial Kras mutation initiating urethane carcinogenesis. *Nat Commun* 11: 1800

Lo Iacono M, Monica V, Righi L, Grosso F, Libener R, Vatrano S, Bironzo P, Novello S, Musmeci L, Volante M *et al* (2015) Targeted next-generation sequencing of cancer genes in advanced stage malignant pleural mesothelioma: a retrospective study. *J Thorac Oncol* 10: 492 – 499

Marazioti A, Lilis I, Vreka M, Apostolopoulou H, Kalogeropoulou A, Giopanou I, Giotopoulou GA, Krontira AC, Iliopoulou M, Kanellakis NI *et al* (2018) Myeloid-derived interleukin-1β drives oncogenic KRAS-NF-κB addiction in malignant pleural effusion. *Nat Commun* 9: 672

Marazioti A, Papadia K, Giannou A, Stathopoulos GT, Antimisiaris SG (2019) Prolonged retention of liposomes in the pleural cavity of normal mice and high tumor distribution in mice with malignant pleural effusion, after intrapleural injection. *Int J Nanomed* 14: 3773 – 3784

Marazioti A, Voulgaridis A, Psallidas I, Lamort AS, Iliopoulou M, Krontira AC, Lilis I, Asciak R, Kanellakis NI, Rahman NM *et al* (2021) Clinical identification of malignant pleural effusions. *medRxiv* https://doi.org/10.1101/2020.05.31.20118307 [PREPRINT]

Marino S, Vooijs M, van Der Gulden H, Jonkers J, Berns A (2000) Induction of medulloblastomas in p53-null mutant mice by somatic inactivation of Rb in the external granular layer cells of the cerebellum. *Genes Dev* 14: 994 – 1004

Markoutsa E, Papadia K, Giannou AD, Spella M, Cagnotto A, Salmona M, Stathopoulos GT, Antimisiaris SG (2014) Mono and dually decorated nanoliposomes for brain targeting, *in vitro* and *in vivo* studies. *Pharm Res* 31: 1275 – 1289

Mason RJ, Kalina M, Nielsen LD, Malkinson AM, Shannon JM (2000) Surfactant protein C expression in urethane-induced murine pulmonary tumors. *Am J Pathol* 156: 175 – 182

Matallanas D, Romano D, Al-Mulla F, O'Neill E, Al-Ali W, Crespo P, Doyle B, Nixon C, Sansom O, Drosten M *et al* (2011) Mutant K-Ras activation of the proapoptotic MST2 pathway is antagonized by wild-type K-Ras. *Mol Cell* 44: 893 – 906

Menges CW, Kadariya Y, Altomare D, Talarchek J, Neumann-Domer E, Wu Y, Xiao G-H, Shapiro IM, Kolev VN, Pachter JA *et al* (2014) Tumor suppressor alterations cooperate to drive aggressive mesotheliomas with enriched cancer stem cells via a p53-miR-34a-c-Met axis. *Cancer Res* 74: 1261 – 1271

Meylan E, Dooley AL, Feldser DM, Shen L, Turk E, Ouyang C, Jacks T (2009) Requirement for NF-kappaB signalling in a mouse model of lung adenocarcinoma. *Nature* 462: 104 – 107

Mezzapelle R, Miglio U, Rena O, Paganotti A, Allegrini S, Antona J, Molinari F, Frattini M, Monga G, Alabiso O *et al* (2013) Mutation analysis of the EGFR gene and downstream signalling pathway in histologic samples of malignant pleural mesothelioma. *Br J Cancer* 108: 1743 – 1749

Mutti L, Peikert T, Robinson BWS, Scherpereel A, Tsao AS, de Perrot M, Woodard GA, Jablons DM, Wiens J, Hirsch FR *et al* (2018) Scientific advances and new frontiers in mesothelioma therapeutics. *J Thorac Oncol* 13: 1269 – 1283

Muzumdar MD, Tasic B, Miyamichi K, Li L, Luo L (2007) A global double-fluorescent Cre reporter mouse. *Genesis* 45: 593 – 605

Nagai H, Okazaki Y, Chew SH, Misawa N, Yamashita Y, Akatsuka S, Ishihara T, Yamashita K, Yoshikawa Y, Yasui H *et al* (2011) Diameter and rigidity of multiwalled carbon nanotubes are critical factors in mesothelial injury and carcinogenesis. *Proc Natl Acad Sci USA* 108: E1330 – E1338

Nasu M, Emi M, Pastorino S, Tanji M, Powers A, Luk H, Baumann F, Zhang Y-A, Gazdar A, Kanodia S *et al* (2015) High incidence of somatic BAP1 alterations in sporadic malignant mesothelioma. *J Thorac Oncol* 10: 565 – 576

Paajanen J, Laaksonen S, Ilonen I, Wolff H, Husgafvel-Pursiainen K, Kuosma E, Ollila H, Myllärniemi M, Vehmas T (2018) Computed tomography in the evaluation of malignant pleural mesothelioma-Association of tumor size to a sarcomatoid histology, a more advanced TNM stage and poor survival. *Lung Cancer* 116: 73 – 79

Pass H, Giroux D, Kennedy C, Ruffini E, Cangir AK, Rice D, Asamura H, Waller D, Edwards J, Weder W *et al* (2016) The IASLC mesothelioma staging project: improving staging of a rare disease through international participation. *J Thorac Oncol* 11: 2082 – 2088

Patel MR, Jacobson BA, De A, Frizelle SP, Janne P, Thumma SC, Whitson BA, Farassati F, Kratzke RA (2007) Ras pathway activation in malignant mesothelioma. *J Thorac Oncol* 2: 789 – 795

Patil NS, Righi L, Koeppen H, Zou W, Izzo S, Grosso F, Libener R, Loiacono M, Monica V, Buttigliero C *et al* (2018) Molecular and histopathological characterization of the tumor immune microenvironment in advanced stage of malignant pleural mesothelioma. *J Thorac Oncol* 13: 124 – 133

Pauli C, Hopkins BD, Prandi D, Shaw R, Fedrizzi T, Sboner A, Sailer V, Augello M, Puca L, Rosati R *et al* (2017) Personalized *in vitro* and *in vivo* cancer models to guide precision medicine. *Cancer Discov* 7: 462 – 477

Pfaffl MW (2001) A new mathematical model for relative quantification in real-time RT-PCR. *Nucleic Acids Res* 29: e45

Poole JC, Wu S-F, Lu TT, Vibat CRT, Pham A, Samuelsz E, Patel M, Chen J, Daher T, Singh VM *et al* (2019) Analytical validation of the target selector ctDNA platform featuring single copy detection sensitivity for clinically actionable EGFR, BRAF, and KRAS mutations. *PLoS One* 14: e0223112

Quetel L, Meiller C, Assié J-B, Blum Y, Imbeaud S, Montagne F, Tranchant R, Wolf J, Caruso S, Copin M-C *et al* (2020) Genetic alterations of malignant pleural mesothelioma: association with tumor heterogeneity and overall survival. *Mol Oncol* 14: 1207 – 1223

Robinson BW, Musk AW, Lake RA (2005) Malignant mesothelioma. *Lancet* 366: 397 – 408

Robinson JT, Thorvaldsdóttir H, Winckler W, Guttman M, Lander ES, Getz G, Mesirov JP (2011) Integrative genomics viewer. *Nat Biotechnol* 29: 24

Rusch VW, Chansky K, Kindler HL, Nowak AK, Pass HI, Rice DC, Shemanski L, Galateau-Sallé F, McCaughan BC, Nakano T *et al* (2016) The IASLC mesothelioma staging project: proposals for the M descriptors and for revision of the TNM stage groupings in the forthcoming (Eighth) edition of the TNM classification for mesothelioma. *J Thorac Oncol* 11: 2112 – 2119

Ryman-Rasmussen JP, Cesta MF, Brody AR, Shipley-Phillips JK, Everitt JI, Tewksbury EW, Moss OR, Wong BA, Dodd DE, Andersen ME *et al* (2009) Inhaled carbon nanotubes reach the subpleural tissue in mice. *Nat Nanotechnol* 4: 747–751

Ryu JS, Ryu HJ, Lee SN, Memon A, Lee SK, Nam HS, Kim HJ, Lee KH, Cho JH, Hwang SS (2014) Prognostic impact of minimal pleural effusion in non-small-cell lung cancer. *J Clin Oncol* 32: 960–967

Sanchez-Vega F, Mina M, Armenia J, Chatila WK, Luna A, La KC, Dimitriadoy S, Liu DL, Kantheti HS, Saghafinia S *et al* (2018) Oncogenic signaling pathways in the cancer genome atlas. *Cell* 173: 321–337

Scherpereel A, Astoul P, Baas P, Berghmans T, Clayson H, de Vuyst P, Dienemann H, Galateau-Salle F, Hennequin C, Hillerdal G *et al* (2010) Guidelines of the European Respiratory Society and the European Society of Thoracic Surgeons for the management of malignant pleural mesothelioma. *Eur Respir J* 35: 479–495

Scherpereel A, Wallyn F, Albelda SM, Munck C (2018) Novel therapies for malignant pleural mesothelioma. *Lancet Oncol* 19: e161–e172

Schindelin J, Arganda-Carreras I, Frise E, Kaynig V, Longair M, Pietzsch T, Preibisch S, Rueden C, Saalfeld S, Schmid B *et al* (2012) Fiji: an open-source platform for biological-image analysis. *Nat Methods* 9: 676–682

Shukuya T, Serizawa M, Watanabe M, Akamatsu H, Abe M, Imai H, Tokito T, Ono A, Taira T, Kenmotsu H *et al* (2014) Identification of actionable mutations in malignant pleural mesothelioma. *Lung Cancer* 86: 35–40

Smeele P, d'Almeida SM, Meiller C, Chéné A-L, Liddell C, Cellerin L, Montagne F, Deshayes S, Benziane S, Copin M-C *et al* (2018) Brain-derived neurotrophic factor, a new soluble biomarker for malignant pleural mesothelioma involved in angiogenesis. *Mol Cancer* 17: 148

Smith JC, Sheltzer JM (2018) Systematic identification of mutations and copy number alterations associated with cancer patient prognosis. *Elife* 7: e39217

Spella M, Lilis I, Pepe MAA, Chen Y, Armaka M, Lamort A-S, Zazara DE, Roumelioti F, Vreka M, Kanellakis NI *et al* (2019) Club cells form lung adenocarcinomas and maintain the alveoli of adult mice. *Elife* 8: e45571

Stathopoulos GT, Zhu Z, Everhart MB, Kalomenidis I, Lawson WE, Bilaceroglu S, Peterson TE, Mitchell D, Yull FE, Light RW *et al* (2006) Nuclear factor-kappaB affects tumor progression in a mouse model of malignant pleural effusion. *Am J Respir Cell Mol Biol* 34: 142–150

Stathopoulos GT, Kanellakis NI, Pepe M (2017) Gene Expression Omnibus GSE94415: Transcriptomic profiling of KPM cell lines through RNA-Seq (https://www.ncbi.nlm.nih.gov/geo/query/acc.cgi?acc=GSE94415). [DATASET]

Stephen AG, Esposito D, Bagni RK, McCormick F (2014) Dragging ras back in the ring. *Cancer Cell* 25: 272–281

Stott FJ, Bates S, James MC, McConnell BB, Starborg M, Brookes S, Palmero I, Ryan K, Hara E, Vousden KHJ *et al* (1998) The alternative product from the human CDKN2A locus, p14(ARF), participates in a regulatory feedback loop with p53 and MDM2. *EMBO J* 17: 5001–5014

Subramanian A, Tamayo P, Mootha VK, Mukherjee S, Ebert BL, Gillette MA, Paulovich A, Pomeroy SL, Golub TR, Lander ES *et al* (2005) Gene set enrichment analysis: a knowledge-based approach for interpreting genome-wide expression profiles. *Proc Natl Acad Sci USA* 102: 15545–15550

Thomas R, Fysh ETH, Smith NA, Lee P, Kwan BCH, Yap E, Horwood FC, Piccolo F, Lam DCL, Garske LA *et al* (2017) Effect of an indwelling pleural catheter vs talc pleurodesis on hospitalization days in patients with malignant pleural effusion: the AMPLE randomized clinical trial. *JAMA* 318: 1903–1912

Tikoo A, Varga M, Ramesh V, Gusella J, Maruta H (1994) An anti-Ras function of neurofibromatosis type 2 gene product (NF2/Merlin). *J Biol Chem* 269: 23387–23390

Tsao AS, Wistuba I, Roth JA, Kindler HL (2009) Malignant pleural mesothelioma. *J Clin Oncol* 27: 2081–2090

Westbom CM, Shukla A, MacPherson MB, Yasewicz EC, Miller JM, Beuschel SL, Steele C, Pass HI, Vacek PM, Shukla A (2014) CREB-induced inflammation is important for malignant mesothelioma growth. *Am J Pathol* 184: 2816–2827

Xu J, Kadariya Y, Cheung M, Pei J, Talarchek J, Sementino E, Tan Y, Menges CW, Cai KQ, Litwin S *et al* (2014) Germline mutation of Bap1 accelerates development of asbestos-induced malignant mesothelioma. *Cancer Res* 74: 4388–4397

Yap TA, Aerts JG, Popat S, Fennell DA (2017) Novel insights into mesothelioma biology and implications for therapy. *Nat Rev Cancer* 17: 475–488

Zalcman G, Mazieres J, Margery J, Greillier L, Audigier-Valette C, Moro-Sibilot D, Molinier O, Corre R, Monnet I, Gounant V *et al* (2016) French Cooperative Thoracic Intergroup (IFCT). Bevacizumab for newly diagnosed pleural mesothelioma in the Mesothelioma Avastin Cisplatin Pemetrexed Study (MAPS): a randomised, controlled, open-label, phase 3 trial. *Lancet* 387: 1405–1414

Zimmermann G, Papke B, Ismail S, Vartak N, Chandra A, Hoffmann M, Hahn SA, Triola G, Wittinghofer A, Bastiaens PIH *et al* (2013) Small molecule inhibition of the KRAS-PDEδ interaction impairs oncogenic KRAS signalling. *Nature* 497: 638–642

# Paper II

Reproduced with permission of the ERS 2023: European Respiratory Journal 60 (1) 2101674; doi: 10.1183/13993003.01674-2021 Published 7 July 2022

EUROPEAN RESPIRATORY JOURNAL
ORIGINAL RESEARCH ARTICLE
A-S. LAMORT ET AL.

## Prognostic phenotypes of early-stage lung adenocarcinoma

Anne-Sophie Lamort[1,2,9], Jan Christian Kaiser[3,9], Mario A.A. Pepe[1,2], Ioannis Lilis[4], Giannoula Ntaliarda[4], Kalman Somogyi[2,5], Magda Spella[4], Sabine J. Behrend[1,2], Georgia A. Giotopoulou[1,2], Willem Kujawa[1,2], Michael Lindner[2,6], Ina Koch[2,6], Rudolf A. Hatz[2,6], Juergen Behr[2,7], Rocio Sotillo[2,5,8], Andrea C. Schamberger[1,2] and Georgios T. Stathopoulos[1,2,9]

[1]Comprehensive Pneumology Center (CPC) and Institute for Lung Biology and Disease (iLBD), Helmholtz Center Munich–German Research Center for Environmental Health (HMGU), Munich, Germany. [2]German Center for Lung Research, Giessen, Germany. [3]Institute of Radiation Medicine (IRM), Helmholtz Center Munich–German Research Center for Environmental Health (HMGU), Neuherberg, Germany. [4]Dept of Physiology, Faculty of Medicine, University of Patras, Rio, Greece. [5]Division of Molecular Thoracic Oncology, German Cancer Research Center (DKFZ), Heidelberg, Germany. [6]Center for Thoracic Surgery Munich, Ludwig Maximilian University of Munich and Asklepios Medical Center, Gauting, Germany. [7]Dept of Medicine V, University Hospital, Ludwig Maximilian University of Munich, Munich, Germany. [8]Translational Lung Research Center Heidelberg (TRLC), German Center for Lung Research (DZL), Heidelberg, Germany. [9]These authors contributed equally to this work.

Corresponding author: Georgios T. Stathopoulos (stathopoulos@helmholtz-muenchen.de)

Shareable abstract (@ERSpublications)
**Clinical-grade immunodetection of TP53, NF1, CD45, PD-1, PCNA, TUNEL and FVIII in tumour samples identifies two phenotypes of resected lung adenocarcinomas that display different prognosis and can be used for patient management and trial design** https://bit.ly/3DpM5Ll

**Cite this article as:** Lamort A-S, Kaiser JC, Pepe MAA, *et al*. Prognostic phenotypes of early-stage lung adenocarcinoma. *Eur Respir J* 2022; 60: 2101674 [DOI: 10.1183/13993003.01674-2021].



This article has an editorial commentary: https://doi.org/10.1183/13993003.00569-2022

Received: 14 June 2021
Accepted: 11 Nov 2021

### Abstract

***Background*** Survival after curative resection of early-stage lung adenocarcinoma (LUAD) varies and prognostic biomarkers are urgently needed.

***Methods*** Large-format tissue samples from a prospective cohort of 200 patients with resected LUAD were immunophenotyped for cancer hallmarks TP53, NF1, CD45, PD-1, PCNA, TUNEL and FVIII, and were followed for a median of 2.34 (95% CI 1.71–3.49) years.

***Results*** Unsupervised hierarchical clustering revealed two patient subgroups with similar clinicopathological features and genotype, but with markedly different survival: "proliferative" patients (60%) with elevated TP53, NF1, CD45 and PCNA expression had 50% 5-year overall survival, while "apoptotic" patients (40%) with high TUNEL had 70% 5-year survival (hazard ratio 2.23, 95% CI 1.33–3.80; p=0.0069). Cox regression and machine learning algorithms including random forests built clinically useful models: a score to predict overall survival and a formula and nomogram to predict tumour phenotype. The distinct LUAD phenotypes were validated in The Cancer Genome Atlas and KMplotter data, and showed prognostic power supplementary to International Association for the Study of Lung Cancer tumour–node–metastasis stage and World Health Organization histologic classification.

***Conclusions*** Two molecular subtypes of LUAD exist and their identification provides important prognostic information.

### Introduction

Lung adenocarcinoma (LUAD), the most frequent histologic subtype of lung cancer, accounts for an estimated 1 million annual deaths [1, 2]. Although surgical resection remains the preferred definitive cure for early-stage LUAD [3], survival thereafter is highly variable, necessitating the development and validation of prognostic biomarkers [4]. Such biomarkers can be clinicopathological features [5–7], genomic alterations [8–12], gene expression profiles [13, 14], imaging characteristics [15, 16] and immunohistochemical expression of single markers [17–22]. However, no biomarker to date has found widespread applicability. Patients with resectable LUAD are currently treated with (neo)adjuvant chemotherapy, radiotherapy, targeted therapy and/or immunotherapy dictated by tumour–node–metastasis (TNM) stage and driver mutations, and are followed in a uniform fashion [3, 9–12]. This is in contrast to other cancer types, where immunodetection of key tumour hallmarks dictates therapy and prognosis. For

example, immunohistochemistry (IHC) expression of marker of proliferation Ki-67 and oestrogen, progesterone and epidermal growth factor type 2 receptors dictate treatment and prognosis in breast cancer [23].

Here, we analysed 200 patients with resected LUAD [7] using conventional (non-tissue microarray-based) IHC of large, representative tumour tissue areas and a clinical-grade scoring system for cancer hallmarks [24] tumour protein 53 (TP53), neurofibromatosis 1 (NF1), cluster of differentiation 45 (CD45), programmed cell death-1 (PD-1), proliferating cell nuclear antigen (PCNA), terminal deoxynucleotidyl nick-end labelling (TUNEL) and anti-haemophilic factor (FVIII). We followed patients for prolonged periods of time (cumulative/median follow-up 507/2.34 (95% CI 1.71–3.49) years) to discover two phenotypes of LUAD with markedly different overall survival. These phenotypes were validated in two independent datasets. Clinicians are provided with tools to predict LUAD phenotype and with proposals for their potential clinical implementation.

## Materials and methods

Research resources are listed using Research Resource Identifiers (RRIDs) (https://scicrunch.org/resources) and CAS Registry Numbers (www.cas.org/cas-data/cas-registry), where appropriate.

### *Study design*

The present study was conducted in accordance with the Helsinki Declaration, was prospectively approved by the Ludwig Maximilian University of Munich Ethics Committee (623-15) and was registered at the German Clinical Trials Register (DRKS00012649). All patients gave written informed consent.

During 2011–2017, 200 patients with full clinical data and ample available tissues were recruited for the present study, designed to reflect the whole cohort of 366 patients [7] (supplementary table E1) and to detect medium effect sizes (d=0.25) with $\alpha$=0.05 and $\beta$=0.90 using G*Power academic software (www.psychologie.hhu.de/arbeitsgruppen/allgemeine-psychologie-und-arbeitspsychologie/gpower; RRID:SCR_013726).

### *Patient data and tumour samples*

Anonymised data and samples were comprehensively reviewed by a dedicated panel (A-S.L., J.C.K., M.A. A.P., S.J.B., G.A.G., A.C.S., M.L., I.K., R.A.H., J.B. and G.T.S.), including International Association for the Study of Lung Cancer (IASLC) TNM stage (the 7th edition (TNM7) was used due to the timing of the study) [25], World Health Organization (WHO) histologic growth pattern (the 2015 classification was used) [2, 5] and "spread through air spaces" (STAS) [26–28]. Tissue samples were cut into two equal parts for IHC and for DNA/RNA extraction using guanidinium thiocyanate–phenol–chloroform extraction (TRIzol; Thermo Fisher, Waltham, MA, USA).

### *IHC and TUNEL*

Tissues were formalin-fixed (CAS 50-00-0) and paraffin-embedded (CAS 8002-74-2), cut into serial tissue sections (5 µm thick), and stained with primary antibodies and their corresponding horseradish peroxidase-linked secondary antibodies (supplementary table E2). For negative controls, primary antibodies were omitted. TUNEL was performed with the Click-iT TUNEL kit (Thermo Fisher). For negative controls, dUTP (CAS 94736-09) was omitted. Slides were counterstained with haematoxylin (Roth, Karlsruhe, Germany; CAS 517-28-2) and coverslipped using Entellan (Merck, Darmstadt, Germany). 10 different areas of each tumour and five different fields of view of each tissue section were analysed by three trained blinded readers (A-S.L., W.K. and G.T.S.) at low magnification (×20), the percentage of stained cells was semiquantitatively scored as 0 (<5%), 1 (5–24%), 2 (25–49%), 3 (50–74%) or 4 (>74%) on an Eclipse E400 microscope (Nikon, Melville, NY, USA; RRID:SCR_020320) using TCapture software (Tucsen Photonics, Fuzhou, China; RRID:SCR_020956) and the results were averaged by patient, as routinely done and described elsewhere [17–20, 23]. Cancer-specific hallmark expression was also determined in randomly selected paired normal lung tissues (n=50).

### *Digital droplet PCR*

DNA was purified with GenElute Mammalian Genomic DNA Miniprep (Sigma-Aldrich, St Louis, MO, USA), and *KRAS* codon 12/13 and *EGFR* exon 19 were analysed with digital droplet PCR *KRAS* G12/G13 and *EGFR* exon 19 del Screening Kits, respectively, using QuantaSoft Analysis Pro software (Bio-Rad, Hercules, CA, USA). Data were normalised by accepted droplet numbers to yield absolute mutation allelic frequencies; 25% mutant droplets was used as the cut-off to discriminate wild-type from mutant tumours.

### ALK *fusion detection*

50 ng RNA was used for reverse transcription using the Quantitect Reverse Transcription Kit (Qiagen, Hilden, Germany). The manufacturer's protocol was followed, except that 0.25 µL *ALK*-specific reverse

primer (hAlk.cdna.rev1) was added to the primer mix to enrich transcripts carrying the 3′ part of the *ALK* gene. RNA from human cell lines (NCI-H3122, *EML4/ALK* variant 1, RRID:CVCL_5160; NCI-H2228, *EML4/ALK* variant 3, RRID:CVCL_1543) served as positive controls. 10 µL PCR reactions were performed using HotStarTaq Master Mix (Qiagen) and 200 ng cDNA template. PCR products were run on 10% agarose gels. *EML4-ALK*-positive reactions were repeated, and the PCR products were purified and sequenced to confirm *EML4/ALK* transcripts. Variant-specific forward (hEml4.cdna.v1.for1; hEml4.cDNA.v2.for1; hEml4.cdna.v3.for1) and universal reverse (hAlk.cdna.rev2) primer sequences were: hAlk.cdna.rev1, CTCCTTCAGGTCACTGATGG; hAlk.cdna.rev2, TTGCCAGCAAAGCAGTAGTTGG; hEml4.cdna.v1.for1, AGTTTCACCCAACAGATGCAAATACC; hEml4.cdna.v2.for1, TAGATGAACCAGGACACTGTGCAG; hEml4.cdna.v3.for1, AGCCCTCTTCACAACCTCTCC.

### *Computational analyses and statistics*

Statistics and heatmap visualisations were done using R* (www.r-project.org; RRID:SCR_001905) and Prism version 8.0 (GraphPad, San Diego, CA, USA; RRID:SCR_002798). Unsupervised hierarchical clustering was performed using Euclidean distance and clustering method "ward.D2" on the R* package pheatmap (RRID:SCR_016418). To investigate predictors of overall survival and prevalence of the proliferative phenotype, a combination of machine learning and regression techniques was applied. Kaplan–Meier, Cox regression and random forests were selected to determine optimal cut-offs and overall survival at different end-points (1 and 3 years). Random forests were grown using the R* package randomforestSRC (RRID:SCR_015718). Covariables for further regression analysis were confirmed based on mean decreased accuracy. From simulated random forests, nonparametric estimates of probabilities for overall survival depending on pertinent covariables (TP53, NF1, CD45, PD-1, PCNA, TUNEL and FVIII) were derived. Partial probability estimates were generated by focusing on a single covariable of interest for which the influence of the remaining covariables was averaged out by summation. Random forest results were used to obtain suggestions for pertinent covariables, to guide the introduction of nonlinear categorical dependencies, and to produce a formula and a nomogram for single-patient phenotype prediction. Overall survival analyses were done with Kaplan–Meier estimates and Cox regression (RRID:SCR_021137). Moreover, survival objects were formed in R* based on right-censored follow-up and survival status which were used in random forest generation and Cox regression. The quality of data explanation for random forests was judged by area under the curve (AUC) in classification mode. However, random forests were mainly applied to guide the regression analysis and not for rigorous prediction assessment. Finally, the preferred regression models were chosen based on goodness-of-fit measured by the Akaike Information Criterion (AIC) and biological plausibility. To characterise the predictive power of a given model, the AUC for logistic regression and the integrated AUC (or concordance) for Cox regression were reported. Associations between variables were examined using Mann–Whitney tests, two-way ANOVA with Šídák's post-tests, Chi-squared tests, Fischer's exact tests and Spearman's correlations. Two-tailed probabilities $p<0.05$ were considered significant. Graphs and tables were generated in Prism version 8.0 and Excel (Microsoft, Redmond, WA, USA).

## Results

We selected 200 patients with complete clinical information and ample LUAD and adjacent lung tissues that were representative of the originating cohort (supplementary table E1) [7]. All 200 large-format tumour samples as well as 50 randomly selected normal tumour-adjacent lung samples were immunolabelled for TP53, NF1, CD45, PD-1, PCNA, TUNEL and FVIII, and 10 independent tumour areas were scored for immunoreactivity on a clinically relevant semiquantitative 0 (none)–4 (highest) scale, using normal lung tissues as background controls. Average relative interobserver variability was <5% for any blinded reader comparison and the three scores for each sample/marker were averaged. Raw data are given in supplementary figure E1 and supplementary table E3.

All seven cancer hallmarks were overexpressed in tumour compared with adjacent lung tissues (figure 1). Unsupervised hierarchical clustering of IHC data alone using Euclidean metrics identified two patient clusters: a majority cluster highly expressing the intercorrelated markers TP53, NF1, CD45 and PCNA comprised of 121 (60%) patients (hereafter called "proliferative") and a minority highly TUNEL-labelled cluster encompassing 79 (40%) patients (hereafter called "apoptotic") (figure 2a and b, and supplementary figure E2). Interestingly, cancer hallmark IHC and the two patient clusters were only marginally or not at all correlated with clinicopathological variables (including sex, smoking status, chronic obstructive pulmonary disease stage, histologic growth pattern, STAS, pathologic TNM7 stage and oncogene status), likely reflecting something novel (figure 2b and c, and supplementary figures E3 and E4). Importantly, proliferative compared with apoptotic patients displayed markedly decreased overall survival (5-year survival 50% *versus* 70%, respectively; hazard ratio (HR) 2.23, 95% CI 1.33–3.80; log-rank p=0.0069), while STAS and mutation status had no impact on overall survival (figure 2d). To validate the existence of

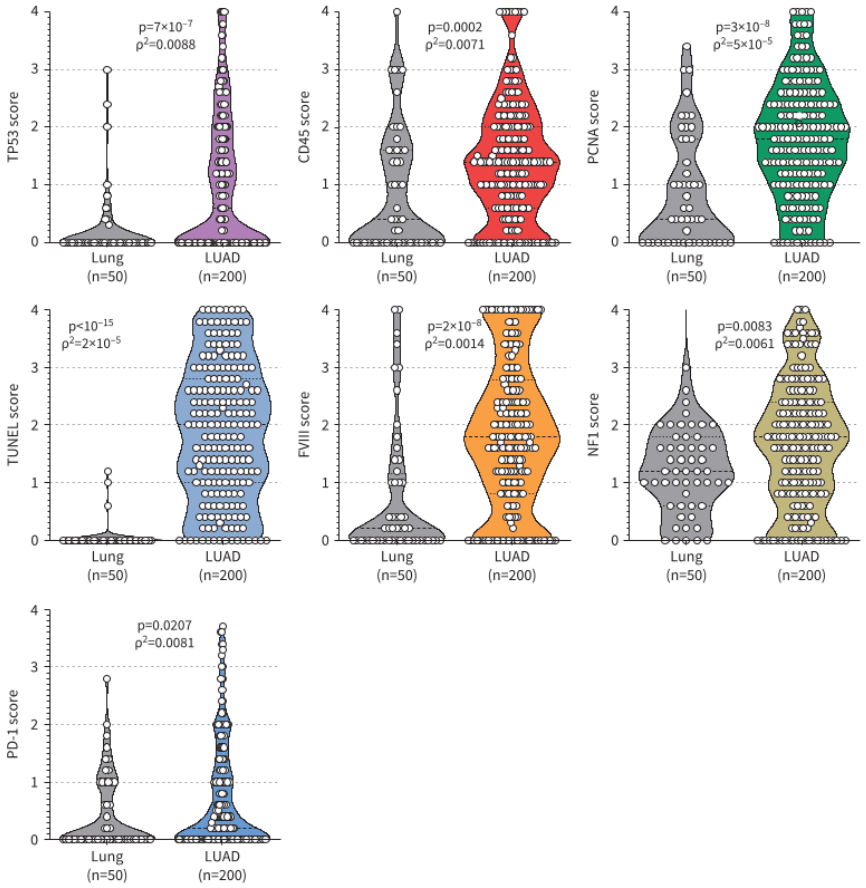


**FIGURE 1** Immunophenotyping of early-stage lung adenocarcinoma (LUAD) (n=200) and randomly selected adjacent normal lung tissues (n=50) for seven cancer hallmarks. Data are shown as raw data points (circles) on a semiquantitative scale from 0 (no expression) to 4 (highest expression), rotated kernel density distributions (violins), medians (dashed lines), quartiles (dotted lines), patient numbers (n), p-values (Mann–Whitney test) and squared Spearman's correlation coefficients ($\rho^2$) for n=50 tumour–normal tissue pairs. Note that all seven cancer hallmarks are overexpressed in cancerous compared with adjacent tissues and that expression values between the two compartments are not correlated. TP53: tumour protein 53; CD45: cluster of differentiation 45; PCNA: proliferating cell nuclear antigen; TUNEL: terminal deoxynucleotidyl transferase dUTP nick-end labelling; FVIII: coagulation factor VIII; NF1: neurofibromatosis 1; PD-1: programmed cell death protein 1.

these two molecular LUAD phenotypes, we analysed The Cancer Genome Atlas LUAD pan-cancer data (https://bit.ly/3blzgFp), which include reverse-phase protein assay data for TP53 and PCNA (but none of the other markers) from 340 patients [29]. Similar to our findings, TP53 and PCNA protein expression were tightly correlated, unsupervised hierarchical clustering identified two patient clusters with high (n=134 (39%)) and low (n=206 (61%)) TP53/PCNA expression ratios, and patients with a high PCNA/TP53 expression ratio displayed significantly worse overall survival (figure 3). Collectively, these results suggest the existence of two LUAD phenotypes, *i.e.* proliferative and apoptotic, in two independent patient cohorts (figure 4a).

We next analysed the impact of individual cancer hallmarks on overall survival using univariate Kaplan–Meier estimates of our cohort stratified by optimal cut-offs defined by the KMplotter custom module (http://kmplot.com/analysis/index.php?p=service&cancer=custom_plot), performed multivariate Cox

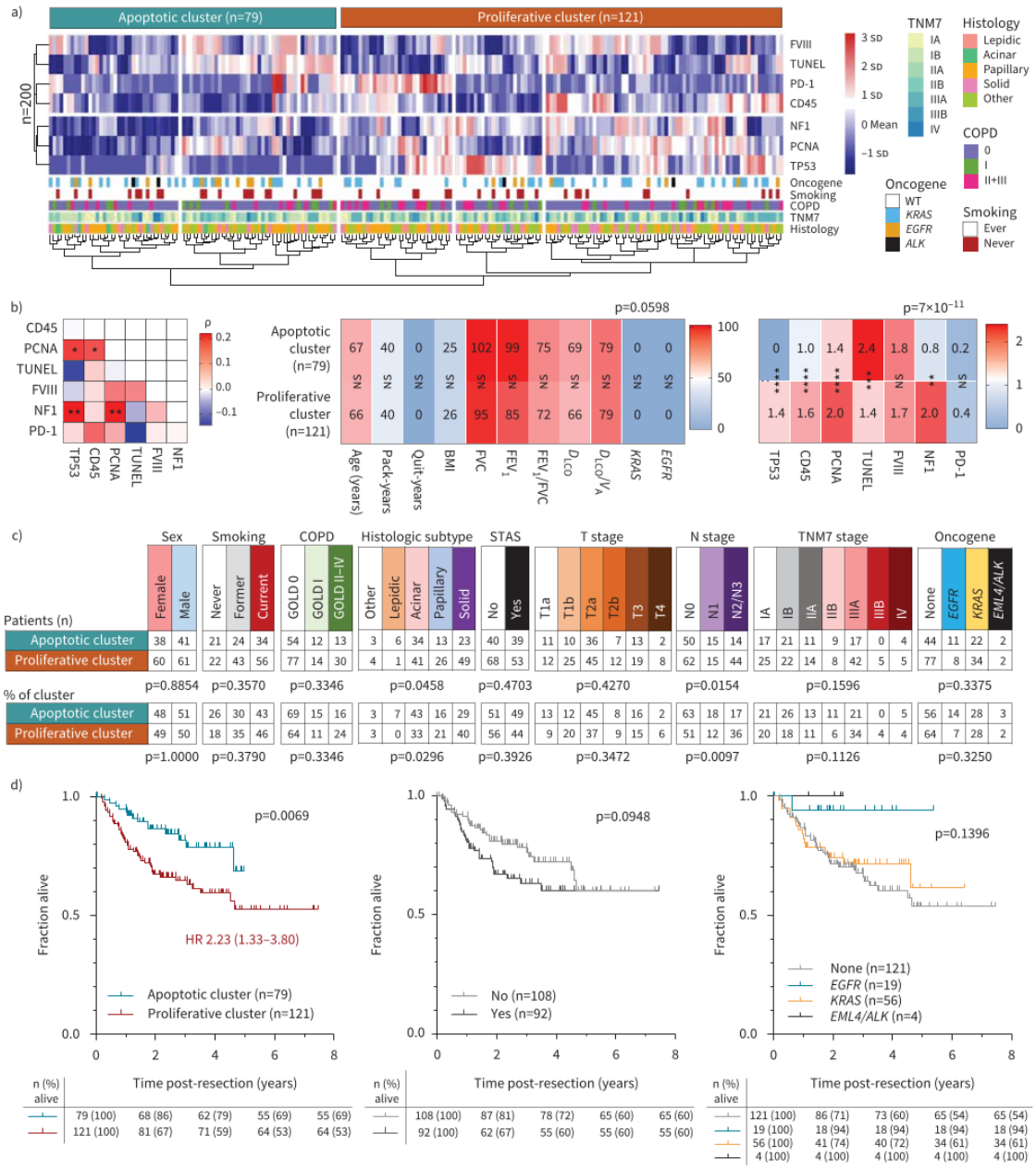


**FIGURE 2** Two patient clusters of early-stage lung adenocarcinoma (LUAD) with markedly different survival. a) Heatmap shows unsupervised hierarchical clustering of n=200 patients by immunohistochemistry of tumour tissues for seven cancer hallmarks. Each column represents one patient and each row represents one marker. b) Heatmaps show Spearman's correlation coefficients (ρ) between immunoreactivity for the seven markers (left), as well as median parametric clinical variables (middle) and median marker expression (right) for proliferative and apoptotic patient clusters. Data are shown as ρ (left) and median values (middle and right), patient numbers (n), and p-values (two-way ANOVA). Left: *: p<0.05; **: p<0.01, Spearman's correlation. Middle and right: NS: nonsignificant (p>0.05); **: p<0.01; ***: p<0.001; ****: p<0.0001, for comparison between the two clusters (Šídák's post-test). c) Cross-tabulations of proliferative and apoptotic cluster patient numbers (n) and percentages (%) stratified by nonparametric variables, with p-values (Chi-squared test or Fischer's exact test). d) Overall survival of all patients stratified by immunophenotypic

cluster (left), "spread through air spaces" (STAS) (middle) and oncogene status (right). Data are shown as patient numbers (n), Kaplan–Meier survival estimates (lines), censored observations (line marks), survival tables, hazard ratio (95% CI) and log-rank p-values. FVIII: coagulation factor VIII; TUNEL: terminal deoxynucleotidyl transferase dUTP nick-end labelling; PD-1: programmed cell death protein 1; CD45: cluster of differentiation 45; NF1: neurofibromatosis 1; PCNA: proliferating cell nuclear antigen; TP53: tumour protein 53; COPD: chronic obstructive pulmonary disease; TNM: tumour–node–metastasis; WT: wild-type; BMI: body mass index ($kg \cdot m^{-2}$); FVC: forced vital capacity (% pred); $FEV_1$: forced expiratory volume in 1 s (% pred); $D_{LCO}$: diffusing capacity of the lung for carbon monoxide (% pred); $V_A$: alveolar volume (L); GOLD: Global Initiative for Chronic Obstructive Lung Disease.

regression and grew random forests. High TP53 and PCNA expression emerged as significant predictors of worse overall survival by all three methods, while high CD45 expression was associated with worse overall survival on Cox and random forest analyses (figure 4b–e). Importantly, TP53, PCNA and CD45 competed with important clinicopathological predictors of overall survival identified previously in several independent cohorts, such as T and N stage and histologic growth pattern, as well as patient age, lung function and smoking status (figure 4f) [4–7]. In addition to TP53, PCNA and CD45, there was also a trend for the remaining cancer hallmarks to impact overall survival (figure 5a, graphs). These findings show that IHC-assessed expression of stand-alone cancer hallmarks, especially TP53, PCNA and CD45, possesses some weak prognostic power for incipient overall survival of resected LUAD.

To improve the prognostic power of individual cancer hallmarks and to provide clinicians with a tool to manage individual patients, all cancer hallmarks were incorporated in an unweighted immunophenotypic LUAD death score ($LADERS_{IMM}$), in homology to a clinical LUAD death score ($LADERS_{CLIN}$) developed previously [7], according to cut-offs determined by a single method or a combination of methods (figure 5a, table). We designed $LADERS_{IMM}$ for easy clinical implementation on any individual patient, by incorporating high expression of TP53, NF1, CD45, PCNA and FVIII as predictors of worse overall survival and of TUNEL and PD-1 as predictors of better overall survival. Indeed, 66 patients with high $LADERS_{IMM}$ (5–6 points) had 5-year overall survival of 43%, while 118 patients with intermediate $LADERS_{IMM}$ (3–4 points) 61% and 16 patients with low $LADERS_{IMM}$ (0–2 points) 100%, with 2–3-fold hazard ratios for every low-to-intermediate-to-high $LADERS_{IMM}$ increment (figure 5b and c). When $LADERS_{IMM}$ and $LADERS_{CLIN}$ (a survival score that incorporates age, lung function, N stage, time from diagnosis to resection and histologic growth pattern, and that outperforms TNM7 stage in predicting survival) [7] were compared by correlation, linear regression and κ statistic of agreement, they were only weakly related, hence they are positioned to synergise in predicting overall survival (figure 5d). To this end, 73 patients with intermediate or high values (≥3) for both scores had 25% 5-year overall survival, while the remaining 127 patients had >75% 5-year overall survival, for a >5-fold hazard ratio (figure 5e). These data support the clinical applicability of $LADERS_{IMM}$ alone or in combination with TNM stage and other clinicopathological prognosticators of overall survival in patients with resected LUAD. To validate $LADERS_{IMM}$, mRNA expression data for the seven cancer hallmarks TP53, NF1, CD45, PD-1, PCNA, TUNEL and FVIII were sought in the KMplotter lung cancer module (https://kmplot.com/analysis/index.php?p=service&cancer=lung). When good probes for our markers were not available, the most relevant genes were used (*CLTA* for CD45, *SPATA2* for PD-1, *MKI67* for PCNA and apopain/*CASP3* for TUNEL). Again, all markers independently performed similar to our cohort in predicting better or worse overall survival (figure 6a). When their average expression was examined (apopain/*CASP3* and PD-1 were inverted similar to $LADERS_{IMM}$), the combination of cancer hallmarks equivalent to $LADERS_{IMM}$ predicted overall survival in all lung cancers and in LUAD, but not in squamous cell lung carcinoma (figure 6b). Hence, cancer hallmarks TP53, NF1, CD45, PD-1, PCNA, TUNEL and FVIII alone or combined into a score predict overall survival in two independent LUAD patient cohorts. We further compared $LADERS_{IMM}$ with IASLC TNM7 stage and WHO histologic subtype in predicting overall survival using Kaplan–Meier and Cox analyses. $LADERS_{IMM}$ was inferior to TNM7, but superior to WHO histology (figure 7a–c), and its prognostic power was stronger in patients with advanced TNM7 stage or solid growth pattern known to have poor overall survival [2, 5, 25], indicating its complementarity to the TNM7 and WHO classifications.

As opposed to using individual cancer hallmarks to directly predict overall survival, we next examined whether cancer hallmark IHC can be integrally used to identify individual patient phenotype and to indirectly prognose overall survival. Using logistic regression and random forests, all cancer hallmarks except PD-1 predicted phenotype (figure 8a and b). In figure 8c we provide a formula and its performance measures designed for clinical use to predict LUAD phenotype. The formula for Microsoft Excel is $P_{PROLIFERATIVE}$=1/(1+e^(−(−4.9+2.5*TP53+1.9*CD45+1.2*PCNA−1.1*TUNEL−0.7*FVIII+1.7*NF1))), where cancer hallmark scores range from 0 (none) to 4 (highest). For this, we used cross-validation with the leave-one-out method. Cut-off $P_{PROLIFERATIVE}$=0.538 was determined for maximal specificity/

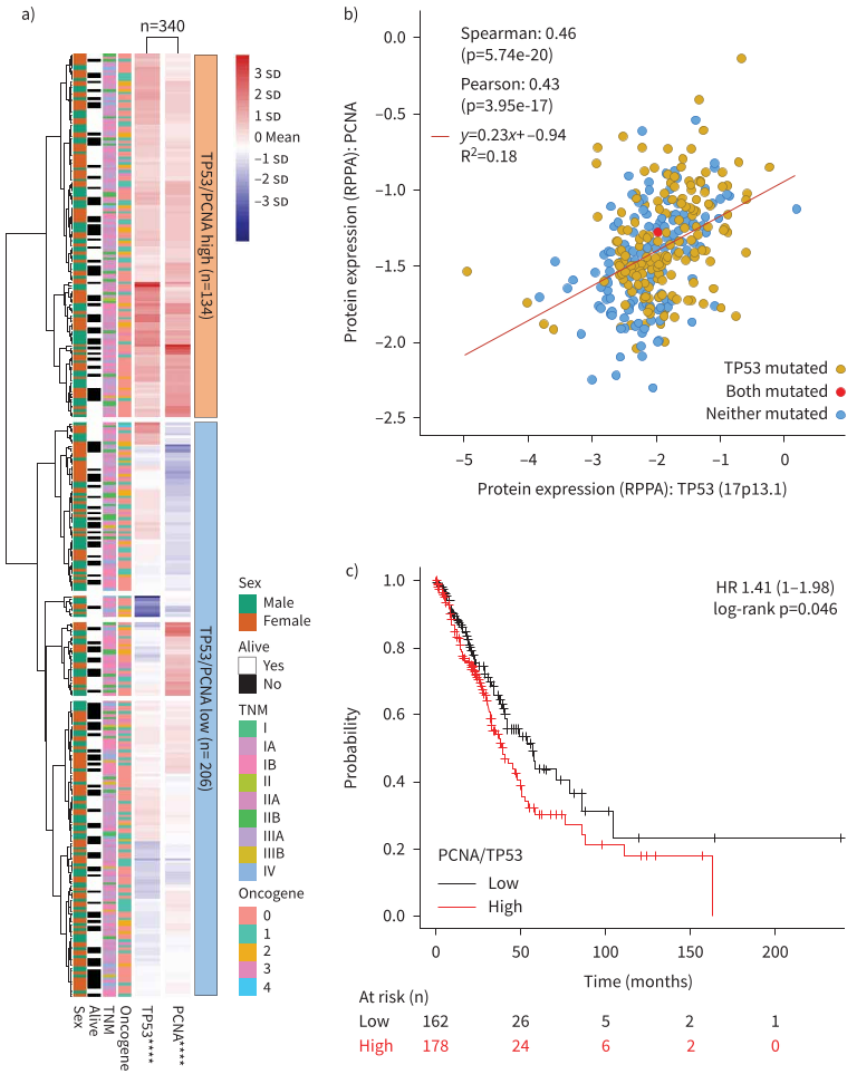


**FIGURE 3** The Cancer Genome Atlas (TCGA) protein data support the existence of two lung adenocarcinoma (LUAD) phenotypes. Tumour protein 53 (TP53) and proliferating cell nuclear antigen (PCNA) protein expression (no others from the selected markers are available) in n=340 patients with LUAD from the TCGA pan-cancer dataset define two patient clusters, are tightly correlated and determine overall survival. Data were retrieved from www.cbioportal.org on 19 March 2021. a) Heatmap shows unsupervised hierarchical clustering of n=340 patients by protein expression of tumour tissues for TP53 and PCNA assessed by reverse-phase protein assay (RPPA). Each row represents one patient and each column represents one marker. ****: p<0.0001, for comparison between the two clusters (Šídák's post-test). b) Correlation and linear regression between TP53 and PCNA protein expression. Shown are raw data points (circles) colour-coded by mutation status, Spearman's correlation coefficients and p-values, as well as linear regression line, formula and p-value. c) Overall survival of all patients stratified by PCNA/TP53 expression ratio. Data are shown as patient numbers (n), Kaplan–Meier survival estimates (lines), censored observations (line marks), survival table, hazard ratio (95% CI) and log-rank p-value. Raw data were analysed using the KMplotter custom module on 19 March 2021 (https://kmplot.com/analysis/index.php?p=service&cancer=custom_plot). TNM: tumour–node–metastasis.

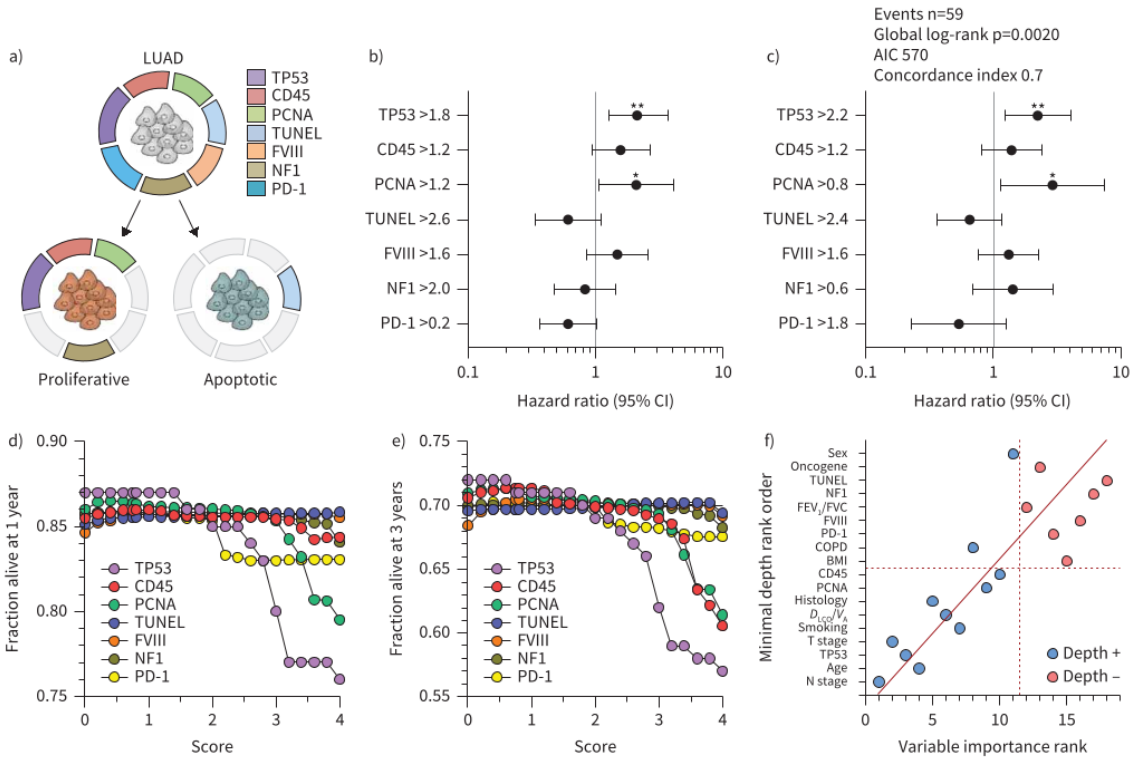


**FIGURE 4** Single-marker analyses targeted at overall survival. a) Schematic of the two identified lung adenocarcinoma (LUAD) phenotypes and their respective cancer hallmark expression patterns. b–f) Overall survival analyses by single-marker cut-offs optimised using b) univariate Kaplan–Meier estimates, c) multivariate Cox regression, d, e) random forest analyses with end-points set at d) 1 year and e) 3 years, and f) variable importance plot of variable importance rank from random forest probability values *versus* minimal depth rank order from logistic regression. Data in b, c) are shown as immunoreactivity cut-offs (*y*-axis numbers) and hazard ratios (95% CI). *: p<0.05; **: p<0.01, compared with hazard ratio=1 (log-rank test in b) and Cox regression in c)). Data in d, e) are shown as probability of overall survival by marker expression. Data in f) are shown as estimates (circles), cut-offs (dashed lines) and regression (solid line). TP53: tumour protein 53; CD45: cluster of differentiation 45; PCNA: proliferating cell nuclear antigen; TUNEL: terminal deoxynucleotidyl transferase dUTP nick-end labelling; FVIII: coagulation factor VIII; NF1: neurofibromatosis 1; PD-1: programmed cell death protein 1; AIC: Akaike Information Criterion; $FEV_1$: forced expiratory volume in 1 s; FVC: forced vital capacity; BMI: body mass index; $D_{LCO}$: diffusing capacity of the lung for carbon monoxide; $V_A$: alveolar volume; T: tumour; N: node.

sensitivity as the median of n=200 $P_{OPTIMAL}$ from cross-validation. $P_{PROLIFERATIVE}$>0.538 means classification of a patient as proliferative, whereas $P_{PROLIFERATIVE}$⩽0.538 means classification of a patient as apoptotic. The formula is visualised as a nomogram (figure 8d) and is easily applicable (patient examples in supplementary figure E5). The receiver operator characteristic curve of the formula (figure 8e) achieves AUC 96%, while the agreement of the formula and nomogram with actual patient phenotype was almost perfect (κ 0.833, 95% CI 0.755–0.912). Formula/nomogram-predicted phenotype significantly affected overall survival, performing equal to actual phenotype (figure 8f). Hence, cancer hallmarks collectively can determine patient phenotype using a formula or a nomogram, indirectly prognosticating overall survival.

## Discussion

Here, we assessed the expression of seven key cancer hallmarks [24] of genomic instability (TP53), KRAS pathway activation (NF1), tumour-associated inflammation (CD45), immune checkpoint activity (PD-1), cellular proliferation (PCNA), tumour cell apoptosis (TUNEL) and angiogenesis (FVIII) in a cohort of patients with early-stage resected LUAD hypothesising that this will aid prognosis. We examined large-format tumour and normal tissues, and applied clinical-grade semiquantitative scoring to multiple

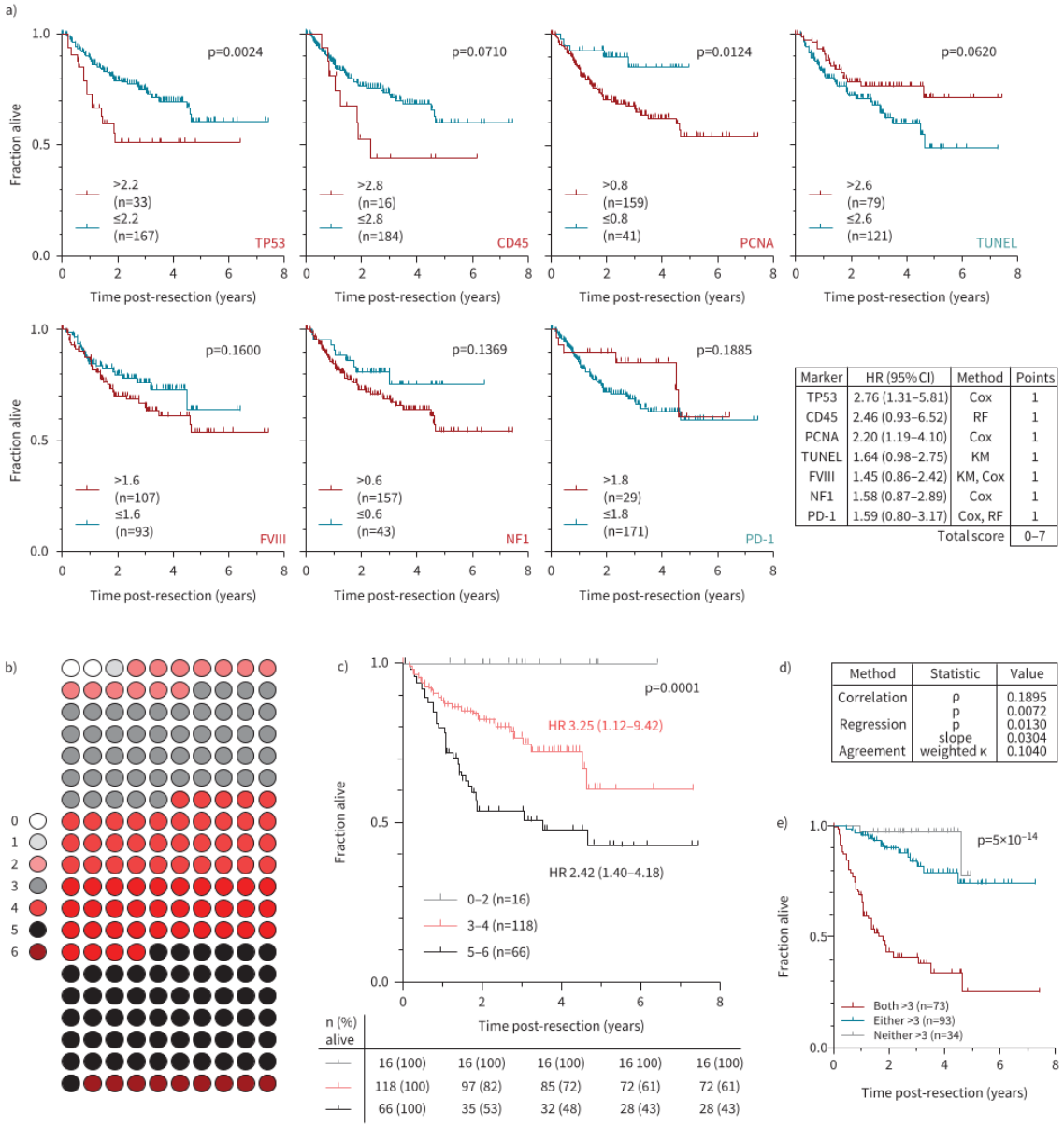


**FIGURE 5** An immunophenotypic score determines survival in lung adenocarcinoma (LUAD). a) Univariate (Kaplan–Meier (KM)), multivariate (Cox) and random forest (RF) survival analyses identified optimised cut-offs of single-marker immunoreactivity. Shown is overall survival of all patients stratified by single-marker immunoreactivity (graphs) and composite immunophenotypic survival score (table). b) Patient distribution by immunophenotypic LUAD death score ($LADERS_{IMM}$). c) Overall survival of all patients stratified by $LADERS_{IMM}$. d) Comparison of $LADERS_{IMM}$ with a previously derived clinical LUAD death score ($LADERS_{CLIN}$) shows that these are only marginally related. Shown are Spearman's correlation coefficient (ρ) and p-value, linear regression p-value and slope, and weighted agreement coefficient (κ). e) Overall survival of all patients stratified by both $LADERS_{IMM}$ and $LADERS_{CLIN}$ [7]. Data in a, c, e) are shown as patient numbers (n), KM survival estimates (lines), censored observations (line marks) and p-values (log-rank test), with or without hazard ratio (95% CI). TP53: tumour protein 53; CD45: cluster of differentiation 45; PCNA: proliferating cell nuclear antigen; TUNEL: terminal deoxynucleotidyl transferase dUTP nick-end labelling; FVIII: coagulation factor VIII; NF1: neurofibromatosis 1; PD-1: programmed cell death protein 1.

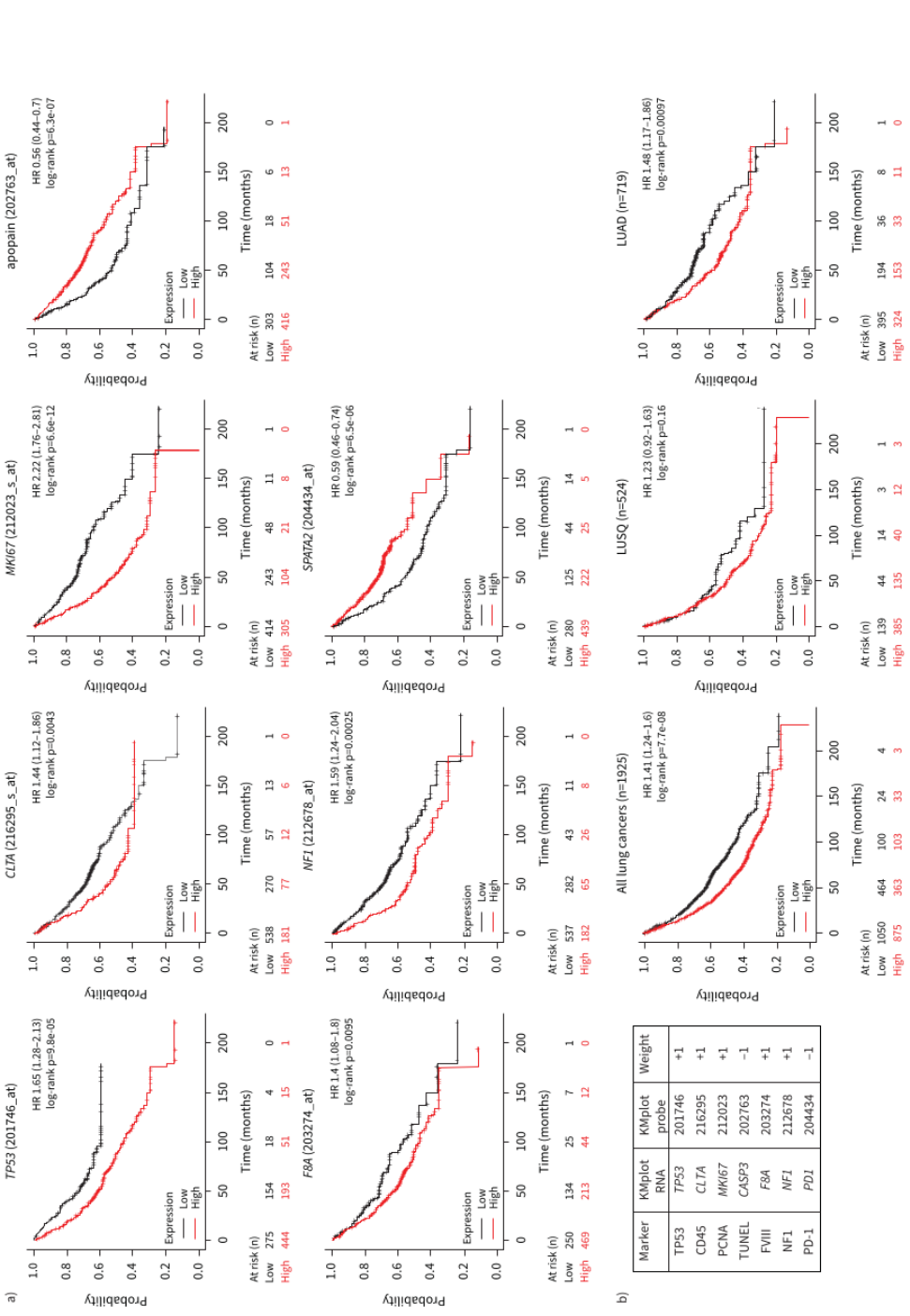


**FIGURE 6** A gene expression profile related to immunophenotype determines survival in lung adenocarcinoma (LUAD). Univariate overall survival analyses by optimised cut-offs of a) LUAD patients by single markers and b) all lung cancer patients by median expression of all markers (apopain and *SPATA2* inverted). Data are shown as patient numbers, Kaplan–Meier survival estimates (lines), censored observations (line marks), survival tables, hazard ratios (95% CI) and log-rank p-values. Data were from the KMplotter lung cancer genechip module (https://kmplot.com/analysis/index.php?p=service&cancer=lung). TP53: tumour protein 53; CD45: cluster of differentiation 45; PCNA: proliferating cell nuclear antigen; TUNEL: terminal deoxynucleotidyl transferase dUTP nick-end labelling; FVIII: coagulation factor VIII; NF1: neurofibromatosis 1; PD-1: programmed cell death protein 1; LUSQ: squamous cell lung carcinoma.

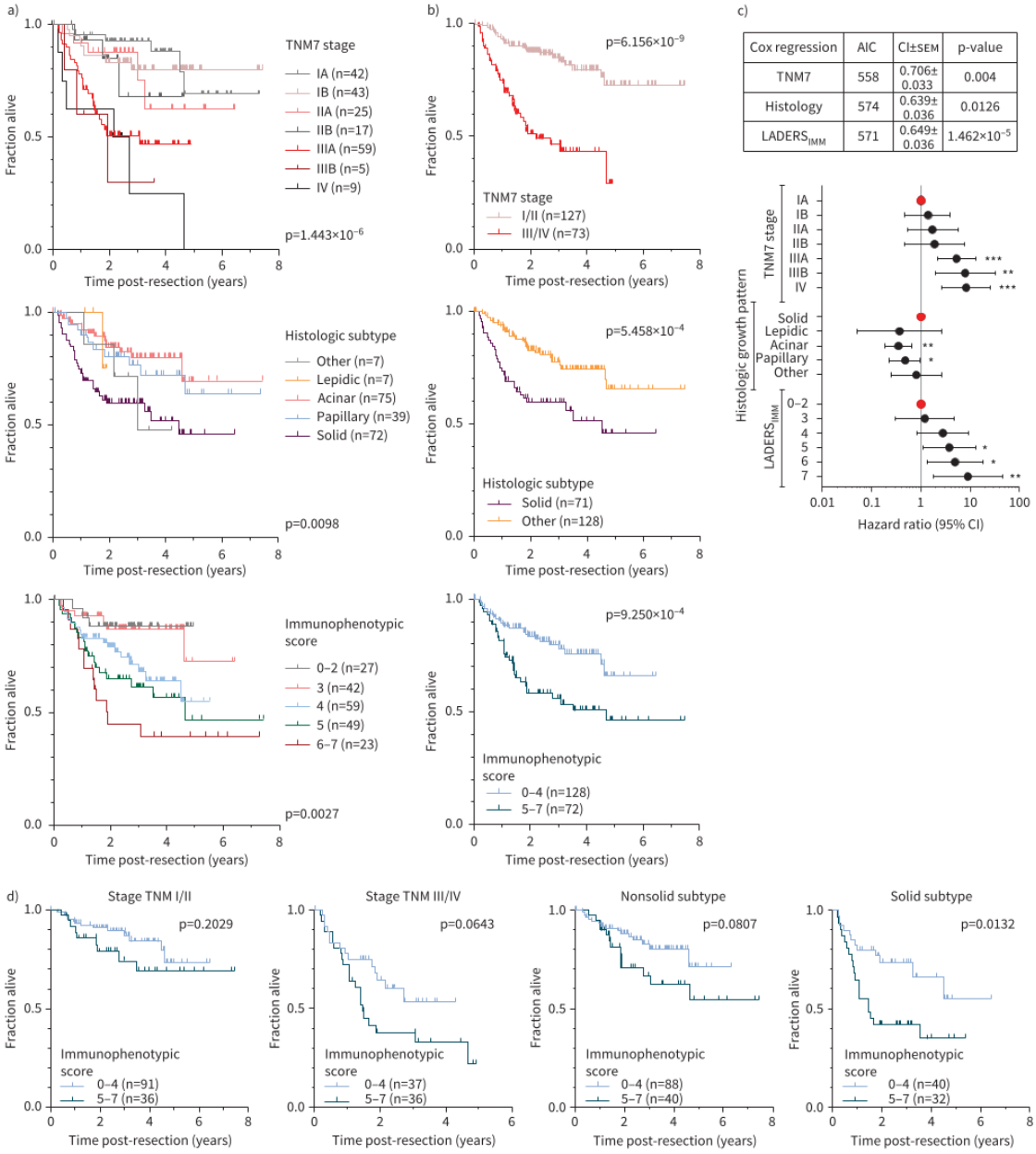


**FIGURE 7** Lung adenocarcinoma (LUAD) immunophenotypic score complements International Association for the Study of Lung Cancer (IASLC) 7th edition tumor–node–metastasis (TNM7) stage and World Health Organization (WHO) histologic subtype. a, b) Overall survival of all patients stratified by TNM7 stage, histologic subtype and immunophenotypic score a) without and b) with category grouping shows that immunophenotypic score outperforms WHO histologic subtype and is outperformed by IASLC TNM7 stage. c) Results of Cox regression using TNM7 stage, histologic growth pattern and immunophenotypic score ($LADERS_{IMM}$) as inputs and overall survival as the target, showing Akaike Information Criterion (AIC), concordance index (CI)±SEM and overall log-rank p-value. *: p<0.05; **: p<0.01; ***: p<0.001, Cox regression. d) Overall survival of early- and advanced-stage patients with solid or other histologic growth patterns stratified by immunophenotype shows the increased value of the latter in advanced and solid disease. Data in a, b, d) are shown as patient numbers (n), Kaplan–Meier survival estimates (lines), censored observations (line marks) and log-rank p-values.

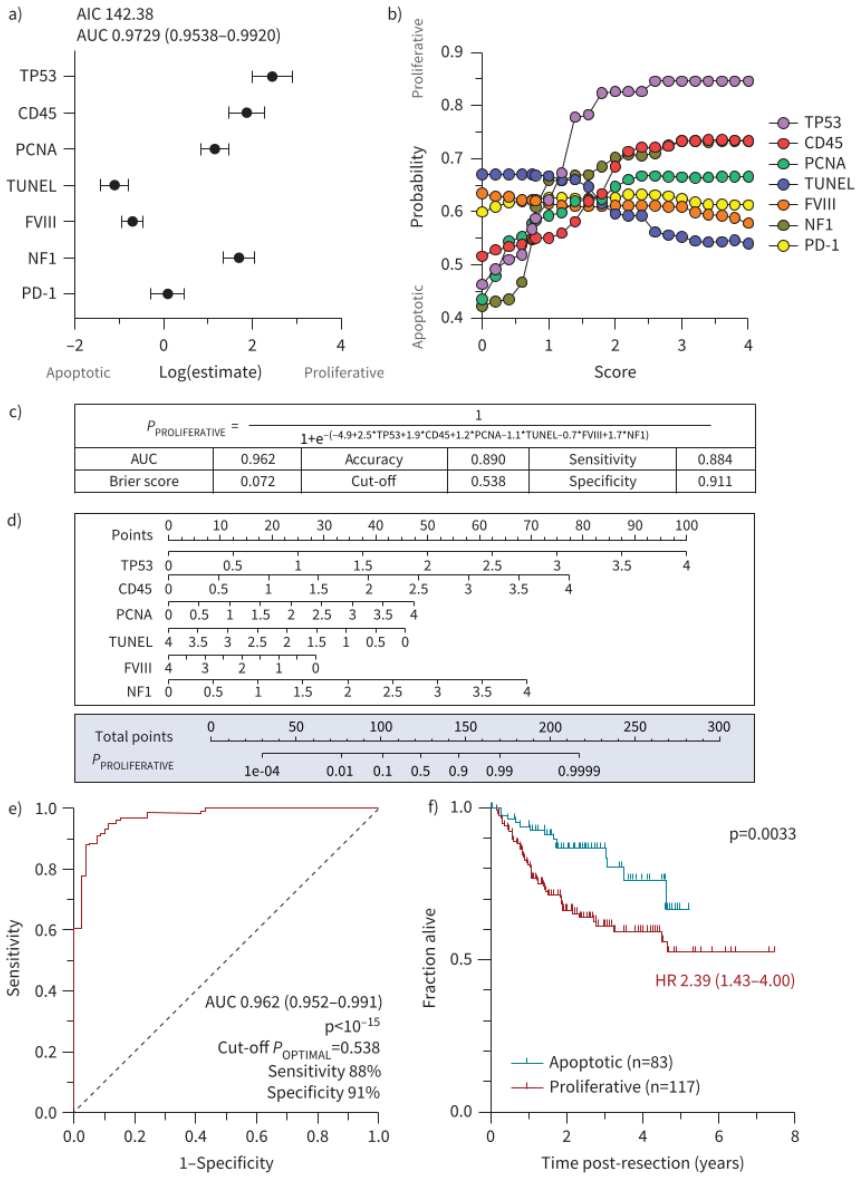


**FIGURE 8** Cancer hallmarks predict lung adenocarcinoma (LUAD) phenotype and overall survival. a, b) Phenotype-predictive power of single cancer hallmarks using a) binary logistic regression and b) random forest analyses. Data in a) are shown as hazard ratios (95% CI), with area under the curve (AUC) (95% CI). c) Formula with its performance measures and d) nomogram for single-patient phenotype prediction by integral cancer hallmark expression. For examples of how to use the formula and nomogram, see the text and supplementary figure E5. e) Receiver operator characteristic of formula/nomogram in LUAD phenotype prediction. f) Overall survival of all patients stratified by formula-predicted phenotype. Data are shown as patient numbers (n), Kaplan–Meier survival estimates (lines), censored observations (line marks), hazard ratio (95% CI) and log-rank p-value. AIC: Akaike Information Criterion; TP53: tumour protein 53; CD45: cluster of differentiation 45; PCNA: proliferating cell nuclear antigen; TUNEL: terminal deoxynucleotidyl transferase dUTP nick-end labelling; FVIII: coagulation factor VIII; NF1: neurofibromatosis 1; PD-1: programmed cell death protein 1.

tumour areas and sections, as is done in routine pathology. Advanced statistics and machine learning identify two LUAD phenotypes solely detectable by cancer hallmarks and not any other clinical, pathological or molecular feature. Proliferative *versus* apoptotic LUAD phenotypes define overall survival to an extent comparable to IASLC TNM7 stage and WHO histologic pattern. A score, a formula and a nomogram to identify LUAD phenotypes and to predict overall survival are provided.

The hallmarks of cancer [24] have streamlined our perceptions of tumour biology, but their clinical impact is still under exploration. Phenotyping of bodily cancers by clinical-grade IHC provides pertinent guidance for treatment and prognosis, with the best example being breast cancer [23]. However, patients with early-stage resectable LUAD are still treated in a uniform fashion, grouped with other nonsmall cell lung tumours [2, 3], despite the fact that multiple studies have found that TNM stage-based overall survival prediction can be enhanced by many clinical, pathological and molecular variables [5–22]. We examined the possibility that LUAD patients might benefit from the current approach to breast cancer, which is treated and prognosticated based on validated molecular variables including IHC expression of marker of proliferation Ki-67 and oestrogen, progesterone and epidermal growth factor type 2 receptors [23]. We designed the present study in order to bridge this gap and investigated the value of IHC for cancer hallmarks in prediction of overall survival of LUAD patients. Indeed, we describe two LUAD phenotypes with markedly divergent overall survival. These proliferative $TP53^{hi}NF1^{hi}CD45^{hi}PCNA^{hi}$ and apoptotic $TUNEL^{hi}$ phenotypes can be discriminated immediately after surgery with 96% accuracy and can accurately predict overall survival. The findings can be readily tested in other cohorts using the score, formula and nomogram provided, and can potentially be incorporated in clinical trial design and/or patient management. For example, the findings can be used to prompt clinical and radiological vigilance for proliferative cases, but also to enhance clinical trial design for novel adjuvant therapies. To this end, we postulate that proliferative and apoptotic patients may exhibit differential therapeutic responses to adjuvant chemotherapy, targeted therapy and immunotherapy post-resection, based on their differential expression of PCNA (a proliferation marker), NF1 (a KRAS inhibitor) and CD45 (an inflammatory marker).

Our findings also trigger mechanistic hypotheses on LUAD evolution. In addition to histologic growth pattern and genomic landscape [5, 9], epidemiological data from atom bomb survivors [30] spark hypotheses on the existence of multiple molecular varieties of LUAD. The results presented here support such hypotheses: two phenotypes of LUAD are discovered solely based on expression of cancer hallmarks, which cannot be identified by driver mutation or any other clinicopathological feature. These phenotypes may be related to early initiating events such as environmental cause, replicative stress and/or cell of origin, or, more likely in our view, to late tumour diversity emanating from divergent mutagenic processes. Whatever the reason for their existence, we provide the means for characterisation of two molecular phenotypes of LUAD, which can be used for clinical management, trial design, as well as mechanistic studies on LUAD pathobiology. Notwithstanding the limitations of the present work, such as the use of an older TNM staging system and of a limited number of markers, future validation and clinical implementation of the proliferative and apoptotic phenotypes of LUAD described here may lead to therapeutic and research innovation.

Author contributions: M. Lindner, I. Koch and R.A. Hatz performed surgeries and procured data that were produced during surgeries. J. Behr performed clinical and physiological assessment. M.A.A. Pepe, M. Spella, I. Lilis, G. Ntaliarda, S.J. Behrend, G.A. Giotopoulou and A.C. Schamberger processed samples and provided important intellectual input. A-S. Lamort and W. Kujawa performed IHC. M.A.A. Pepe performed digital droplet PCR and analysed data; K. Somogyi and R. Sotillo analysed *ALK* fusions. A-S. Lamort, J.C. Kaiser and G.T. Stathopoulos designed and guided the study, analysed data, and wrote the manuscript. All authors critically reviewed and edited the paper for important intellectual content and approved the final submitted version. A-S. Lamort, J.C. Kaiser and G.T. Stathopoulos had full access to all the data of the study, had final responsibility for the decision to submit it for publication and are the guarantors of the study's integrity.

This study is registered at the German Clinical Trials Register with identifier number DRKS00012649.

Conflict of interest: The authors declare no potential conflicts of interest.

Support statement: This work was supported by European Research Council 2010 Starting Independent Investigator (260524) and 2015 Proof of Concept (679345) grants, the Graduate College (Graduiertenkolleg) 2338 of the German Research Society (Deutsche Forschungsgemeinschaft), the target validation project for pharmaceutical development ALTERNATIVE of the German Ministry for Education and Research (Bundesministerium für Bildung und Forschung), and a Translational Research Grant by the German Center for Lung Research (Deutsches Zentrum

für Lungenforschung) (all to G.T. Stathopoulos). The study sponsors had no role in study design, data collection, analysis and interpretation, and in writing and submitting the paper for publication. Funding information for this article has been deposited with the Crossref Funder Registry.

## References

1 Global Burden of Disease Cancer Collaboration. Global, regional, and national cancer incidence, mortality, years of life lost, years lived with disability, and disability-adjusted life-years for 29 cancer groups, 1990 to 2017: a systematic analysis for the global burden of disease study. *JAMA Oncol* 2019; 5: 1749–1768.
2 Travis WD, Brambilla E, Nicholson AG, *et al.* The 2015 World Health Organization classification of lung tumors: impact of genetic, clinical and radiologic advances since the 2004 classification. *J Thorac Oncol* 2015; 10: 1243–1260.
3 Postmus PE, Kerr KM, Oudkerk M, *et al.* Early and locally advanced non-small-cell lung cancer (NSCLC): ESMO Clinical Practice Guidelines for diagnosis, treatment and follow-up. *Ann Oncol* 2017; 28: iv1–iv21.
4 Liang W, Zhang L, Jiang G, *et al.* Development and validation of a nomogram for predicting survival in patients with resected non-small-cell lung cancer. *J Clin Oncol* 2015; 33: 861–869.
5 Ujiie H, Kadota K, Chaft JE, *et al.* Solid predominant histologic subtype in resected stage I lung adenocarcinoma is an independent predictor of early, extrathoracic, multisite recurrence and of poor postrecurrence survival. *J Clin Oncol* 2015; 33: 2877–2884.
6 Duhig EE, Dettrick A, Godbolt DB, *et al.* Mitosis trumps T stage and proposed International Association for the Study of Lung Cancer/American Thoracic Society/European Respiratory Society classification for prognostic value in resected stage 1 lung adenocarcinoma. *J Thorac Oncol* 2015; 10: 673–681.
7 Klotz LV, Courty Y, Lindner M, *et al.* Comprehensive clinical profiling of the Gauting locoregional lung adenocarcinoma donors. *Cancer Med* 2019; 8: 1486–1499.
8 Warth A, Penzel R, Lindenmaier H, *et al. EGFR*, *KRAS*, *BRAF* and *ALK* gene alterations in lung adenocarcinomas: patient outcome, interplay with morphology and immunophenotype. *Eur Respir J* 2014; 43: 872–883.
9 Qian J, Zhao S, Zou Y, *et al.* Genomic underpinnings of tumor behavior in *in situ* and early lung adenocarcinoma. *Am J Respir Crit Care Med* 2019; 201: 697–706.
10 Izar B, Zhou H, Heist RS, *et al.* The prognostic impact of KRAS, its codon and amino acid specific mutations, on survival in resected stage I lung adenocarcinoma. *J Thorac Oncol* 2014; 9: 1363–1369.
11 Blackhall FH, Peters S, Bubendorf L, *et al.* Prevalence and clinical outcomes for patients with ALK-positive resected stage I to III adenocarcinoma: results from the European Thoracic Oncology Platform Lungscape Project. *J Clin Oncol* 2014; 32: 2780–2787.
12 Rizvi NA, Hellmann MD, Snyder A, *et al.* Cancer immunology. Mutational landscape determines sensitivity to PD-1 blockade in non-small cell lung cancer. *Science* 2015; 348: 124–128.
13 Cui Y, Fang W, Li C, *et al.* Development and validation of a novel signature to predict overall survival in "driver gene-negative" lung adenocarcinoma (LUAD): results of a multicenter study. *Clin Cancer Res* 2019; 25: 1546–1556.
14 Gentles AJ, Bratman SV, Lee LJ, *et al.* Integrating tumor and stromal gene expression signatures with clinical indices for survival stratification of early-stage non-small cell lung cancer. *J Natl Cancer Inst* 2015; 107: djv211.
15 Varghese C, Rajagopalan S, Karwoski RA, *et al.* Computed tomography-based Score Indicative of Lung Cancer Aggression (SILA) predicts the degree of histologic tissue invasion and patient survival in lung adenocarcinoma spectrum. *J Thorac Oncol* 2019; 14: 1419–1429.
16 Lee HY, Lee SW, Lee KS, *et al.* Role of CT and PET imaging in predicting tumor recurrence and survival in patients with lung adenocarcinoma: a comparison with the International Association for the Study of Lung Cancer/American Thoracic Society/European Respiratory Society Classification of Lung Adenocarcinoma. *J Thorac Oncol* 2015; 10: 1785–1794.
17 Takada K, Okamoto T, Shoji F, *et al.* Clinical significance of PD-L1 protein expression in surgically resected primary lung adenocarcinoma. *J Thorac Oncol* 2016; 11: 1879–1890.
18 Yanagawa N, Leduc C, Kohler D, *et al.* Loss of phosphatase and tensin homolog protein expression is an independent poor prognostic marker in lung adenocarcinoma. *J Thorac Oncol* 2012; 7: 1513–1521.
19 Cappuzzo F, Tallini G, Finocchiaro G, *et al.* Insulin-like growth factor receptor 1 (IGF1R) expression and survival in surgically resected non-small-cell lung cancer (NSCLC) patients. *Ann Oncol* 2010; 21: 562–567.
20 Kilvaer TK, Paulsen E-E, Khanehkenari MR, *et al.* The presence of intraepithelial CD45RO$^{+}$ cells in resected lymph nodes with metastases from NSCLC patients is an independent predictor of disease-specific survival. *Br J Cancer* 2016; 114: 1145–1151.
21 Ishida T, Kaneko S, Akazawa K, *et al.* Proliferating cell nuclear antigen expression and argyrophilic nucleolar organizer regions as factors influencing prognosis of surgically treated lung cancer patients. *Cancer Res* 1993; 53: 5000–5003.

22 Duarte IG, Bufkin BL, Pennington MF, *et al.* Angiogenesis as a predictor of survival after surgical resection for stage I non-small-cell lung cancer. *J Thorac CardiovascSurg* 1998; 115: 652–658.

23 Cardoso F, Kyriakides S, Ohno S, *et al.* Early breast cancer: ESMO Clinical Practice Guidelines for diagnosis, treatment and follow-up. *Ann Oncol* 2019; 30: 1194–1220.

24 Hanahan D, Weinberg RA. Hallmarks of cancer: the next generation. *Cell* 2011; 144: 646–674.

25 Groome PA, Bolejack V, Crowley JJ, *et al.* The IASLC Lung Cancer Staging Project: validation of the proposals for revision of the T, N, and M descriptors and consequent stage groupings in the forthcoming (seventh) edition of the TNM classification of malignant tumours. *J Thorac Oncol* 2007; 2: 694–705.

26 Kadota K, Nitadori JI, Sima CS, *et al.* Tumor spread through air spaces is an important pattern of invasion and impacts the frequency and location of recurrences after limited resection for small stage I lung adenocarcinomas. *J Thorac Oncol* 2015; 10: 806–814.

27 Lu S, Tan KS, Kadota K, *et al.* Spread through Air Spaces (STAS) is an independent predictor of recurrence and lung cancer-specific death in squamous cell carcinoma. *J Thorac Oncol* 2017; 12: 223–234.

28 Yagi Y, Aly RG, Tabata K, *et al.* Three-dimensional histologic, immunohistochemical, and multiplex immunofluorescence analyses of dynamic vessel co-option of spread through air spaces in lung adenocarcinoma. *J Thorac Oncol* 2020; 15: 589–600.

29 Campbell JD, Alexandrov A, Kim J, *et al.* Distinct patterns of somatic genome alterations in lung adenocarcinomas and squamous cell carcinomas. *Nat Genet* 2016; 48: 607–616.

30 Castelletti N, Kaiser JC, Simonetto C, *et al.* Risk of lung adenocarcinoma from smoking and radiation arises in distinct molecular pathways. *Carcinogenesis* 2019; 40: 1240–1250.

# References

[1] Hanahan D, Weinberg RA. The hallmarks of cancer. Cell. 2000;100(1):57-70. doi: 10.1016/s0092-8674(00)81683-9.

[2] Blanpain C. Tracing the cellular origin of cancer. Nat Cell Biol. 2013;15(2):126-34. doi: 10.1038/ncb2657.

[3] Travis WD, Brambilla E, Nicholson AG, Yatabe Y, Austin JHM, Beasley MB, Chirieac LR, Dacic S, Duhig E, Flieder DB, Geisinger K, Hirsch FR, Ishikawa Y, Kerr KM, Noguchi M, Pelosi G, Powell CA, Tsao MS, Wistuba I. The 2015 World Health Organization Classification of Lung Tumors: Impact of Genetic, Clinical and Radiologic Advances Since the 2004 Classification. J Thorac Oncol. 2015;10(9):1243-60. doi: 10.1097/jto.0000000000000630.

[4] Sung H, Ferlay J, Siegel RL, Laversanne M, Soerjomataram I, Jemal A, Bray F. Global Cancer Statistics 2020: GLOBOCAN Estimates of Incidence and Mortality Worldwide for 36 Cancers in 185 Countries. CA Cancer J Clin. 2021;71(3):209-49. doi: 10.3322/caac.21660.

[5] Collins LG, Haines C, Perkel R, Enck RE. Lung cancer: diagnosis and management. Am Fam Physician. 2007;75(1):56-63. doi.

[6] Nooreldeen R, Bach H. Current and Future Development in Lung Cancer Diagnosis. Int J Mol Sci. 2021;22(16). doi: 10.3390/ijms22168661.

[7] Hecht SS. Tobacco smoke carcinogens and lung cancer. J Natl Cancer Inst. 1999;91(14):1194-210. doi: 10.1093/jnci/91.14.1194.

[8] Huang R, Wei Y, Hung RJ, Liu G, Su L, Zhang R, Zong X, Zhang ZF, Morgenstern H, Brüske I, Heinrich J, Hong YC, Kim JH, Cote M, Wenzlaff A, Schwartz AG, Stucker I, McLaughlin J, Marcus MW, Davies MP, Liloglou T, Field JK, Matsuo K, Barnett M, Thornquist M, Goodman G, Wang Y, Chen S, Yang P, Duell EJ, Andrew AS, Lazarus P, Muscat J, Woll P, Horsman J, Teare MD, Flugelman A, Rennert G, Zhang Y, Brenner H, Stegmaier C, van der Heijden EH, Aben K, Kiemeney L, Barros-Dios J, Pérez-Ríos M, Ruano-Ravina A, Caporaso NE, Bertazzi PA, Landi MT, Dai J, Hongbing Shen H, Fernandez-Tardon G, Rodriguez-Suarez M, Tardon A, Christiani DC. Associated Links Among Smoking, Chronic Obstructive Pulmonary Disease, and Small Cell Lung Cancer: A Pooled Analysis in the International Lung Cancer Consortium. EBioMedicine. 2015;2(11):1677-85. doi: 10.1016/j.ebiom.2015.09.031.

[9] Li Y, Hecht SS. Carcinogenic components of tobacco and tobacco smoke: A 2022 update. Food Chem Toxicol. 2022;165:113179. doi: 10.1016/j.fct.2022.113179.

[10] Alberg AJ, Brock MV, Ford JG, Samet JM, Spivack SD. Epidemiology of lung cancer: Diagnosis and management of lung cancer, 3rd ed: American College of Chest Physicians evidence-based clinical practice guidelines. Chest. 2013;143(5 Suppl):e1S-e29S. doi: 10.1378/chest.12-2345.

[11] Furukawa K, Preston DL, Lönn S, Funamoto S, Yonehara S, Matsuo T, Egawa H, Tokuoka S, Ozasa K, Kasagi F, Kodama K, Mabuchi K. Radiation and smoking effects on lung cancer incidence among atomic bomb survivors. Radiat Res. 2010;174(1):72-82. doi: 10.1667/rr2083.1.

[12] McCunney RJ, Li J. Radiation risks in lung cancer screening programs: a comparison with nuclear industry workers and atomic bomb survivors. Chest. 2014;145(3):618-24. doi: 10.1378/chest.13-1420.

[13] Raaschou-Nielsen O, Andersen ZJ, Beelen R, Samoli E, Stafoggia M, Weinmayr G, Hoffmann B, Fischer P, Nieuwenhuijsen MJ, Brunekreef B, Xun WW, Katsouyanni K, Dimakopoulou K, Sommar J, Forsberg B, Modig L, Oudin A, Oftedal B, Schwarze PE, Nafstad P, De Faire U, Pedersen NL, Ostenson CG, Fratiglioni L, Penell J, Korek M, Pershagen G, Eriksen KT, Sørensen M, Tjønneland A, Ellermann T, Eeftens M, Peeters PH, Meliefste K, Wang M, Bueno-de-Mesquita B, Key TJ, de Hoogh K, Concin H, Nagel G, Vilier A, Grioni S, Krogh V, Tsai MY, Ricceri F, Sacerdote C, Galassi C, Migliore E, Ranzi A, Cesaroni G, Badaloni C, Forastiere F, Tamayo I, Amiano P, Dorronsoro M, Trichopoulou A, Bamia C, Vineis P, Hoek G. Air pollution and lung cancer incidence in 17

European cohorts: prospective analyses from the European Study of Cohorts for Air Pollution Effects (ESCAPE). Lancet Oncol. 2013;14(9):813-22. doi: 10.1016/s1470-2045(13)70279-1.

[14] Lamichhane DK, Kim HC, Choi CM, Shin MH, Shim YM, Leem JH, Ryu JS, Nam HS, Park SM. Lung Cancer Risk and Residential Exposure to Air Pollution: A Korean Population-Based Case-Control Study. Yonsei Med J. 2017;58(6):1111-8. doi: 10.3349/ymj.2017.58.6.1111.

[15] Driscoll T, Nelson DI, Steenland K, Leigh J, Concha-Barrientos M, Fingerhut M, Prüss-Ustün A. The global burden of disease due to occupational carcinogens. Am J Ind Med. 2005;48(6):419-31. doi: 10.1002/ajim.20209.

[16] Darby S, Hill D, Auvinen A, Barros-Dios JM, Baysson H, Bochicchio F, Deo H, Falk R, Forastiere F, Hakama M, Heid I, Kreienbrock L, Kreuzer M, Lagarde F, Mäkeläinen I, Muirhead C, Oberaigner W, Pershagen G, Ruano-Ravina A, Ruosteenoja E, Rosario AS, Tirmarche M, Tomásek L, Whitley E, Wichmann HE, Doll R. Radon in homes and risk of lung cancer: collaborative analysis of individual data from 13 European case-control studies. Bmj. 2005;330(7485):223. doi: 10.1136/bmj.38308.477650.63.

[17] Gray A, Read S, McGale P, Darby S. Lung cancer deaths from indoor radon and the cost effectiveness and potential of policies to reduce them. Bmj. 2009;338:a3110. doi: 10.1136/bmj.a3110.

[18] Rodríguez-Martínez Á, Torres-Durán M, Barros-Dios JM, Ruano-Ravina A. Residential radon and small cell lung cancer. A systematic review. Cancer Lett. 2018;426:57-62. doi: 10.1016/j.canlet.2018.04.003.

[19] Brenner DR, McLaughlin JR, Hung RJ. Previous lung diseases and lung cancer risk: a systematic review and meta-analysis. PLoS One. 2011;6(3):e17479. doi: 10.1371/journal.pone.0017479.

[20] Qu YL, Liu J, Zhang LX, Wu CM, Chu AJ, Wen BL, Ma C, Yan XY, Zhang X, Wang DM, Lv X, Hou SJ. Asthma and the risk of lung cancer: a meta-analysis. Oncotarget. 2017;8(7):11614-20. doi: 10.18632/oncotarget.14595.

[21] Søgaard KK, Farkas DK, Pedersen L, Weiss NS, Thomsen RW, Sørensen HT. Pneumonia and the incidence of cancer: a Danish nationwide cohort study. J Intern Med. 2015;277(4):429-38. doi: 10.1111/joim.12270.

[22] Zhan P, Suo LJ, Qian Q, Shen XK, Qiu LX, Yu LK, Song Y. Chlamydia pneumoniae infection and lung cancer risk: a meta-analysis. Eur J Cancer. 2011;47(5):742-7. doi: 10.1016/j.ejca.2010.11.003.

[23] Brenner DR, Boffetta P, Duell EJ, Bickeböller H, Rosenberger A, McCormack V, Muscat JE, Yang P, Wichmann HE, Brueske-Hohlfeld I, Schwartz AG, Cote ML, Tjønneland A, Friis S, Le Marchand L, Zhang ZF, Morgenstern H, Szeszenia-Dabrowska N, Lissowska J, Zaridze D, Rudnai P, Fabianova E, Foretova L, Janout V, Bencko V, Schejbalova M, Brennan P, Mates IN, Lazarus P, Field JK, Raji O, McLaughlin JR, Liu G, Wiencke J, Neri M, Ugolini D, Andrew AS, Lan Q, Hu W, Orlow I, Park BJ, Hung RJ. Previous lung diseases and lung cancer risk: a pooled analysis from the International Lung Cancer Consortium. Am J Epidemiol. 2012;176(7):573-85. doi: 10.1093/aje/kws151.

[24] Sigel K, Makinson A, Thaler J. Lung cancer in persons with HIV. Curr Opin HIV AIDS. 2017;12(1):31-8. doi: 10.1097/coh.0000000000000326.

[25] Rudin CM, Brambilla E, Faivre-Finn C, Sage J. Small-cell lung cancer. Nat Rev Dis Primers. 2021;7(1):3. doi: 10.1038/s41572-020-00235-0.

[26] Kalemkerian GP, Akerley W, Bogner P, Borghaei H, Chow LQ, Downey RJ, Gandhi L, Ganti AK, Govindan R, Grecula JC, Hayman J, Heist RS, Horn L, Jahan T, Koczywas M, Loo BW, Jr., Merritt RE, Moran CA, Niell HB, O'Malley J, Patel JD, Ready N, Rudin CM, Williams CC, Jr., Gregory K, Hughes M. Small cell lung cancer. J Natl Compr Canc Netw. 2013;11(1):78-98. doi: 10.6004/jnccn.2013.0011.

[27] Govindan R, Page N, Morgensztern D, Read W, Tierney R, Vlahiotis A, Spitznagel EL, Piccirillo J. Changing epidemiology of small-cell lung cancer in the United States over the

last 30 years: analysis of the surveillance, epidemiologic, and end results database. J Clin Oncol. 2006;24(28):4539-44. doi: 10.1200/jco.2005.04.4859.

[28] Joshi M, Ayoola A, Belani CP. Small-cell lung cancer: an update on targeted therapies. Adv Exp Med Biol. 2013;779:385-404. doi: 10.1007/978-1-4614-6176-0_18.

[29] Taniguchi H, Sen T, Rudin CM. Targeted Therapies and Biomarkers in Small Cell Lung Cancer. Front Oncol. 2020;10:741. doi: 10.3389/fonc.2020.00741.

[30] Schabath MB, Cote ML. Cancer Progress and Priorities: Lung Cancer. Cancer Epidemiol Biomarkers Prev. 2019;28(10):1563-79. doi: 10.1158/1055-9965.Epi-19-0221.

[31] Sangha R, Price J, Butts CA. Adjuvant therapy in non-small cell lung cancer: current and future directions. Oncologist. 2010;15(8):862-72. doi: 10.1634/theoncologist.2009-0186.

[32] Hotta K, Matsuo K, Ueoka H, Kiura K, Tabata M, Tanimoto M. Role of adjuvant chemotherapy in patients with resected non-small-cell lung cancer: reappraisal with a meta-analysis of randomized controlled trials. J Clin Oncol. 2004;22(19):3860-7. doi: 10.1200/jco.2004.01.153.

[33] Lemjabbar-Alaoui H, Hassan OU, Yang YW, Buchanan P. Lung cancer: Biology and treatment options. Biochim Biophys Acta. 2015;1856(2):189-210. doi: 10.1016/j.bbcan.2015.08.002.

[34] Aupérin A, Le Péchoux C, Pignon JP, Koning C, Jeremic B, Clamon G, Einhorn L, Ball D, Trovo MG, Groen HJ, Bonner JA, Le Chevalier T, Arriagada R. Concomitant radio-chemotherapy based on platin compounds in patients with locally advanced non-small cell lung cancer (NSCLC): a meta-analysis of individual data from 1764 patients. Ann Oncol. 2006;17(3):473-83. doi: 10.1093/annonc/mdj117.

[35] Rowell NP, O'Rourke NP. Concurrent chemoradiotherapy in non-small cell lung cancer. Cochrane Database Syst Rev. 2004(4):Cd002140. doi: 10.1002/14651858.CD002140.pub2.

[36] Chen R, Manochakian R, James L, Azzouqa AG, Shi H, Zhang Y, Zhao Y, Zhou K, Lou Y. Emerging therapeutic agents for advanced non-small cell lung cancer. J Hematol Oncol. 2020;13(1):58. doi: 10.1186/s13045-020-00881-7.

[37] Mutti L, Peikert T, Robinson BWS, Scherpereel A, Tsao AS, de Perrot M, Woodard GA, Jablons DM, Wiens J, Hirsch FR, Yang H, Carbone M, Thomas A, Hassan R. Scientific Advances and New Frontiers in Mesothelioma Therapeutics. J Thorac Oncol. 2018;13(9):1269-83. doi: 10.1016/j.jtho.2018.06.011.

[38] Ismail-Khan R, Robinson LA, Williams CC, Jr., Garrett CR, Bepler G, Simon GR. Malignant pleural mesothelioma: a comprehensive review. Cancer Control. 2006;13(4):255-63. doi: 10.1177/107327480601300402.

[39] Sekido Y. Molecular pathogenesis of malignant mesothelioma. Carcinogenesis. 2013;34(7):1413-9. doi: 10.1093/carcin/bgt166.

[40] Bibby AC, Tsim S, Kanellakis N, Ball H, Talbot DC, Blyth KG, Maskell NA, Psallidas I. Malignant pleural mesothelioma: an update on investigation, diagnosis and treatment. Eur Respir Rev. 2016;25(142):472-86. doi: 10.1183/16000617.0063-2016.

[41] Jain SV, Wallen JM. Malignant Mesothelioma. StatPearls [Internet]. Treasure Island (FL): StatPearls Publishing; 2022.

[42] Skok K, Hladnik G, Grm A, Crnjac A. Malignant Pleural Effusion and Its Current Management: A Review. Medicina (Kaunas). 2019;55(8). doi: 10.3390/medicina55080490.

[43] Attanoos RL, Churg A, Galateau-Salle F, Gibbs AR, Roggli VL. Malignant Mesothelioma and Its Non-Asbestos Causes. Arch Pathol Lab Med. 2018;142(6):753-60. doi: 10.5858/arpa.2017-0365-RA.

[44] GBD 2016 Occupational Carcinogens Collaborators. Global and regional burden of cancer in 2016 arising from occupational exposure to selected carcinogens: a systematic analysis for the Global Burden of Disease Study 2016. Occup Environ Med. 2020;77(3):151-9. doi: 10.1136/oemed-2019-106012.

[45] Rohl AN, Langer AM, Moncure G, Selikoff IJ, Fischbein A. Endemic pleural disease associated with exposure to mixed fibrous dust in Turkey. Science. 1982;216(4545):518-20. doi: 10.1126/science.7071597.

[46] Ortega-Guerrero MA, Carrasco-Núñez G, Barragán-Campos H, Ortega MR. High incidence of lung cancer and malignant mesothelioma linked to erionite fibre exposure in a rural community in Central Mexico. Occup Environ Med. 2015;72(3):216-8. doi: 10.1136/oemed-2013-101957.

[47] Paoletti L, Batisti D, Bruno C, Di Paola M, Gianfagna A, Mastrantonio M, Nesti M, Comba P. Unusually high incidence of malignant pleural mesothelioma in a town of eastern Sicily: an epidemiological and environmental study. Archives of Environmental Health: An International Journal. 2000;55(6):392-8. doi.

[48] Antman KH, Corson JM, Li FP, Greenberger J, Sytkowski A, Henson DE, Weinstein L. Malignant mesothelioma following radiation exposure. J Clin Oncol. 1983;1(11):695-700. doi: 10.1200/jco.1983.1.11.695.

[49] Roviaro GC, Sartori F, Calabrò F, Varoli F. The association of pleural mesothelioma and tuberculosis. Am Rev Respir Dis. 1982;126(3):569-71. doi: 10.1164/arrd.1982.126.3.569.

[50] Gentiloni N, Febbraro S, Barone C, Lemmo G, Neri G, Zannoni G, Capelli A, Gasbarrini G. Peritoneal mesothelioma in recurrent familial peritonitis. J Clin Gastroenterol. 1997;24(4):276-9. doi: 10.1097/00004836-199706000-00023.

[51] Sakamoto Y, Nakae D, Fukumori N, Tayama K, Maekawa A, Imai K, Hirose A, Nishimura T, Ohashi N, Ogata A. Induction of mesothelioma by a single intrascrotal administration of multi-wall carbon nanotube in intact male Fischer 344 rats. J Toxicol Sci. 2009;34(1):65-76. doi: 10.2131/jts.34.65.

[52] Tischoff I, Neid M, Neumann V, Tannapfel A. Pathohistological diagnosis and differential diagnosis. Recent Results Cancer Res. 2011;189:57-78. doi: 10.1007/978-3-642-10862-4_5.

[53] Vigneswaran WT, Kircheva DY, Ananthanarayanan V, Watson S, Arif Q, Celauro AD, Kindler HL, Husain AN. Amount of Epithelioid Differentiation Is a Predictor of Survival in Malignant Pleural Mesothelioma. Ann Thorac Surg. 2017;103(3):962-6. doi: 10.1016/j.athoracsur.2016.08.063.

[54] Vogelzang NJ, Rusthoven JJ, Symanowski J, Denham C, Kaukel E, Ruffie P, Gatzemeier U, Boyer M, Emri S, Manegold C, Niyikiza C, Paoletti P. Phase III study of pemetrexed in combination with cisplatin versus cisplatin alone in patients with malignant pleural mesothelioma. J Clin Oncol. 2003;21(14):2636-44. doi: 10.1200/jco.2003.11.136.

[55] van Meerbeeck JP, Gaafar R, Manegold C, Van Klaveren RJ, Van Marck EA, Vincent M, Legrand C, Bottomley A, Debruyne C, Giaccone G. Randomized phase III study of cisplatin with or without raltitrexed in patients with malignant pleural mesothelioma: an intergroup study of the European Organisation for Research and Treatment of Cancer Lung Cancer Group and the National Cancer Institute of Canada. J Clin Oncol. 2005;23(28):6881-9. doi: 10.1200/jco.20005.14.589.

[56] Davies HE, Mishra EK, Kahan BC, Wrightson JM, Stanton AE, Guhan A, Davies CW, Grayez J, Harrison R, Prasad A, Crosthwaite N, Lee YC, Davies RJ, Miller RF, Rahman NM. Effect of an indwelling pleural catheter vs chest tube and talc pleurodesis for relieving dyspnea in patients with malignant pleural effusion: the TIME2 randomized controlled trial. Jama. 2012;307(22):2383-9. doi: 10.1001/jama.2012.5535.

[57] Rimner A, Zauderer MG, Gomez DR, Adusumilli PS, Parhar PK, Wu AJ, Woo KM, Shen R, Ginsberg MS, Yorke ED, Rice DC, Tsao AS, Rosenzweig KE, Rusch VW, Krug LM. Phase II Study of Hemithoracic Intensity-Modulated Pleural Radiation Therapy (IMPRINT) As Part of Lung-Sparing Multimodality Therapy in Patients With Malignant Pleural Mesothelioma. J Clin Oncol. 2016;34(23):2761-8. doi: 10.1200/jco.2016.67.2675.

[58] MacLeod N, Chalmers A, O'Rourke N, Moore K, Sheridan J, McMahon L, Bray C, Stobo J, Price A, Fallon M, Laird BJ. Is Radiotherapy Useful for Treating Pain in Mesothelioma?: A Phase II Trial. J Thorac Oncol. 2015;10(6):944-50. doi: 10.1097/jto.0000000000000499.

[59] Sinn K, Mosleh B, Hoda MA. Malignant pleural mesothelioma: recent developments. Curr Opin Oncol. 2021;33(1):80-6. doi: 10.1097/cco.0000000000000697.

[60] Zalcman G, Mazieres J, Margery J, Greillier L, Audigier-Valette C, Moro-Sibilot D, Molinier O, Corre R, Monnet I, Gounant V, Rivière F, Janicot H, Gervais R, Locher C, Milleron B, Tran Q, Lebitasy MP, Morin F, Creveuil C, Parienti JJ, Scherpereel A. Bevacizumab for newly diagnosed pleural mesothelioma in the Mesothelioma Avastin Cisplatin Pemetrexed Study (MAPS): a randomised, controlled, open-label, phase 3 trial. Lancet. 2016;387(10026):1405-14. doi: 10.1016/s0140-6736(15)01238-6.

[61] Hanahan D, Weinberg RA. Hallmarks of cancer: the next generation. Cell. 2011;144(5):646-74. doi: 10.1016/j.cell.2011.02.013.

[62] Stratton MR, Campbell PJ, Futreal PA. The cancer genome. Nature. 2009;458(7239):719-24. doi: 10.1038/nature07943.

[63] Dawson MA, Kouzarides T. Cancer epigenetics: from mechanism to therapy. Cell. 2012;150(1):12-27. doi: 10.1016/j.cell.2012.06.013.

[64] Melo SA, Esteller M. Dysregulation of microRNAs in cancer: playing with fire. FEBS Lett. 2011;585(13):2087-99. doi: 10.1016/j.febslet.2010.08.009.

[65] Peters A, Nawrot TS, Baccarelli AA. Hallmarks of environmental insults. Cell. 2021;184(6):1455-68. doi: 10.1016/j.cell.2021.01.043.

[66] Kucab JE, Zou X, Morganella S, Joel M, Nanda AS, Nagy E, Gomez C, Degasperi A, Harris R, Jackson SP, Arlt VM, Phillips DH, Nik-Zainal S. A Compendium of Mutational Signatures of Environmental Agents. Cell. 2019;177(4):821-36.e16. doi: 10.1016/j.cell.2019.03.001.

[67] Alexandrov LB, Nik-Zainal S, Wedge DC, Aparicio SA, Behjati S, Biankin AV, Bignell GR, Bolli N, Borg A, Børresen-Dale AL, Boyault S, Burkhardt B, Butler AP, Caldas C, Davies HR, Desmedt C, Eils R, Eyfjörd JE, Foekens JA, Greaves M, Hosoda F, Hutter B, Ilicic T, Imbeaud S, Imielinski M, Jäger N, Jones DT, Jones D, Knappskog S, Kool M, Lakhani SR, López-Otín C, Martin S, Munshi NC, Nakamura H, Northcott PA, Pajic M, Papaemmanuil E, Paradiso A, Pearson JV, Puente XS, Raine K, Ramakrishna M, Richardson AL, Richter J, Rosenstiel P, Schlesner M, Schumacher TN, Span PN, Teague JW, Totoki Y, Tutt AN, Valdés-Mas R, van Buuren MM, van 't Veer L, Vincent-Salomon A, Waddell N, Yates LR, Zucman-Rossi J, Futreal PA, McDermott U, Lichter P, Meyerson M, Grimmond SM, Siebert R, Campo E, Shibata T, Pfister SM, Campbell PJ, Stratton MR. Signatures of mutational processes in human cancer. Nature. 2013;500(7463):415-21. doi: 10.1038/nature12477.

[68] Alexandrov LB, Kim J, Haradhvala NJ, Huang MN, Tian Ng AW, Wu Y, Boot A, Covington KR, Gordenin DA, Bergstrom EN, Islam SMA, Lopez-Bigas N, Klimczak LJ, McPherson JR, Morganella S, Sabarinathan R, Wheeler DA, Mustonen V, Getz G, Rozen SG, Stratton MR. The repertoire of mutational signatures in human cancer. Nature. 2020;578(7793):94-101. doi: 10.1038/s41586-020-1943-3.

[69] Pfeifer GP, You YH, Besaratinia A. Mutations induced by ultraviolet light. Mutat Res. 2005;571(1-2):19-31. doi: 10.1016/j.mrfmmm.2004.06.057.

[70] de Sousa VML, Carvalho L. Heterogeneity in Lung Cancer. Pathobiology. 2018;85(1-2):96-107. doi: 10.1159/000487440.

[71] Oehl K, Vrugt B, Opitz I, Meerang M. Heterogeneity in Malignant Pleural Mesothelioma. Int J Mol Sci. 2018;19(6). doi: 10.3390/ijms19061603.

[72] Dagogo-Jack I, Shaw AT. Tumour heterogeneity and resistance to cancer therapies. Nat Rev Clin Oncol. 2018;15(2):81-94. doi: 10.1038/nrclinonc.2017.166.

[73] Parikh AR. Lung Cancer Genomics. Acta Med Acad. 2019;48(1):78-83. doi: 10.5644/ama2006-124.244.

[74] Bueno R, Stawiski EW, Goldstein LD, Durinck S, De Rienzo A, Modrusan Z, Gnad F, Nguyen TT, Jaiswal BS, Chirieac LR, Sciaranghella D, Dao N, Gustafson CE, Munir KJ, Hackney JA, Chaudhuri A, Gupta R, Guillory J, Toy K, Ha C, Chen YJ, Stinson J, Chaudhuri S, Zhang N, Wu TD, Sugarbaker DJ, de Sauvage FJ, Richards WG, Seshagiri S. Comprehensive genomic analysis of malignant pleural mesothelioma identifies

recurrent mutations, gene fusions and splicing alterations. Nat Genet. 2016;48(4):407-16. doi: 10.1038/ng.3520.

[75] Hylebos M, Van Camp G, van Meerbeeck JP, Op de Beeck K. The Genetic Landscape of Malignant Pleural Mesothelioma: Results from Massively Parallel Sequencing. J Thorac Oncol. 2016;11(10):1615-26. doi: 10.1016/j.jtho.2016.05.020.

[76] Bott M, Brevet M, Taylor BS, Shimizu S, Ito T, Wang L, Creaney J, Lake RA, Zakowski MF, Reva B, Sander C, Delsite R, Powell S, Zhou Q, Shen R, Olshen A, Rusch V, Ladanyi M. The nuclear deubiquitinase BAP1 is commonly inactivated by somatic mutations and 3p21.1 losses in malignant pleural mesothelioma. Nat Genet. 2011;43(7):668-72. doi: 10.1038/ng.855.

[77] Wadowski B, De Rienzo A, Bueno R. The Molecular Basis of Malignant Pleural Mesothelioma. Thorac Surg Clin. 2020;30(4):383-93. doi: 10.1016/j.thorsurg.2020.08.005.

[78] Carbone M, Yang H, Pass HI, Krausz T, Testa JR, Gaudino G. BAP1 and cancer. Nat Rev Cancer. 2013;13(3):153-9. doi: 10.1038/nrc3459.

[79] Quetel L, Tranchant R, Meiller C, Imbeaud S, Renier A, Le Pimpec-Barthes F, Zucman-Rossi J, Jaurand M-C, Jean D. Abstract 112: Genetic alterations in molecular tumor subgroups of malignant pleural mesothelioma. Cancer Research. 2016;76(14_Supplement):112-. doi: 10.1158/1538-7445.Am2016-112.

[80] Hmeljak J, Sanchez-Vega F, Hoadley KA, Shih J, Stewart C, Heiman D, Tarpey P, Danilova L, Drill E, Gibb EA, Bowlby R, Kanchi R, Osmanbeyoglu HU, Sekido Y, Takeshita J, Newton Y, Graim K, Gupta M, Gay CM, Diao L, Gibbs DL, Thorsson V, Iype L, Kantheti H, Severson DT, Ravegnini G, Desmeules P, Jungbluth AA, Travis WD, Dacic S, Chirieac LR, Galateau-Sallé F, Fujimoto J, Husain AN, Silveira HC, Rusch VW, Rintoul RC, Pass H, Kindler H, Zauderer MG, Kwiatkowski DJ, Bueno R, Tsao AS, Creaney J, Lichtenberg T, Leraas K, Bowen J, Felau I, Zenklusen JC, Akbani R, Cherniack AD, Byers LA, Noble MS, Fletcher JA, Robertson AG, Shen R, Aburatani H, Robinson BW, Campbell P, Ladanyi M. Integrative Molecular Characterization of Malignant Pleural Mesothelioma. Cancer Discov. 2018;8(12):1548-65. doi: 10.1158/2159-8290.Cd-18-0804.

[81] Trassl L, Stathopoulos GT. KRAS Pathway Alterations in Malignant Pleural Mesothelioma: An Underestimated Player. Cancers. 2022;14(17):4303. doi.

[82] Hindson BJ, Ness KD, Masquelier DA, Belgrader P, Heredia NJ, Makarewicz AJ, Bright IJ, Lucero MY, Hiddessen AL, Legler TC, Kitano TK, Hodel MR, Petersen JF, Wyatt PW, Steenblock ER, Shah PH, Bousse LJ, Troup CB, Mellen JC, Wittmann DK, Erndt NG, Cauley TH, Koehler RT, So AP, Dube S, Rose KA, Montesclaros L, Wang S, Stumbo DP, Hodges SP, Romine S, Milanovich FP, White HE, Regan JF, Karlin-Neumann GA, Hindson CM, Saxonov S, Colston BW. High-throughput droplet digital PCR system for absolute quantitation of DNA copy number. Anal Chem. 2011;83(22):8604-10. doi: 10.1021/ac202028g.

[83] Kanagal-Shamanna R. Digital PCR: Principles and Applications. Methods Mol Biol. 2016;1392:43-50. doi: 10.1007/978-1-4939-3360-0_5.

[84] Verheul RC, van Deutekom JC, Datson NA. Digital Droplet PCR for the Absolute Quantification of Exon Skipping Induced by Antisense Oligonucleotides in (Pre-)Clinical Development for Duchenne Muscular Dystrophy. PLoS One. 2016;11(9):e0162467. doi: 10.1371/journal.pone.0162467.

[85] Jennings LJ, George D, Czech J, Yu M, Joseph L. Detection and quantification of BCR-ABL1 fusion transcripts by droplet digital PCR. J Mol Diagn. 2014;16(2):174-9. doi: 10.1016/j.jmoldx.2013.10.007.

[86] McCombie WR, McPherson JD, Mardis ER. Next-Generation Sequencing Technologies. Cold Spring Harb Perspect Med. 2019;9(11). doi: 10.1101/cshperspect.a036798.

[87] Postel M, Roosen A, Laurent-Puig P, Taly V, Wang-Renault SF. Droplet-based digital PCR and next generation sequencing for monitoring circulating tumor DNA: a cancer diagnostic perspective. Expert Rev Mol Diagn. 2018;18(1):7-17. doi: 10.1080/14737159.2018.1400384.

[88] Voso MT, Ottone T, Lavorgna S, Venditti A, Maurillo L, Lo-Coco F, Buccisano F. MRD in AML: The Role of New Techniques. Front Oncol. 2019;9:655. doi: 10.3389/fonc.2019.00655.

[89] Hu B, Tao Y, Shao Z, Zheng Y, Zhang R, Yang X, Liu J, Li X, Sun R. A Comparison of Blood Pathogen Detection Among Droplet Digital PCR, Metagenomic Next-Generation Sequencing, and Blood Culture in Critically Ill Patients With Suspected Bloodstream Infections. Front Microbiol. 2021;12:641202. doi: 10.3389/fmicb.2021.641202.

[90] Marazioti A, Krontira AC, Behrend SJ, Giotopoulou GA, Ntaliarda G, Blanquart C, Bayram H, Iliopoulou M, Vreka M, Trassl L, Pepe MAA, Hackl CM, Klotz LV, Weiss SAI, Koch I, Lindner M, Hatz RA, Behr J, Wagner DE, Papadaki H, Antimisiaris SG, Jean D, Deshayes S, Grégoire M, Kayalar Ö, Mortazavi D, Dilege Ş, Tanju S, Erus S, Yavuz Ö, Bulutay P, Fırat P, Psallidas I, Spella M, Giopanou I, Lilis I, Lamort AS, Stathopoulos GT. KRAS signaling in malignant pleural mesothelioma. EMBO Mol Med. 2022;14(2):e13631. doi: 10.15252/emmm.202013631.

[91] Callens C, Bidard FC, Curto-Taribo A, Trabelsi-Grati O, Melaabi S, Delaloge S, Hardy-Bessard AC, Bachelot T, Clatot F, De La Motte Rouge T, Canon JL, Arnould L, Andre F, Marques S, Stern MH, Pierga JY, Vincent-Salomon A, Benoist C, Jeannot E, Berger F, Bieche I, Pradines A. Real-Time Detection of ESR1 Mutation in Blood by Droplet Digital PCR in the PADA-1 Trial: Feasibility and Cross-Validation with NGS. Anal Chem. 2022;94(16):6297-303. doi: 10.1021/acs.analchem.2c00446.

[92] Batlle E, Clevers H. Cancer stem cells revisited. Nat Med. 2017;23(10):1124-34. doi: 10.1038/nm.4409.

[93] Lundin A, Driscoll B. Lung cancer stem cells: progress and prospects. Cancer Lett. 2013;338(1):89-93. doi: 10.1016/j.canlet.2012.08.014.

[94] Rock JR, Onaitis MW, Rawlins EL, Lu Y, Clark CP, Xue Y, Randell SH, Hogan BL. Basal cells as stem cells of the mouse trachea and human airway epithelium. Proc Natl Acad Sci U S A. 2009;106(31):12771-5. doi: 10.1073/pnas.0906850106.

[95] Rawlins EL, Okubo T, Xue Y, Brass DM, Auten RL, Hasegawa H, Wang F, Hogan BL. The role of Scgb1a1+ Clara cells in the long-term maintenance and repair of lung airway, but not alveolar, epithelium. Cell Stem Cell. 2009;4(6):525-34. doi: 10.1016/j.stem.2009.04.002.

[96] Zheng D, Limmon GV, Yin L, Leung NH, Yu H, Chow VT, Chen J. Regeneration of alveolar type I and II cells from Scgb1a1-expressing cells following severe pulmonary damage induced by bleomycin and influenza. PLoS One. 2012;7(10):e48451. doi: 10.1371/journal.pone.0048451.

[97] Zuo W, Zhang T, Wu DZ, Guan SP, Liew AA, Yamamoto Y, Wang X, Lim SJ, Vincent M, Lessard M, Crum CP, Xian W, McKeon F. p63(+)Krt5(+) distal airway stem cells are essential for lung regeneration. Nature. 2015;517(7536):616-20. doi: 10.1038/nature13903.

[98] Spella M, Lilis I, Pepe MA, Chen Y, Armaka M, Lamort AS, Zazara DE, Roumelioti F, Vreka M, Kanellakis NI, Wagner DE, Giannou AD, Armenis V, Arendt KA, Klotz LV, Toumpanakis D, Karavana V, Zakynthinos SG, Giopanou I, Marazioti A, Aidinis V, Sotillo R, Stathopoulos GT. Club cells form lung adenocarcinomas and maintain the alveoli of adult mice. Elife. 2019;8. doi: 10.7554/eLife.45571.

[99] Barkauskas CE, Cronce MJ, Rackley CR, Bowie EJ, Keene DR, Stripp BR, Randell SH, Noble PW, Hogan BL. Type 2 alveolar cells are stem cells in adult lung. J Clin Invest. 2013;123(7):3025-36. doi: 10.1172/jci68782.

[100] Desai TJ, Brownfield DG, Krasnow MA. Alveolar progenitor and stem cells in lung development, renewal and cancer. Nature. 2014;507(7491):190-4. doi: 10.1038/nature12930.

[101] Kim CF, Jackson EL, Woolfenden AE, Lawrence S, Babar I, Vogel S, Crowley D, Bronson RT, Jacks T. Identification of bronchioalveolar stem cells in normal lung and lung cancer. Cell. 2005;121(6):823-35. doi: 10.1016/j.cell.2005.03.032.

[102] Behrend SJ, Giotopoulou GA, Spella M, Stathopoulos GT. A role for club cells in smoking-associated lung adenocarcinoma. Eur Respir Rev. 2021;30(162):210122. doi: 10.1183/16000617.0122-2021.

[103] McFadden DG, Politi K, Bhutkar A, Chen FK, Song X, Pirun M, Santiago PM, Kim-Kiselak C, Platt JT, Lee E, Hodges E, Rosebrock AP, Bronson RT, Socci ND, Hannon GJ, Jacks T, Varmus H. Mutational landscape of EGFR-, MYC-, and Kras-driven genetically engineered mouse models of lung adenocarcinoma. Proc Natl Acad Sci U S A. 2016;113(42):E6409-e17. doi: 10.1073/pnas.1613601113.

[104] Westcott PM, Halliwill KD, To MD, Rashid M, Rust AG, Keane TM, Delrosario R, Jen KY, Gurley KE, Kemp CJ, Fredlund E, Quigley DA, Adams DJ, Balmain A. The mutational landscapes of genetic and chemical models of Kras-driven lung cancer. Nature. 2015;517(7535):489-92. doi: 10.1038/nature13898.

[105] Kanellakis NI, Giannou AD, Pepe MAA, Agalioti T, Zazara DE, Giopanou I, Psallidas I, Spella M, Marazioti A, Arendt KAM, Lamort AS, Champeris Tsaniras S, Taraviras S, Papadaki H, Lilis I, Stathopoulos GT. Tobacco chemical-induced mouse lung adenocarcinoma cell lines pin the prolactin orthologue proliferin as a lung tumour promoter. Carcinogenesis. 2019;40(11):1352-62. doi: 10.1093/carcin/bgz047.

[106] Stathopoulos GT, Sherrill TP, Cheng DS, Scoggins RM, Han W, Polosukhin VV, Connelly L, Yull FE, Fingleton B, Blackwell TS. Epithelial NF-kappaB activation promotes urethane-induced lung carcinogenesis. Proc Natl Acad Sci U S A. 2007;104(47):18514-9. doi: 10.1073/pnas.0705316104.

[107] Gurley KE, Moser RD, Kemp CJ. Induction of Lung Tumors in Mice with Urethane. Cold Spring Harb Protoc. 2015;2015(9):pdb.prot077446. doi: 10.1101/pdb.prot077446.

[108] Izar B, Zhou H, Heist RS, Azzoli CG, Muzikansky A, Scribner EE, Bernardo LA, Dias-Santagata D, Iafrate AJ, Lanuti M. The prognostic impact of KRAS, its codon and amino acid specific mutations, on survival in resected stage I lung adenocarcinoma. J Thorac Oncol. 2014;9(9):1363-9. doi: 10.1097/jto.0000000000000266.

[109] Chapman AM, Sun KY, Ruestow P, Cowan DM, Madl AK. Lung cancer mutation profile of EGFR, ALK, and KRAS: Meta-analysis and comparison of never and ever smokers. Lung Cancer. 2016;102:122-34. doi: 10.1016/j.lungcan.2016.10.010.

[110] El Osta B, Behera M, Kim S, Berry LD, Sica G, Pillai RN, Owonikoko TK, Kris MG, Johnson BE, Kwiatkowski DJ, Sholl LM, Aisner DL, Bunn PA, Khuri FR, Ramalingam SS. Characteristics and Outcomes of Patients With Metastatic KRAS-Mutant Lung Adenocarcinomas: The Lung Cancer Mutation Consortium Experience. J Thorac Oncol. 2019;14(5):876-89. doi: 10.1016/j.jtho.2019.01.020.

[111] Ferrer I, Zugazagoitia J, Herbertz S, John W, Paz-Ares L, Schmid-Bindert G. KRAS-Mutant non-small cell lung cancer: From biology to therapy. Lung Cancer. 2018;124:53-64. doi: 10.1016/j.lungcan.2018.07.013.

[112] Pylayeva-Gupta Y, Grabocka E, Bar-Sagi D. RAS oncogenes: weaving a tumorigenic web. Nat Rev Cancer. 2011;11(11):761-74. doi: 10.1038/nrc3106.

[113] Muzumdar MD, Tasic B, Miyamichi K, Li L, Luo L. A global double-fluorescent Cre reporter mouse. Genesis. 2007;45(9):593-605. doi: 10.1002/dvg.20335.

[114] Mainardi S, Mijimolle N, Francoz S, Vicente-Dueñas C, Sánchez-García I, Barbacid M. Identification of cancer initiating cells in K-Ras driven lung adenocarcinoma. Proc Natl Acad Sci U S A. 2014;111(1):255-60. doi: 10.1073/pnas.1320383110.

[115] Sutherland KD, Song JY, Kwon MC, Proost N, Zevenhoven J, Berns A. Multiple cells-of-origin of mutant K-Ras-induced mouse lung adenocarcinoma. Proc Natl Acad Sci U S A. 2014;111(13):4952-7. doi: 10.1073/pnas.1319963111.

[116] Xu X, Rock JR, Lu Y, Futtner C, Schwab B, Guinney J, Hogan BL, Onaitis MW. Evidence for type II cells as cells of origin of K-Ras-induced distal lung adenocarcinoma. Proc Natl Acad Sci U S A. 2012;109(13):4910-5. doi: 10.1073/pnas.1112499109.

[117] Vaz M, Hwang SY, Kagiampakis I, Phallen J, Patil A, O'Hagan HM, Murphy L, Zahnow CA, Gabrielson E, Velculescu VE, Easwaran HP, Baylin SB. Chronic Cigarette Smoke-Induced Epigenomic Changes Precede Sensitization of Bronchial Epithelial Cells to

Single-Step Transformation by KRAS Mutations. Cancer Cell. 2017;32(3):360-76.e6. doi: 10.1016/j.ccell.2017.08.006.

[118] Li S, MacAlpine DM, Counter CM. Capturing the primordial Kras mutation initiating urethane carcinogenesis. Nat Commun. 2020;11(1):1800. doi: 10.1038/s41467-020-15660-8.

[119] Jamal-Hanjani M, Wilson GA, McGranahan N, Birkbak NJ, Watkins TBK, Veeriah S, Shafi S, Johnson DH, Mitter R, Rosenthal R, Salm M, Horswell S, Escudero M, Matthews N, Rowan A, Chambers T, Moore DA, Turajlic S, Xu H, Lee SM, Forster MD, Ahmad T, Hiley CT, Abbosh C, Falzon M, Borg E, Marafioti T, Lawrence D, Hayward M, Kolvekar S, Panagiotopoulos N, Janes SM, Thakrar R, Ahmed A, Blackhall F, Summers Y, Shah R, Joseph L, Quinn AM, Crosbie PA, Naidu B, Middleton G, Langman G, Trotter S, Nicolson M, Remmen H, Kerr K, Chetty M, Gomersall L, Fennell DA, Nakas A, Rathinam S, Anand G, Khan S, Russell P, Ezhil V, Ismail B, Irvin-Sellers M, Prakash V, Lester JF, Kornaszewska M, Attanoos R, Adams H, Davies H, Dentro S, Taniere P, O'Sullivan B, Lowe HL, Hartley JA, Iles N, Bell H, Ngai Y, Shaw JA, Herrero J, Szallasi Z, Schwarz RF, Stewart A, Quezada SA, Le Quesne J, Van Loo P, Dive C, Hackshaw A, Swanton C. Tracking the Evolution of Non-Small-Cell Lung Cancer. N Engl J Med. 2017;376(22):2109-21. doi: 10.1056/NEJMoa1616288.

[120] Govindan R, Ding L, Griffith M, Subramanian J, Dees ND, Kanchi KL, Maher CA, Fulton R, Fulton L, Wallis J, Chen K, Walker J, McDonald S, Bose R, Ornitz D, Xiong D, You M, Dooling DJ, Watson M, Mardis ER, Wilson RK. Genomic landscape of non-small cell lung cancer in smokers and never-smokers. Cell. 2012;150(6):1121-34. doi: 10.1016/j.cell.2012.08.024.

[121] Klotz LV, Courty Y, Lindner M, Petit-Courty A, Stowasser A, Koch I, Eichhorn ME, Lilis I, Morresi-Hauf A, Arendt KAM, Pepe M, Giopanou I, Ntaliarda G, Behrend SJ, Oplopoiou M, Gissot V, Guyetant S, Marchand-Adam S, Behr J, Kaiser JC, Hatz RA, Lamort AS, Stathopoulos GT. Comprehensive clinical profiling of the Gauting locoregional lung adenocarcinoma donors. Cancer Med. 2019;8(4):1486-99. doi: 10.1002/cam4.2031.

[122] Lamort AS, Kaiser JC, Pepe MAA, Lilis I, Ntaliarda G, Somogyi K, Spella M, Behrend SJ, Giotopoulou GA, Kujawa W, Lindner M, Koch I, Hatz RA, Behr J, Sotillo R, Schamberger AC, Stathopoulos GT. Prognostic phenotypes of early-stage lung adenocarcinoma. Eur Respir J. 2022;60(1):2101674. doi: 10.1183/13993003.01674-2021.

[123] Sabbah DA, Hajjo R, Sweidan K. Review on Epidermal Growth Factor Receptor (EGFR) Structure, Signaling Pathways, Interactions, and Recent Updates of EGFR Inhibitors. Curr Top Med Chem. 2020;20(10):815-34. doi: 10.2174/1568026620666200303123102.

[124] Shaw AT, Yeap BY, Mino-Kenudson M, Digumarthy SR, Costa DB, Heist RS, Solomon B, Stubbs H, Admane S, McDermott U, Settleman J, Kobayashi S, Mark EJ, Rodig SJ, Chirieac LR, Kwak EL, Lynch TJ, Iafrate AJ. Clinical features and outcome of patients with non-small-cell lung cancer who harbor EML4-ALK. J Clin Oncol. 2009;27(26):4247-53. doi: 10.1200/jco.2009.22.6993.

[125] Locatelli-Sanchez M, Couraud S, Arpin D, Riou R, Bringuier PP, Souquet PJ. Routine EGFR molecular analysis in non-small-cell lung cancer patients is feasible: exons 18-21 sequencing results of 753 patients and subsequent clinical outcomes. Lung. 2013;191(5):491-9. doi: 10.1007/s00408-013-9482-4.

[126] Cardoso F, Kyriakides S, Ohno S, Penault-Llorca F, Poortmans P, Rubio IT, Zackrisson S, Senkus E. Early breast cancer: ESMO Clinical Practice Guidelines for diagnosis, treatment and follow-up†. Ann Oncol. 2019;30(8):1194-220. doi: 10.1093/annonc/mdz173.

[127] Yap TA, Aerts JG, Popat S, Fennell DA. Novel insights into mesothelioma biology and implications for therapy. Nat Rev Cancer. 2017;17(8):475-88. doi: 10.1038/nrc.2017.42.

[128] Patel MR, Jacobson BA, De A, Frizelle SP, Janne P, Thumma SC, Whitson BA, Farassati F, Kratzke RA. Ras pathway activation in malignant mesothelioma. J Thorac Oncol. 2007;2(9):789-95. doi: 10.1097/JTO.0b013e31811f3aab.

[129] Matallanas D, Romano D, Al-Mulla F, O'Neill E, Al-Ali W, Crespo P, Doyle B, Nixon C, Sansom O, Drosten M, Barbacid M, Kolch W. Mutant K-Ras activation of the proapoptotic

MST2 pathway is antagonized by wild-type K-Ras. Mol Cell. 2011;44(6):893-906. doi: 10.1016/j.molcel.2011.10.016.

[130] Enomoto Y, Kasai T, Takeda M, Takano M, Morita K, Kadota E, Iizuka N, Maruyama H, Haratake J, Kojima Y, Ikeda N, Inatsugi N, Nonomura A. Epidermal growth factor receptor mutations in malignant pleural and peritoneal mesothelioma. J Clin Pathol. 2012;65(6):522-7. doi: 10.1136/jclinpath-2011-200631.

[131] Mezzapelle R, Miglio U, Rena O, Paganotti A, Allegrini S, Antona J, Molinari F, Frattini M, Monga G, Alabiso O, Boldorini R. Mutation analysis of the EGFR gene and downstream signalling pathway in histologic samples of malignant pleural mesothelioma. Br J Cancer. 2013;108(8):1743-9. doi: 10.1038/bjc.2013.130.

[132] Shukuya T, Serizawa M, Watanabe M, Akamatsu H, Abe M, Imai H, Tokito T, Ono A, Taira T, Kenmotsu H, Naito T, Murakami H, Takahashi T, Endo M, Ohde Y, Nakajima T, Yamamoto N, Koh Y. Identification of actionable mutations in malignant pleural mesothelioma. Lung Cancer. 2014;86(1):35-40. doi: 10.1016/j.lungcan.2014.08.004.

[133] Guo G, Chmielecki J, Goparaju C, Heguy A, Dolgalev I, Carbone M, Seepo S, Meyerson M, Pass HI. Whole-exome sequencing reveals frequent genetic alterations in BAP1, NF2, CDKN2A, and CUL1 in malignant pleural mesothelioma. Cancer Res. 2015;75(2):264-9. doi: 10.1158/0008-5472.Can-14-1008.

[134] Lo Iacono M, Monica V, Righi L, Grosso F, Libener R, Vatrano S, Bironzo P, Novello S, Musmeci L, Volante M, Papotti M, Scagliotti GV. Targeted next-generation sequencing of cancer genes in advanced stage malignant pleural mesothelioma: a retrospective study. J Thorac Oncol. 2015;10(3):492-9. doi: 10.1097/jto.0000000000000436.

[135] De Rienzo A, Archer MA, Yeap BY, Dao N, Sciaranghella D, Sideris AC, Zheng Y, Holman AG, Wang YE, Dal Cin PS, Fletcher JA, Rubio R, Croft L, Quackenbush J, Sugarbaker PE, Munir KJ, Battilana JR, Gustafson CE, Chirieac LR, Ching SM, Wong J, Tay LC, Rudd S, Hercus R, Sugarbaker DJ, Richards WG, Bueno R. Gender-Specific Molecular and Clinical Features Underlie Malignant Pleural Mesothelioma. Cancer Res. 2016;76(2):319-28. doi: 10.1158/0008-5472.Can-15-0751.

[136] Kato S, Tomson BN, Buys TP, Elkin SK, Carter JL, Kurzrock R. Genomic Landscape of Malignant Mesotheliomas. Mol Cancer Ther. 2016;15(10):2498-507. doi: 10.1158/1535-7163.Mct-16-0229.

[137] Klotz LV, Lindner M, Eichhorn ME, Grützner U, Koch I, Winter H, Kauke T, Duell T, Hatz RA. Pleurectomy/decortication and hyperthermic intrathoracic chemoperfusion using cisplatin and doxorubicin for malignant pleural mesothelioma. J Thorac Dis. 2019;11(5):1963-72. doi: 10.21037/jtd.2019.04.93.

[138] Gueugnon F, Leclercq S, Blanquart C, Sagan C, Cellerin L, Padieu M, Perigaud C, Scherpereel A, Gregoire M. Identification of novel markers for the diagnosis of malignant pleural mesothelioma. Am J Pathol. 2011;178(3):1033-42. doi: 10.1016/j.ajpath.2010.12.014.

[139] Smeele P, d'Almeida SM, Meiller C, Chéné AL, Liddell C, Cellerin L, Montagne F, Deshayes S, Benziane S, Copin MC, Hofman P, Le Pimpec-Barthes F, Porte H, Scherpereel A, Grégoire M, Jean D, Blanquart C. Brain-derived neurotrophic factor, a new soluble biomarker for malignant pleural mesothelioma involved in angiogenesis. Mol Cancer. 2018;17(1):148. doi: 10.1186/s12943-018-0891-0.

[140] Ikediobi ON, Davies H, Bignell G, Edkins S, Stevens C, O'Meara S, Santarius T, Avis T, Barthorpe S, Brackenbury L, Buck G, Butler A, Clements J, Cole J, Dicks E, Forbes S, Gray K, Halliday K, Harrison R, Hills K, Hinton J, Hunter C, Jenkinson A, Jones D, Kosmidou V, Lugg R, Menzies A, Mironenko T, Parker A, Perry J, Raine K, Richardson D, Shepherd R, Small A, Smith R, Solomon H, Stephens P, Teague J, Tofts C, Varian J, Webb T, West S, Widaa S, Yates A, Reinhold W, Weinstein JN, Stratton MR, Futreal PA, Wooster R. Mutation analysis of 24 known cancer genes in the NCI-60 cell line set. Mol Cancer Ther. 2006;5(11):2606-12. doi: 10.1158/1535-7163.Mct-06-0433.

[141] Forbes SA, Beare D, Gunasekaran P, Leung K, Bindal N, Boutselakis H, Ding M, Bamford S, Cole C, Ward S, Kok CY, Jia M, De T, Teague JW, Stratton MR, McDermott U, Campbell PJ. COSMIC: exploring the world's knowledge of somatic mutations in

human cancer. Nucleic Acids Res. 2015;43(Database issue):D805-11. doi: 10.1093/nar/gku1075.

[142] Fridlender ZG, Sun J, Kim S, Kapoor V, Cheng G, Ling L, Worthen GS, Albelda SM. Polarization of tumor-associated neutrophil phenotype by TGF-beta: "N1" versus "N2" TAN. Cancer Cell. 2009;16(3):183-94. doi: 10.1016/j.ccr.2009.06.017.

[143] Agalioti T, Giannou AD, Krontira AC, Kanellakis NI, Kati D, Vreka M, Pepe M, Spella M, Lilis I, Zazara DE, Nikolouli E, Spiropoulou N, Papadakis A, Papadia K, Voulgaridis A, Harokopos V, Stamou P, Meiners S, Eickelberg O, Snyder LA, Antimisiaris SG, Kardamakis D, Psallidas I, Marazioti A, Stathopoulos GT. Mutant KRAS promotes malignant pleural effusion formation. Nat Commun. 2017;8:15205. doi: 10.1038/ncomms15205.

[144] Jongsma J, van Montfort E, Vooijs M, Zevenhoven J, Krimpenfort P, van der Valk M, van de Vijver M, Berns A. A conditional mouse model for malignant mesothelioma. Cancer Cell. 2008;13(3):261-71. doi: 10.1016/j.ccr.2008.01.030.

[145] Guo Y, Chirieac LR, Bueno R, Pass H, Wu W, Malinowska IA, Kwiatkowski DJ. Tsc1-Tp53 loss induces mesothelioma in mice, and evidence for this mechanism in human mesothelioma. Oncogene. 2014;33(24):3151-60. doi: 10.1038/onc.2013.280.

[146] Xu J, Kadariya Y, Cheung M, Pei J, Talarchek J, Sementino E, Tan Y, Menges CW, Cai KQ, Litwin S, Peng H, Karar J, Rauscher FJ, Testa JR. Germline mutation of Bap1 accelerates development of asbestos-induced malignant mesothelioma. Cancer Res. 2014;74(16):4388-97. doi: 10.1158/0008-5472.Can-14-1328.

[147] Kukuyan AM, Sementino E, Kadariya Y, Menges CW, Cheung M, Tan Y, Cai KQ, Slifker MJ, Peri S, Klein-Szanto AJ, Rauscher FJ, 3rd, Testa JR. Inactivation of Bap1 Cooperates with Losses of Nf2 and Cdkn2a to Drive the Development of Pleural Malignant Mesothelioma in Conditional Mouse Models. Cancer Res. 2019;79(16):4113-23. doi: 10.1158/0008-5472.Can-18-4093.

[148] Jackson EL, Willis N, Mercer K, Bronson RT, Crowley D, Montoya R, Jacks T, Tuveson DA. Analysis of lung tumor initiation and progression using conditional expression of oncogenic K-ras. Genes Dev. 2001;15(24):3243-8. doi: 10.1101/gad.943001.

[149] Meylan E, Dooley AL, Feldser DM, Shen L, Turk E, Ouyang C, Jacks T. Requirement for NF-kappaB signalling in a mouse model of lung adenocarcinoma. Nature. 2009;462(7269):104-7. doi: 10.1038/nature08462.

[150] Giannou AD, Marazioti A, Spella M, Kanellakis NI, Apostolopoulou H, Psallidas I, Prijovich ZM, Vreka M, Zazara DE, Lilis I, Papaleonidopoulos V, Kairi CA, Patmanidi AL, Giopanou I, Spiropoulou N, Harokopos V, Aidinis V, Spyratos D, Teliousi S, Papadaki H, Taraviras S, Snyder LA, Eickelberg O, Kardamakis D, Iwakura Y, Feyerabend TB, Rodewald HR, Kalomenidis I, Blackwell TS, Agalioti T, Stathopoulos GT. Mast cells mediate malignant pleural effusion formation. J Clin Invest. 2015;125(6):2317-34. doi: 10.1172/jci79840.

[151] Nagai H, Okazaki Y, Chew SH, Misawa N, Yamashita Y, Akatsuka S, Ishihara T, Yamashita K, Yoshikawa Y, Yasui H, Jiang L, Ohara H, Takahashi T, Ichihara G, Kostarelos K, Miyata Y, Shinohara H, Toyokuni S. Diameter and rigidity of multiwalled carbon nanotubes are critical factors in mesothelial injury and carcinogenesis. Proc Natl Acad Sci U S A. 2011;108(49):E1330-8. doi: 10.1073/pnas.1110013108.

[152] Patil NS, Righi L, Koeppen H, Zou W, Izzo S, Grosso F, Libener R, Loiacono M, Monica V, Buttigliero C, Novello S, Hegde PS, Papotti M, Kowanetz M, Scagliotti GV. Molecular and Histopathological Characterization of the Tumor Immune Microenvironment in Advanced Stage of Malignant Pleural Mesothelioma. J Thorac Oncol. 2018;13(1):124-33. doi: 10.1016/j.jtho.2017.09.1968.

[153] Robinson BW, Musk AW, Lake RA. Malignant mesothelioma. Lancet. 2005;366(9483):397-408. doi: 10.1016/s0140-6736(05)67025-0.

[154] Byrd AL, Segre JA. Infectious disease. Adapting Koch's postulates. Science. 2016;351(6270):224-6. doi: 10.1126/science.aad6753.

[155] Zimmermann G, Papke B, Ismail S, Vartak N, Chandra A, Hoffmann M, Hahn SA, Triola G, Wittinghofer A, Bastiaens PI, Waldmann H. Small molecule inhibition of the KRAS-PDEδ interaction impairs oncogenic KRAS signalling. Nature. 2013;497(7451):638-42. doi: 10.1038/nature12205.

[156] De Rienzo A, Richards WG, Yeap BY, Coleman MH, Sugarbaker PE, Chirieac LR, Wang YE, Quackenbush J, Jensen RV, Bueno R. Sequential binary gene ratio tests define a novel molecular diagnostic strategy for malignant pleural mesothelioma. Clin Cancer Res. 2013;19(9):2493-502. doi: 10.1158/1078-0432.Ccr-12-2117.

[157] Abbosh C, Birkbak NJ, Wilson GA, Jamal-Hanjani M, Constantin T, Salari R, Le Quesne J, Moore DA, Veeriah S, Rosenthal R, Marafioti T, Kirkizlar E, Watkins TBK, McGranahan N, Ward S, Martinson L, Riley J, Fraioli F, Al Bakir M, Grönroos E, Zambrana F, Endozo R, Bi WL, Fennessy FM, Sponer N, Johnson D, Laycock J, Shafi S, Czyzewska-Khan J, Rowan A, Chambers T, Matthews N, Turajlic S, Hiley C, Lee SM, Forster MD, Ahmad T, Falzon M, Borg E, Lawrence D, Hayward M, Kolvekar S, Panagiotopoulos N, Janes SM, Thakrar R, Ahmed A, Blackhall F, Summers Y, Hafez D, Naik A, Ganguly A, Kareht S, Shah R, Joseph L, Marie Quinn A, Crosbie PA, Naidu B, Middleton G, Langman G, Trotter S, Nicolson M, Remmen H, Kerr K, Chetty M, Gomersall L, Fennell DA, Nakas A, Rathinam S, Anand G, Khan S, Russell P, Ezhil V, Ismail B, Irvin-Sellers M, Prakash V, Lester JF, Kornaszewska M, Attanoos R, Adams H, Davies H, Oukrif D, Akarca AU, Hartley JA, Lowe HL, Lock S, Iles N, Bell H, Ngai Y, Elgar G, Szallasi Z, Schwarz RF, Herrero J, Stewart A, Quezada SA, Peggs KS, Van Loo P, Dive C, Lin CJ, Rabinowitz M, Aerts H, Hackshaw A, Shaw JA, Zimmermann BG, Swanton C. Phylogenetic ctDNA analysis depicts early-stage lung cancer evolution. Nature. 2017;545(7655):446-51. doi: 10.1038/nature22364.

# Appendix A: Paper III

Reproduced with permission of the ERS 2023: European Respiratory Review 30 (162) 210122; doi: 10.1183/16000617.0122-2021 Published 20 October 2021

EUROPEAN RESPIRATORY REVIEW
LUNG SCIENCE CONFERENCE
S.J. BEHREND ET AL.

## A role for club cells in smoking-associated lung adenocarcinoma

Sabine J. Behrend [1,2], Georgia A. Giotopoulou[1,2], Magda Spella[3] and Georgios T. Stathopoulos [1,2]

[1]Comprehensive Pneumology Center (CPC) and Institute for Lung Biology and Disease (iLBD); Helmholtz Center Munich-German Research Center for Environmental Health (HMGU) and Ludwig-Maximilian-University (LMU) Munich, Munich, Germany. [2]German Center for Lung Research (DZL), Giessen, Germany. [3]Laboratory for Molecular Respiratory Carcinogenesis, Dept of Physiology, Faculty of Medicine, University of Patras, Patras, Greece.

Corresponding author: Georgios T. Stathopoulos (stathopoulos@helmholtz-muenchen.de)

Shareable abstract (@ERSpublications)
**Multiple lung epithelial cells are targets of carcinogenic hits. Club cells are such cells that can metabolically activate tobacco pre-carcinogens, being thus positioned as cells of origin of lung adenocarcinomas in smokers.** https://bit.ly/3iOshcy

**Cite this article as:** Behrend SJ, Giotopoulou GA, Spella M, *et al*. A role for club cells in smoking-associated lung adenocarcinoma. *Eur Respir Rev* 2021; 30: 210122 [DOI: 10.1183/16000617.0122-2021].



Received: 22 May 2021
Accepted: 5 Aug 2021

### Abstract

The cellular origin of lung adenocarcinoma remains a focus of intense research efforts. The marked cellular heterogeneity and plasticity of the lungs, as well as the vast variety of molecular subtypes of lung adenocarcinomas perplex the field and account for the extensive variability of experimental results. While most experts would agree on the cellular origins of other types of thoracic tumours, great controversy exists on the tumour-initiating cells of lung adenocarcinoma, since this histologic subtype of lung cancer arises in the distal pulmonary regions where airways and alveoli converge, occurs in smokers as well as nonsmokers, is likely caused by various environmental agents, and is marked by vast molecular and pathologic heterogeneity. Alveolar type II, club, and their variant cells have all been implicated in lung adenocarcinoma progeny and the lineage hierarchies in the distal lung remain disputed. Here we review the relevant literature in this rapidly expanding field, including results from mouse models and human studies. In addition, we present a case for club cells as cells of origin of lung adenocarcinomas that arise in smokers.

### Introduction

Lung cancer is the most lethal cancer worldwide causing more than 1.7 million deaths in 2018 [1]. Lung adenocarcinoma (LUAD) is the most prevalent histologic subtype of lung cancer and accounts for almost half of all lung cancer deaths because of its indolent clinical presentation and its peripheral location in the lung parenchyma [2, 3]. As most lung cancers, and especially LUAD, are diagnosed when they have already become locally advanced or metastatic, the 5-year survival rate amounts to only 15% [4]. Despite rapid improvements in lung cancer prevention through smoking cessation and screening programmes, as well as targeted and multi-modality therapies in the last few decades, lung cancer remains a dreadful disease [5, 6]. While the incidence and mortality of many other types of lung cancer such as squamous cell lung carcinoma and small cell lung carcinoma are continuously dropping in more developed countries where smoking incidence is declining, LUAD incidence and mortality are constantly rising, a phenomenon ascribed to the changing face of manufactured cigarettes and the increasing occurrence of LUAD in nonsmokers [7–12].

Cancers are defined by both their genetic alterations and their cells and tissues of origin [13]. These precancerous cells and tissues of origin define which cells can potentially lead to cancer, and are likely distinct from stem cells in established tumours, which constitute the subset of cancer cells that possesses stem cell characteristics and can drive tumour progression, therapy resistance, relapse and metastasis [13]. It has been demonstrated that self-renewal pathways such as Wnt, Hedgehog, and Notch that are upregulated in embryonic stem cells are also commonly reactivated in tumour-initiating and cancer stem cells as well as in mature lung cancers, driving proliferation, resistance to apoptosis, epithelial-to-mesenchymal transition, metastasis, acquisition of new blood vessels and further genomic permutation [14]. Such lung

cancer initiating and stem cells possess self-renewal properties and are able to execute programmes of repair and normal tissue replacement during precarcinogenesis and established carcinogenesis [15].

Several cell types of the lungs hold tumour-initiating and stem cell properties and are thus potential cells of origin of lung cancer. To this end, p63(+)Krt5(+) distal airway stem cells likely relevant to airway basal cells have been shown to maintain and repopulate the airway and alveolar epithelium following viral injury, while club cell secretory protein (CCSP)-expressing club cells have also been shown to be capable of maintaining and repairing smaller bronchioles and alveolar structures [16–20]. Similarly, surfactant protein C (SFTPC)-producing alveolar type II (ATII) cells are responsible for maintenance of the alveolar epithelium [21, 22]. However, CCSP+SFTPC+ double positive bronchioalveolar stem cells (BASC) that reside in the terminal and respiratory bronchioles and alveolar ducts and can differentiate into club cells as well as alveolar cells were also shown to possess strong regenerative potential of both airway and alveolar epithelium [23]. An often underestimated and disputed pool of lung stem cells are of mesenchymal origin, located in all human tissues and organs and shown to migrate and differentiate into non-mesodermal cell types [24–26]. Additional cells that are lineage negative have been shown to reside in the lungs and to possess strong regenerative potential, while mesothelial cells were also shown to repopulate mesenchymal cells of the lungs and other internal organs [27, 28]. While lung stem cells and their functions are authoritatively reviewed elsewhere [29–33], the present review will summarise the current knowledge on the cells of origin of lung cancer with a special focus on club cells and their potential role as cancer stem cells of LUAD.

## Methods

In addition to articles already known to the authors, PubMed (https://pubmed.ncbi.nlm.nih.gov/) was queried on 17 May 2021 using theterms: (‘lung cancer’[Title/Abstract] OR ‘lung adenocarcinoma’[Title/Abstract] OR ‘squamous cell lung carcinoma’[Title/Abstract] OR ‘squamous cell lung cancer’[Title/Abstract] OR ‘small cell lung cancer’[Title/Abstract] OR ‘small cell lung carcinoma’[Title/Abstract]) AND (‘stem cell’[Title/Abstract] OR ‘cell of origin’[Title/Abstract]), retrieving 1385 results. Titles and journal names were manually curated to yield 416 articles whose abstracts were screened to yield the articles that built the knowledgebase and reference list of the present review.

## Results

### *The causes of cancer translated to lung adenocarcinoma*

Heredity causes multiple forms of cancer that can be clinically manifest in childhood, but also in adult life, and can be spontaneous or co-precipitated by germline mutations and environmental factors such as smoking [34, 35]. Heredity can also indirectly cause cancer by influencing our interactions with the environment, as is the case with a single nucleotide polymorphism in the habenular nicotinergic acetylcholine receptor which renders individuals susceptible to nicotine addiction and thereby to COPD, lung cancer and peripheral arterial disease [36]. Environmental carcinogens are thought to be even more important than heredity in precipitating chest tumours in humans. The relationship between tobacco smoking and lung cancer is one of the best documented epidemiologic relationships, while the same goes for asbestos exposure and mesothelioma [37–44]. Radiation has also been tightly linked with lung cancer development based on a number of different data sources, including atom bomb survivors, nuclear plant workers, uranium miners, radiotherapy patients, and participants of lung cancer screening programmes [45–54]. Finally, an increasingly stronger case is in the making for the connection between urban air pollution and lung cancer [55–58]. While the list of environmental carcinogens that impact the lungs and pleura is getting longer every day, and are comprehensively reviewed elsewhere [38], a fascinating new hypothesis saw the light of day in recent years: the bad luck hypothesis by Tomasetti and Vogelstein examines the possibility of a significant proportion of human cancers resulting from stem cell divisions gone awry [59–62]. This ground-breaking work was based on measurements of cell division rates in the various organs using proliferating cell nuclear antigen (PCNA) and marker of proliferation Ki-67 staining of proliferating cells and extrapolation of the data by organ size and cell number. Indeed, PCNA+ cells in the resting lung are very sparse, and increase tremendously in lung cancers [59–62].

Hence, several different environmental and endogenous causes can precipitate lung cancer originating from the same and/or different lung lineages, and this heterogeneity is most evident with LUAD. It is highly likely that different molecular subtypes of LUAD exist, which emanate from different cells of origin that were tumour-initiated by different triggers, and such patient subgroups are evident in molecular and epidemiologic datasets. For example, we identified two subgroups of patients with LUAD in atom bomb survivors from Hiroshima and Nagasaki included in the Life Span Study that can be explained by exposures to smoking and to irradiation, and validated their existence in the TCGA cohort from the US [48]. In addition, molecular subsets of *KRAS*-mutant LUAD were identified within the TCGA cohort *via* elegant

genomic analyses [63]. This interpatient heterogeneity of LUAD needs to be addressed by future studies on the cell of origin of lung tumours, which should ascertain the tumour subtype under study.

### *Evidence from genetic mouse models of LUAD*

Studies on the origins of LUAD have been boosted tremendously by the use of genetically engineered mouse models, which are valuable tools for tumour induction and lineage tracing. Model organisms have been genetically manipulated to conditionally express oncogenic or tumour suppressive alleles, in conjunction with CRE recombinase expressed under the control of a promoter active specifically in one of the different respiratory cell lineages, and are therefore ideal for the tracing of a specific cell population carrying specific mutations in time and space. Prominent focus has been given to the development of mouse models harbouring KRAS proto-oncogene GTPase (encoded by the human *KRAS* and the murine *Kras* genes) and tumour protein 53 (encoded by the human *TP53* and the murine *Trp53* genes) mutations, as oncogenic mutations of the *KRAS* and *TP53* genes are found in 34% and 54% of human LUAD [64, 65]. As a result, several mutant *Kras/KRAS* knock-in and *Trp53* knockout mouse models have been generated, with the most widely used among them being the *Lox-Stop-Lox-KRAS*$^{G12D}$ model, which develops LUAD within 4 months post intranasal administration of adenoviral CRE, and the *Lox-Trp53-Lox* model, in which *Trp53* can be deleted in specific lineages and can cause more aggressive LUAD when combined with the *Lox-Stop-Lox-KRAS*$^{G12D}$ model, as well as other transgenic mouse models that cannot be all mentioned here [64–68]. Pulmonary lineage tracing studies in the respiratory epithelium of these genetically modified mice following forced expression of the *Kras*$^{G12D}$ mutation in club airway epithelial cells expressing CCSP, or in ATII alveolar epithelial cells expressing SFTPC, or in bronchoalveolar epithelial cells expressing both markers, resulted interchangeably in LUAD formation, leading to inconclusive data as to the progenitors of LUAD in adult mice [22, 23, 69–71]. This is partly attributable to the fact that some of the above-referenced lineage tracing mouse models feature incomplete and/or promiscuous lung cell labelling, to the heterogeneity among ATII cells regarding their proliferative and to tumour-initiating cell properties [22], but also to the viral-induced injury itself, since it was also shown that adenoviral infection alone contributed to the transformation of lung cells towards LUAD [71]. Similar genetically engineered mouse models reproducing other LUAD driver mutations such as *EGFR* mutations and *EML4-ALK* fusions have also been established and have proven the oncogenicity of the respective molecular changes when forcefully expressed in alveolar cells, implying that ATII cells are the cellular origins of multiple oncogene-driven LUAD tumours [72–74].

### *Evidence from environmental LUAD induction in mice*

Although the above-referenced genetic mouse models have enhanced our mechanistic understanding of LUAD development, oncogene function and cell of origin, they do not fully capture the mutation diversity and burden of human LUAD, which is caused by environmental carcinogens rather than single oncogenes [74, 75]. To better recapitulate the mutational acquisition pattern and dissect the complex pathobiology of human LUAD, alternative strategies can be employed that combine conditional respiratory lineage tracing with carcinogenic insults. This approach is advantageous in recapitulating pathophysiologic endogenous carcinogenic events and in unravelling key events taking place during early tumour initiation, knowledge which can prove valuable for the development of LUAD early detection of chemoprevention strategies. Along these lines, we recently showed that as early as two weeks following treatment of lineage-marked mice with urethane (ethyl carbamate, a chemical carcinogen contained in tobacco smoke) [76], *Kras*$^{Q61R}$ driver mutations accumulate specifically in club and not in ATII cells [20], in line with evidence from human airway epithelial cells found to be sensitised by tobacco smoke to a single-hit *KRAS* mutation [77] and from a massive parallel sequencing approach [78]. These results are also in accord with earlier studies that dictate that only club cells possess the cytochrome CYP2E1 [79, 80] that is required to convert the tobacco pre-carcinogen urethane (ethyl carbamate) to carcinogenic derivatives vinyl carbamate and its epoxide [81, 82], which in turn have a half-life of a few femtoseconds and can thus only injure the DNA of the same cell that metabolically activates them [83, 84]. Thus, club cells are likely to be the cellular source of LUAD triggered by the tobacco carcinogen urethane as opposed to ATII cells as cells of origin of transgenic lung tumours in mice [20, 85].

Indeed, environmental-induced LUAD in susceptible inbred mouse strains is a versatile research tool. To this end, single-hit LUAD emerge in sensitive FVB and A/J mice 6–9 months post-treatment with intraperitoneal urethane (ethyl carbamate), N-nitrosodiethylamine (DEN), 4-(methylnitrosamino)-1-(3-pyridyl)-1-butanone (NNK), N′-nitrosonornicotine (NNN), and N-methyl-N-nitrosourea (MNU), and uniquely recapitulate the mutational landscape of human LUAD [20, 75, 86–93]. Such models have been successfully used to study oncogene function in the genomic context and to reproduce human-relevant LUAD mutanomes in mice [75, 93]. Although chemical models of LUAD do not necessarily rely on human-relevant *Kras* mutations, they rather generate a human-relevant mutation spectrum in terms of

single nucleotide variants in the mono- and tri-nucleotide, as well as the gene contexts [75, 87]. For example, urethane-induced LUAD in mice feature the *Kras*$^{Q61R}$ mutation, which is very rare in human LUAD, but at the same time they harbour multiple mutations in critical LUAD genes such as *Alk* and *Crebbp* that are highly relevant to human LUAD [75]. Combining such tools with lineage tracing allows spatiotemporal exploration of whole adverse outcome pathways leading from a specific carcinogen to lineage-restricted molecular initiating events, key progression events and clinicopathologic and molecular signatures that indicate the initiating agent and cell type. Using such an approach, club cells were shown to contribute to lung maintenance, repair and carcinogenesis, to possess stem cell features and to sustain chemical-induced *KRAS* mutations as LUAD cells of origin would [20, 85].

### *Evidence from human LUAD*

Human LUAD patient cohorts have also been interrogated for cell of origin signatures, since abundant evidence supports that cell of origin is imprinted and deductible from molecular data [94, 95]. These studies have been sparse but imperative, since there are marked differences between mouse and human lung epithelial cell biology, rendering translation of mouse lineage tracing data to the human setting uncertain. Such studies are marked by inherent uncertainty, since lineage plasticity in the lungs is tremendous and even malignant lung tumours can switch histology and molecular profiles upon acquisition of new genomic alterations [96, 97]. To this end, one study exploited the finding of co-mutations of *KRAS* and *KEAP1* in 5% of LUAD [63] to ascribe different cells of origin (airway *versus* alveolar), as well as immunometabolic profiles to *KRAS*-mutant LUAD with or without *KEAP1* alterations [98]. In another effort to determine genomic imprints of cell fate, squamous and adenomatous lung tumours appeared highly similar, suggesting a common ancestor [99]. In our view, tumours of smokers and nonsmokers may very well have different cellular origins, and hence studies should focus on molecular hallmarks of smoking when examining lineage of origin, since such markers have been described, including KRAS and TP53 mutations, as well as the C>A transversions described elsewhere [100–102]. These data show the need for genetic lineage tracing models in the search for cells of origin of lung tumours, and for biomarkers of environmental and endogenous lung cancer causative agents. Furthermore, they illustrate the marked heterogeneity of LUAD, which needs to be taken into account in such lineage tracing studies.

## Conclusions

The contribution of cells with stemness properties to tissue homeostasis, regeneration and tumour progression is undeniable, and this trait renders them attractive therapeutic targets. In heterogeneous tumours, stem cells will sustain tumour growth and possibly tumour recurrence. Chemical carcinogenesis mouse models faithfully recapitulate human LUAD, and have highlighted club cells as a central respiratory cell population with a key role in early initiation events leading to LUAD. Future perspectives should therefore be targeted to better characterise this cell type and to increase our comprehension of the mechanisms regulating cell biology, biomarker expression, mutational acquisition spatiotemporal patterns, molecular dynamics of tumour evolution and tumour architecture. Novel technologies, such as organoids, 3D whole organ imaging with single cell resolution, and single cell sequencing, have been developed to compliment the knowledge gained from transgenic mouse models and better understand the underlying tumour pathobiology. The new knowledge should be tested on human-relevant experimental pre-clinical models, so that effective therapies can be developed.

Acknowledgements: This work was supported by the Graduate College (Graduiertenkolleg, GRK) #2338 of the German Research Society (Deutsche Forschungsgemeinschaft, DFG), the target validation project for pharmaceutical development ALTERNATIVE of the German Ministry for Education and Research (Bundesministerium für Bildung und Forschung, BMBF), and a Translational Research Grant by the German Centre for Lung Research (Deutsches Zentrum für Lungenforschung, DZL) (all to GTS); the Greek State Scholarship Foundation Program 'Reinforcement of Postdoctoral Researchers-1st and 2nd cycles' co-financed by the European Union Social Fund and Greek national funds (NSRF 2014–2020 and MIS-5033021) and General Secretariat for Research and Innovation and Hellenic Foundation for Research and Innovation grant #1853a (all to MS).

Provenance: Commissioned article, peer reviewed.

Author Contributions: S.J. Behrend, G.A. Giotopoulou, M. Spella and G.T. Stathopoulos conceived the idea, analysed data, generated graphs and figures, and wrote the paper. All authors reviewed and concurred with the submitted manuscript.

Conflict of interest: None declared.

Support statement: Funding was received from Bundesministerium für Bildung und Forschung (Grant: ALTERNATIVE), Deutsches Zentrum für Lungenforschung (Grant: Translational Research Grant), Greek State Scholarship Foundation Program 'Reinforcement of Postdoctoral Researchers-1st and 2nd cycles' co-financed by the European Union Social Fund and Greek national funds (Grant: NSRF 2014-2020 and MIS-5033021), General Secretariat for Research and Innovation and Hellenic Foundation for Research and Innovation (Grant: #1853a) and Deutsche Forschungsgemeinschaft (Grant: GRK2338). Funding information for this article has been deposited with the Crossref Funder Registry.

## References

1 Bray F, Ferlay J, Soerjomataram I, *et al.* Global cancer statistics 2018: GLOBOCAN estimates of incidence and mortality worldwide for 36 cancers in 185 countries. *CA Cancer J Clin* 2018; 68: 394–424.
2 Houston KA, Henley SJ, Li J, *et al.* Patterns in lung cancer incidence rates and trends by histologic type in the United States, 2004–2009. *Lung Cancer* 2014; 86: 22–28.
3 Kenfield SA, Wei EK, Stampfer MJ, *et al.* Comparison of aspects of smoking among the four histological types of lung cancer. *Tob Control* 2008; 17: 198–204.
4 Minna JD, Schiller JH. Lung Cancer. *In*: Harrison's Principles of Internal Medicine. 17th Edn. MacGraw-Hill, Philadelphia, 2008; pp. 551–562.
5 Schabath MB, Cote ML. Cancer progress and priorities: lung cancer. *Cancer Epidemiol Biomarkers Prev* 2019; 28: 1563–1579.
6 Hirsch FR, Scagliotti GV, Mulshine JL, *et al.* Lung cancer: current therapies and new targeted treatments. *Lancet* 2017; 389: 299–311.
7 Janssen-Heijnen ML, Nab HW, van Reek J, *et al.* Striking changes in smoking behaviour and lung cancer incidence by histological type in south-east Netherlands, 1960–1991. *Eur J Cancer* 1995; 31a: 949–952.
8 Levi F, Franceschi S, La Vecchia C, *et al.* Lung carcinoma trends by histologic type in Vaud and Neuchâtel, Switzerland, 1974–1994. *Cancer* 1997; 79: 906–914.
9 Russo A, Crosignani P, Franceschi S, *et al.* Changes in lung cancer histological types in Varese Cancer Registry, Italy 1976–1992. *Eur J Cancer* 1997; 33: 1643–1647.
10 Wingo PA, Ries LA, Giovino GA, *et al.* Annual report to the nation on the status of cancer, 1973–1996, with a special section on lung cancer and tobacco smoking. *J Natl Cancer Inst* 1999; 91: 675–690.
11 Sobue T, Ajiki W, Tsukuma H, *et al.* Trends of lung cancer incidence by histologic type: a population-based study in Osaka, Japan. *Jpn J Cancer Res* 1999; 90: 6–15.
12 Cha Q, Chen Y, Du Y. The trends in histological types of lung cancer during 1980–1988, Guangzhou, China. *Lung Cancer* 1997; 17: 219–230.
13 Batlle E, Clevers H. Cancer stem cells revisited. *Nat Med* 2017; 23: 1124–1134.
14 Lundin A, Driscoll B. Lung cancer stem cells: progress and prospects. *Cancer Lett* 2013; 338: 89–93.
15 Heng WS, Gosens R, Kruyt FAE. Lung cancer stem cells: origin, features, maintenance mechanisms and therapeutic targeting. *Biochem Pharmacol* 2019; 160: 121–133.
16 Rock JR, Onaitis MW, Rawlins EL, *et al.* Basal cells as stem cells of the mouse trachea and human airway epithelium. *Proc Natl Acad Sci USA* 2009; 106: 12771–12775.
17 Rawlins EL, Okubo T, Xue Y, *et al.* The role of Scgb1a1+ Clara cells in the long-term maintenance and repair of lung airway, but not alveolar, epithelium. *Cell Stem Cell* 2009; 4: 525–534.
18 Zheng D, Limmon GV, Yin L, *et al.* Regeneration of alveolar type I and II cells from Scgb1a1- expressing cells following severe pulmonary damage induced by bleomycin and influenza. *PLoS ONE* 2012; 7: e48451.
19 Zuo W, Zhang T, Wu DZ, *et al.* p63(+)Krt5(+) distal airway stem cells are essential for lung regeneration. *Nature* 2015; 517: 616–620.
20 Spella M, Lilis I, Pepe MA, *et al.* Club cells form lung adenocarcinomas and maintain the alveoli of adult mice. *Elife* 2019; 8: e45571.
21 Barkauskas CE, Cronce MJ, Rackley CR, *et al.* Type 2 alveolar cells are stem cells in adult lung. *J Clin Invest* 2013; 123: 3025–3036.
22 Desai TJ, Brownfield DG, Krasnow MA. Alveolar progenitor and stem cells in lung development, renewal and cancer. *Nature* 2014; 507: 190–194.
23 Kim CF, Jackson EL, Woolfenden AE, *et al.* Identification of bronchioalveolar stem cells in normal lung and lung cancer. *Cell* 2005; 121: 823–835.
24 Chamberlain G, Fox J, Ashton B, *et al.* Concise review: mesenchymal stem cells: their phenotype, differentiation capacity, immunological features, and potential for homing. *Stem Cells* 2007; 25: 2739–2749.
25 Kotton DN, Ma BY, Cardoso WV, *et al.* Bone marrow-derived cells as progenitors of lung alveolar epithelium. *Development* 2001; 128: 5181–5188.
26 Lee JH, Tammela T, Hofree M, *et al.* Anatomically and functionally distinct lung mesenchymal populations marked by Lgr5 and Lgr6. *Cell* 2017; 170: 1149–1163.
27 Vaughan AE, Brumwell AN, Xi Y, *et al.* Lineage-negative progenitors mobilize to regenerate lung epithelium after major injury. *Nature* 2015; 517: 621–625.

28 Rinkevich Y, Mori T, Sahoo D, *et al.* Identification and prospective isolation of a mesothelial precursor lineage giving rise to smooth muscle cells and fibroblasts for mammalian internal organs, and their vasculature. *Nat Cell Biol* 2012; 14: 1251–1260.
29 Wu H, Tang N. Stem cells in pulmonary alveolar regeneration. *Development* 2021; 148: dev193458.
30 Nadkarni RR, Abed S, Draper JS. Stem cells in pulmonary disease and regeneration. *Chest* 2018; 153: 994–1003.
31 Tata PR, Rajagopal J. Plasticity in the lung: making and breaking cell identity. *Development* 2017; 144: 755–766.
32 Chen F, Fine A. Stem cells in lung injury and repair. *Am J Pathol* 2016; 186: 2544–2550.
33 Leeman KT, Fillmore CM, Kim CF. Lung stem and progenitor cells in tissue homeostasis and disease. *Curr Top Dev Biol* 2014; 107: 207–233.
34 Sweet-Cordero EA, Biegel JA. The genomic landscape of pediatric cancers: Implications for diagnosis and treatment. *Science* 2019; 363: 1170–1175.
35 Nenekidis I, Stathopoulos GT, Anagnostakou V, *et al.* Atypical pulmonary carcinoid tumour in a 28-year-old nonsmoker with Prader-Willi syndrome. *Eur Respir J* 2011; 38: 1230–1233.
36 Thorgeirsson TE, Geller F, Sulem P, *et al.* A variant associated with nicotine dependence, lung cancer and peripheral arterial disease. *Nature* 2008; 452: 638–642.
37 Hecht SS. Tobacco smoke carcinogens and lung cancer. *J Natl Cancer Inst* 1999; 91: 1194–1210.
38 Alberg AJ, Brock MV, Ford JG, *et al.* Epidemiology of lung cancer: Diagnosis and management of lung cancer, 3rd ed: American College of Chest Physicians evidence-based clinical practice guidelines. *Chest* 2013; 143: Suppl 5, e1S–e29S.
39 Sun S, Schiller JH, Gazdar AF. Lung cancer in never smokers – a different disease. *Nat Rev Cancer* 2007; 7: 778–790.
40 Rudin CM, Brambilla E, Faivre-Finn C, *et al.* Small-cell lung cancer. *Nat Rev Dis Primers* 2021; 7: 3.
41 Bibby AC, Tsim S, Kanellakis N, *et al.* Malignant pleural mesothelioma: an update on investigation, diagnosis and treatment. *Eur Respir Rev* 2016; 25: 472–486.
42 Liu B, van Gerwen M, Bonassi S, *et al.* Epidemiology of environmental exposure and malignant mesothelioma. *J Thorac Oncol* 2017; 12: 1031–1045.
43 Tsao AS, Wistuba I, Roth JA, *et al.* Malignant pleural mesothelioma. *J Clin Oncol* 2009; 27: 2081–2090.
44 Yap TA, Aerts JG, Popat S, *et al.* Novel insights into mesothelioma biology and implications for therapy. *Nat Rev Cancer* 2017; 17: 475–488.
45 Brenner DJ, Doll R, Goodhead DT, *et al.* Cancer risks attributable to low doses of ionizing radiation: assessing what we really know. *Proc Natl Acad Sci USA* 2003; 100: 13761–13766.
46 Darby SC, Doll R, Gill SK, *et al.* Long term mortality after a single treatment course with X-rays in patients treated for ankylosing spondylitis. *Br J Cancer* 1987; 55: 179–190.
47 Sachs RK, Brenner DJ. Solid tumor risks after high doses of ionizing radiation. *Proc Natl Acad Sci USA* 2005; 102: 13040–13045.
48 Castelletti N, Kaiser JC, Simonetto C, *et al.* Risk of lung adenocarcinoma from smoking and radiation arises in distinct molecular pathways. *Carcinogenesis* 2019; 40: 1240–1250.
49 Furukawa K, Preston DL, Lönn S, *et al.* Radiation and smoking effects on lung cancer incidence among atomic bomb survivors. *Radiat Res* 2010; 174: 72–82.
50 Egawa H, Furukawa K, Preston D, *et al.* Radiation and smoking effects on lung cancer incidence by histological types among atomic bomb survivors. *Radiat Res* 2012; 178: 191–201.
51 McCunney RJ, Li J. Radiation risks in lung cancer screening programs: a comparison with nuclear industry workers and atomic bomb survivors. *Chest* 2014; 145: 618–624.
52 Lubin JH, Boice JD Jr, Edling C, *et al.* Lung cancer in radon-exposed miners and estimation of risk from indoor exposure. *J Natl Cancer Inst* 1995; 87: 817–827.
53 Darby S, Hill D, Auvinen A, *et al.* Radon in homes and risk of lung cancer: collaborative analysis of individual data from 13 European case-control studies. *BMJ* 2005; 330: 223.
54 Gray A, Read S, McGale P, *et al.* Lung cancer deaths from indoor radon and the cost effectiveness and potential of policies to reduce them. *BMJ* 2009; 338: a3110.
55 Eckel SP, Cockburn M, Shu YH, *et al.* Air pollution affects lung cancer survival. *Thorax* 2016; 71: 891–898.
56 Moore JX, Akinyemiju T, Wang HE. Pollution and regional variations of lung cancer mortality in the United States. *Cancer Epidemiol* 2017; 49: 118–127.
57 Raaschou-Nielsen O, Andersen ZJ, Beelen R, *et al.* Air pollution and lung cancer incidence in 17 European cohorts: prospective analyses from the European Study of Cohorts for Air Pollution Effects (ESCAPE). *Lancet Oncol* 2013; 14: 813–822.
58 Seow WJ, Shu XO, Nicholson JK, *et al.* Association of untargeted urinary metabolomics and lung cancer risk among never-smoking women in China. *JAMA Netw Open* 2019; 2: e1911970.
59 Tomasetti C, Li L, Vogelstein B. Stem cell divisions, somatic mutations, cancer etiology, and cancer prevention. *Science* 2017; 355: 1330–1334.

60 Tomasetti C, Vogelstein B. Cancer etiology. Variation in cancer risk among tissues can be explained by the number of stem cell divisions. *Science* 2015; 347: 78–81.
61 Tomasetti C, Poling J, Roberts NJ, *et al.* Cell division rates decrease with age, providing a potential explanation for the age-dependent deceleration in cancer incidence. *Proc Natl Acad Sci USA* 2019; 116: 20482–20488.
62 Tomasetti C, Durrett R, Kimmel M, *et al.* Role of stem-cell divisions in cancer risk. *Nature* 2017; 548: E13–E14.
63 Skoulidis F, Byers LA, Diao L, *et al.* Co-occurring genomic alterations define major subsets of KRAS-mutant lung adenocarcinoma with distinct biology, immune profiles, and therapeutic vulnerabilities. *Cancer Discov* 2015; 5: 860–877.
64 Jackson EL, Willis N, Mercer K, *et al.* Analysis of lung tumor initiation and progression using conditional expression of oncogenic K-ras. *Genes Dev* 2001; 15: 3243–3248.
65 Meylan E, Dooley AL, Feldser DM, *et al.* Requirement for NF-kappaB signalling in a mouse model of lung adenocarcinoma. *Nature* 2009; 462: 104–107.
66 Xue W, Meylan E, Oliver TG, *et al.* Response and resistance to NF-κB inhibitors in mouse models of lung adenocarcinoma. *Cancer Discov* 2011; 1: 236–247.
67 Jackson EL, Olive KP, Tuveson DA, *et al.* The differential effects of mutant p53 alleles on advanced murine lung cancer. *Cancer Res* 2005; 65: 10280–10288.
68 Ventura A, Kirsch DG, McLaughlin ME, *et al.* Restoration of p53 function leads to tumour regression *in vivo*. *Nature* 2007; 445: 661–665.
69 Sutherland KD, Song JY, Kwon MC, *et al.* Multiple cells-of-origin of mutant K-Ras-induced mouse lung adenocarcinoma. *Proc Natl Acad Sci USA* 2014; 111: 4952–4957.
70 Mainardi S, Mijimolle N, Francoz S, *et al.* Identification of cancer initiating cells in K-Ras driven lung adenocarcinoma. *Proc Natl Acad Sci USA* 2014; 111: 255–260.
71 Guerra C, Mijimolle N, Dhawahir A, *et al.* Tumor induction by an endogenous K-ras oncogene is highly dependent on cellular context. *Cancer Cell* 2003; 4: 111–120.
72 Politi K, Zakowski MF, Fan PD, *et al.* Lung adenocarcinomas induced in mice by mutant EGF receptors found in human lung cancers respond to a tyrosine kinase inhibitor or to down-regulation of the receptors. *Genes Dev* 2006; 20: 1496–1510.
73 Soda M, Takada S, Takeuchi K, *et al.* A mouse model for EML4-ALK-positive lung cancer. *Proc Natl Acad Sci USA* 2008; 105: 19893–19897.
74 McFadden DG, Politi K, Bhutkar A, *et al.* Mutational landscape of EGFR-, MYC-, and Kras-driven genetically engineered mouse models of lung adenocarcinoma. *Proc Natl Acad Sci USA* 2016; 113: E6409–E6417.
75 Westcott PM, Halliwill KD, To MD, *et al.* The mutational landscapes of genetic and chemical models of Kras-driven lung cancer. *Nature* 2015; 517: 489–492.
76 Schmeltz I, Chiong KG, Hoffmann D. Formation and determination of ethyl carbamate in tobacco and tobacco smoke. *J Anal Toxicol* 1978; 2: 265–268.
77 Vaz M, Hwang SY, Kagiampakis I, *et al.* Chronic cigarette smoke-induced epigenomic changes precede sensitization of bronchial epithelial cells to single-step transformation by KRAS mutations. *Cancer Cell* 2017; 32: 360–376.
78 Li S, MacAlpine DM, Counter CM. Capturing the primordial Kras mutation initiating urethane carcinogenesis. *Nat Commun* 2020; 11: 1800.
79 Forkert PG. CYP2E1 is preferentially expressed in Clara cells of murine lung: localization by in situ hybridization and immunohistochemical methods. *Am J Respir Cell Mol Biol* 1995; 12: 589–596.
80 Hukkanen J, Pelkonen O, Hakkola J, *et al.* Expression and regulation of xenobiotic-metabolizing cytochrome P450 (CYP) enzymes in human lung. *Crit Rev Toxicol* 2002; 32: 391–411.
81 Guengerich FP, Kim DH, Iwasaki M. Role of human cytochrome p-450 IIE1 in the oxidation of many low molecular weight cancer suspects. *Chem Res Toxicol* 1991; 4: 168–179.
82 Forkert PG. Mechanisms of lung tumorigenesis by ethyl carbamate and vinyl carbamate. *Drug Metab Rev* 2010; 42: 355–378.
83 Dahl GA, Miller JA, Miller EC. Vinyl carbamate as a promutagen and a more carcinogenic analog of ethyl carbamate. *Cancer Res* 1978; 38: 3793–3804.
84 Park KK, Liem A, Stewart BC, *et al.* Vinyl carbamate epoxide, a major strong electrophilic, mutagenic and carcinogenic metabolite of vinyl carbamate and ethyl carbamate (urethane). *Carcinogenesis* 1993; 14: 441–450.
85 Spella M, Lilis I, Stathopoulos GT. Shared epithelial pathways to lung repair and disease. *Eur Respir Rev* 2017; 26: 170048.
86 Stathopoulos GT, Sherrill TP, Cheng DS, *et al.* Epithelial NF-kappaB activation promotes urethane-induced lung carcinogenesis. *Proc Natl Acad Sci USA* 2007; 104: 18514–18519.
87 Kanellakis NI, Giannou AD, Pepe MAA, *et al.* Tobacco chemical-induced mouse lung adenocarcinoma cell lines pin the prolactin orthologue proliferin as a lung tumour promoter. *Carcinogenesis* 2019; 40: 1352–1362.

88 Vreka M, Lilis I, Papageorgopoulou M, *et al.* IκB Kinase α is required for development and progression of KRAS-mutant lung adenocarcinoma. *Cancer Res* 2018; 78: 2939–2951.

89 Murphy SE, Isaac IS, Ding X, *et al.* Specificity of cytochrome P450 2A3-catalyzed alpha-hydroxylation of N′-nitrosonornicotine enantiomers. *Drug Metab Dispos* 2000; 28: 1263–1266.

90 Wong HL, Murphy SE, Hecht SS. Cytochrome P450 2A-catalyzed metabolic activation of structurally similar carcinogenic nitrosamines: N′-nitrosonornicotine enantiomers, N-nitrosopiperidine, and N-nitrosopyrrolidine. *Chem Res Toxicol* 2005; 18: 61–69.

91 Xue J, Yang S, Seng S. Mechanisms of cancer induction by tobacco-specific NNK and NNN. *Cancers (Basel)* 2014; 6: 1138–1156.

92 Yuan JM, Knezevich AD, Wang R, *et al.* Urinary levels of the tobacco-specific carcinogen N′-nitrosonornicotine and its glucuronide are strongly associated with esophageal cancer risk in smokers. *Carcinogenesis* 2011; 32: 1366–1371.

93 To MD, Wong CE, Karnezis AN, *et al.* Kras regulatory elements and exon 4A determine mutation specificity in lung cancer. *Nat Genet* 2008; 40: 1240–1244.

94 Hoadley KA, Yau C, Hinoue T, *et al.* Cell-of-origin patterns dominate the molecular classification of 10,000 tumors from 33 types of cancer. *Cell* 2018; 173: 291–304.e6.

95 Sproul D, Kitchen RR, Nestor CE, *et al.* Tissue of origin determines cancer-associated CpG island promoter hypermethylation patterns. *Genome Biol* 2012; 13: R84.

96 Zhang H, Fillmore Brainson C, Koyama S, *et al.* Lkb1 inactivation drives lung cancer lineage switching governed by polycomb repressive complex 2. *Nat Commun* 2017; 8: 14922.

97 van Veen JE, Scherzer M, Boshuizen J, *et al.* Mutationally-activated PI3′-kinase-α promotes de-differentiation of lung tumors initiated by the $BRAF^{V600E}$ oncoprotein kinase. *Elife* 2019; 8: e43668.

98 Best SA, Ding S, Kersbergen A, *et al.* Distinct initiating events underpin the immune and metabolic heterogeneity of KRAS-mutant lung adenocarcinoma. *Nat Commun* 2019; 10: 4190.

99 Tonon G, Brennan C, Protopopov A, *et al.* Common and contrasting genomic profiles among the major human lung cancer subtypes. *Cold Spring Harb Symp Quant Biol* 2005; 70: 11–24.

100 Alexandrov LB, Nik-Zainal S, Wedge DC, *et al.* Signatures of mutational processes in human cancer. *Nature* 2013; 500: 415–421.

101 Govindan R, Ding L, Griffith M, *et al.* Genomic landscape of non-small cell lung cancer in smokers and never-smokers. *Cell* 2012; 150: 1121–1134.

102 Alexandrov LB, Ju YS, Haase K, *et al.* Mutational signatures associated with tobacco smoking in human cancer. *Science* 2016; 354: 618–622.

# Acknowledgements

Special thanks go to my supervisor Dr. Georgios Stathopoulos for giving me the opportunity to do my PhD in his working group Molecular Lung Carcinogenesis at the Comprehensive Pneumology Center and Institute of Lung Biology and Disease of the Helmholtz Center Munich and Ludwig-Maximilians-University (LMU) Munich. I am very grateful to him for my interesting research projects, his great scientific and personal support throughout the whole time as a PhD student, his numerous words of advice, and facilitating me to visit conferences, significantly contributing to making me the scientist I am now.

I would also like to express my sincere gratitude to Professor Dr. Jürgen Behr and Professor Dr. Markus Rehberg for agreeing to being members of my thesis advisory committee. I am thankful for their supervision and helpful and critical input during my progress reports.

Furthermore, I appreciated being a part of the CPC Research School “Lung Biology and Disease”, Munich Medical Research School (MMRS), Helmholtz Graduate School Environmental Health (HELENA), and LMU Research Training Group GRK2338 “Targets in Toxicology”. They provided manifold courses and advanced trainings contributing to my scientific background. I valued that it didn’t come up short to have interactive exchange with my peers, fun activities, and friends.

I am much obliged to my former and current fellow lab mates Dr. Anne-Sophie Lamort, Dr. Mario Pepe, Dr. Kristina Arendt, Dr. Andrea Schamberger, Lilith Traßl, Benteng Deng, Jianlong Jia, and Asma Bin Snkar for the fruitful scientific exchange, troubleshooting, team spirit, and helpfulness creating a fantastic atmosphere and especially making PhD life fun. Special thanks go to Dr. Georgia Giotopoulou with whom together I pursued this whole journey. I want to express my appreciation for everything from scientific discussions to our friendship.

IN addition, I want to thank Dr. Magda Spella, Dr. Ioannis Lilis, Dr. Antonella Marazioti, Giannoula Ntaliarda, and Anthi Krontira of the Molecular Respiratory Carcinogenesis laboratory in the Faculty of Medicine at the University of Patras in Greece for all the pleasant collaborations, common publications, and their kind support during my research stay in their lab. The same goes for the various other co-workers and the interesting collaborations and papers we were allowed to have together.

Finally, I truly appreciate my family and friends for their constant understanding and encouragement during this challenging time.